Multiscale Biodistribution Analysis of a Lipophilic, Poorly Soluble Drug

by

Jason Baik

A dissertation submitted in partial fulfillment
of the requirements for the degree of
Doctor of Philosophy
(Pharmaceutical Sciences)
In The University of Michigan
2012

Doctoral Committee:

Associate Professor Gustavo R. Rosania, Chair
Professor Charles Burant
Professor David E. Smith
Associate Professor Nair Rodriguez-Hornedo

To those who made sacrifices:

my mice, my friends, and my parents

Acknowledgements

I would like to express my sincere gratitude to Dr. Gus Rosania for his support, guidance and patience throughout my Ph.D. training. He taught me perseverance, enthusiasm, and proper scientific attitudes. I also would like to thank my committee members, Dr. Nair Rodriguez-Hornedo, Dr. David Smith, and Dr. Charles Burant for their suggestions and guidance in my project and writing wonderful recommendation letters leading to exciting opportunities in my life.

I am also grateful to the Department of Pharmaceutical Sciences, the Rackham Graduate School and its emergency fund for support during my study and sickness. I also appreciate the funding sources, Warner Lambert & Parke Davis Fellowship, Pharmacological Scientist Training Program, and American Foundation for Pharmaceutical Education Pre-doctoral Fellowship.

I am greatly indebted to all my friends who helped me survive in this lonely, painful journey away from home. My wonderful friends shared the joys and sadness with me. They ate with me, cooked for me, and drank with me. Among the many, I'd like to acknowledge all the current and past students in the department including Cara Hartz Nelson and Lindsay White. Also my best buddies Seokhoon Ahn, Jiseok Lee, and Yong Keun Hwang, for their immeasurable support and friendship.

I thank my brother's family, Robin, Sun, and Julian for their contribution of happiness in my life. Lastly, I am most grateful to my parents who believed in me and offered their support and prayers to keep me going and make me successful.

Table of Contents

List of Figures

List of Appendices

Abstract

Clofazimine is a poorly soluble drug that accumulates as solid deposits in the body during prolonged oral administration. At the outset, we hypothesized that clofazimine accumulated intracellularly by a passive and spontaneous crystallization, and in various levels of experimental set-ups, from a tissue culture to mouse models. We found that clofazimine readily formed amorphous inclusions in complexes with intracellular membranes in MDCK cells, while different types of inclusions were found in the tissue macrophages of clofazimine-diet fed mice. Most of the inclusions *in vivo* appeared as vibrant red, birefringent, 10 – 20 μm length crystal-like structures; however, their physicochemical and morphological characteristics were inconsistent with those of pure clofazimine crystals. Most remarkably, among the inclusions from macrophages, we discovered a new cytoplasmic structure delimited by double membranes with internal supramolecular organizations resembling stacks of lipidic lamellae. Upon prolonged dosing, the intact clofazimine was redistributed from adipose tissues to the lymphatic organs paralleled by anti-inflammatory responses such as splenomegaly, liver microgranulomas, and an expansion of macrophage populations. In conclusion, instead of passive intracellular crystallization hypothesis, I propose that clofazimine accumulates *in vivo* by active sequestration in the immune system. By constructing intracellular crystal- and organelle-like "polyhedrosomes", the macrophages can impact the clofazimine's systemic pharmacokinetics and biodistribution, from micro to macro scale.

Chapter 1

Introduction

1.1 Pharmacokinetics of poorly soluble drugs

The main goal of pharmacokinetics is to study drug absorption, distribution, metabolism and excretion.[1] Such information is useful in identifying the maximum therapeutic use of a drug while allowing us to avoid unwanted toxicity. Therefore, in the drug development process, pharmacokinetic study is required to understand the bodily response to xenobiotic treatment, and is carried out during clinical trials[2] that seize about 70% of the drug development cost estimated from 500 to 900 million dollars.[3, 4] In order to reduce the cost spent on the clinical trials through decreasing the number of test subjects or the failure rate, the characteristics of chemical entities in a drug product must be predicted and addressed as early as possible.[2] Due to such strong demand for inquiry, government, academia, and the pharmaceutical industry have invested significant amounts of effort to develop models with *in silico* simulation,[4-6] *in vitro*[7-12] and *in vivo*,[13, 14] which are implemented for better and earlier prediction of pharmacokinetic behavior.[2]

Among pharmacokinetic parameters, drug plasma concentration is one of the most prominent indicators that reflects how much of a drug is in the body, since it can represent the net level of the drug in the systemic circulation resulting from the interplay

among absorption, distribution, metabolism and excretion components.[1] A decrease in the plasma concentration can be described as plasma half-life ($t_{1/2}$), and it can be linked to the two important pharmacokinetic parameters, which are total drug clearance (CL) and volume of distribution (Vd). For example, a certain case of drug clearance results from metabolism followed by renal excretion indicating how fast an elimination process for a particular drug is carried out in individuals with varying characteristics, such as differences in age, gender, or pathophysiology. The second parameter, the volume of distribution, is the volume accounting for the total amount of a drug in the body. When a steady state drug plasma level is achieved, in other words, when equilibrium has reached between the plasma and tissue concentrations, the volume of distribution can be used to estimate the total amount of drug by multiplying the plasma concentration. It is generalized that the volumes of distribution can be linked to plasma half-life and clearance ($Vd = CL \times t_{1/2} / 0.693$); however, they often result in values with little physiological relevance that are much greater than the bodily fluid estimated to be 42L for a 70kg male adult.[1]

In some cases, some drugs have longer half-lives and larger volumes of distribution than others owing to lipophilicity.[1] By becoming partitioned within fatty tissues, as these drugs favor deposition over dissolution into the blood stream, they could exert a slower rate of elimination and, in return, a longer plasma half-life than the more water-soluble drugs. Not only could lipophilic drugs make the clinician's control of the elimination process more difficult, as fat is a poorly perfused tissue, but it would also require more time to reach a desired plasma level, leading to a more complicated administration process for the same reason. On the other hand, since lipophilicity in general is related to

drug permeability through biological membranes,[15] the absorption can be promoted by increasing lipophilicity,[16] suggesting that the balance of drug permeability and lipophilicity (often anti-correlated to water solubility) becomes the main determinant of pharmacokinetic performance.[15, 17]

1.2 Poorly water soluble drug development and possible adverse effect

Despite the fact that controlling pharmacokinetic behavior is difficult, recent investment in poorly soluble drugs has increased dramatically. In the current industry, 39% of the marketed drugs and 90% of the new molecular entities under development are poorly soluble compounds,[8] and these trends have been supported by the technological advancement of promoting drug absorption and avoiding metabolism. By implementing the physicochemical advantages of formulation, e.g. supersaturation, a greater amount of poorly soluble components could be dissolved and driven through the gut wall into the body by a significant concentration gradient.[18] Also, biotransformation of poorly soluble components has become either less effective against drug encapsulation strategies, e.g. liposomal delivery,[19] or actively utilized by a pro-drug strategy,[20] such that the solubility of a parent compound is enhanced by covalent attachment of a cleavable moiety. However, these trends cast an unprecedented concern owing to the fact that a large amount of poorly water-soluble drug administered into the body could possibly induce idiosyncratic side effects.

Currently, the drug industry is largely focused on enhancing bioavailability as explained above, rather than having researchers consider the possible side effects associated with tissue partitioning, aggregate formation, precipitation or complex

formation of xenobiotics after delivering them into the body. Often, drug formulators rely overly on the belief that the protein binding, which was measured at the early drug discovery stage, would prevent *in vivo* aggregation or solid precipitation, and therefore disregard the potential toxicity, since they seldom encounter such cases. Nevertheless, there are a significant number of case reports of *in vivo* precipitation of drugs or metabolites, sometimes crystallizing in either pure form or as salts, leading to problems in the body.[21-23] For example, indinavir crystalluria[21] or triamterene kidney stone formation[24] are fast-developing symptoms that can cause acute renal failure,[24-27] whereas crystal arthritis or gout[28] are more like slow acting inflammations resulting from the excessive amount of a xenobiotic present in the body over its solubility limit, but one that the body can handle.

1.3 Model drug clofazimine

Past research has shown that the treatment with clofazimine (Lamprene®, Novartis, CAS 2030-63-9, Mw: 473,4)[29-31] results in the red pigmentation of patients due to "drug crystals", which are also reported under search words as "crystals deposition" or "crystal-storing cells".[32-35] At the outset, we hypothesized that clofazimine would accumulate in cells by crystallization, a spontaneous, thermodynamic process. However, other than birefringence and needle-like morphology, we found no direct evidence that these intracellular structures are pure drug crystals, which are unlikely to crystallize under a system as complicated, concentrated, and "dirty" as that of cytoplasm. Therefore, we thought these "crystal-like drug inclusions (CLDIs)" could well be comprised of different components and induced by biological factors instead of "clofazimine to clofazimine"

crystallization. CLDIs could be actively formulated within designated locations in the body as opposed to being physicochemically driven to crystallize and precipitating out at random places.

The drastic skin pigmentation in *Mycobacterium Leprae* infected patients is thought to be due to the physicochemical characteristics of clofazimine that has a logP of 7.3 and water insolubility.[36] The plasma half-life is up to 70 days,[36] and in some cases, clofazimine was reported to stay in the body for a couple of years after discontinuation of the drug which was administered orally as 50 – 100 mg tablets per day.[30, 37, 38] When the drug was dosed with fat, there was a marked increase in absorption; meanwhile, when the drug was chemically modified to a more water soluble version (B720), the drug accumulated and deposited to a lesser extent in the lungs, spleen and liver.[37, 39] This modification advocated the importance of lipophilicity, which affects the drug absorption and distribution.[17] Since clofazimine has high permeability and low solubility (Biopharmaceutics Classification System class 2),[7] at the same time, we could find several references for the clofazimine accumulating inside cells,[40, 41] we sought to further test whether a biological factor could either promote or prevent[42] the drug precipitation.

Since its first synthesis in 1956 by Barry and coworkers,[29] a significant number of observations have been recorded for clofazimine (B663) and its accumulation, which was related to poor solubility.[29, 31] Levy and Banerjee et al. have reported that 99% of the drug was present in an un-dissolved form, indicating significant precipitation had occurred within the first week of treatment in mice.[36, 38] Within this study, the authors reported that 50% of the orally administered drug was excreted unchanged in feces after a single dose, while less than 1% was excreted in urine.[36] The metabolism of clofazimine

has not been fully elucidated, and although 3 metabolic pathways were reported, the biotransformation process remains ineffective, confirmed by metabolite detection in the urine of leprosy patients.[31, 43] Conalty and Jackson have also tested organ pigmentation, and they reported that the liver and lungs developed the drug inclusions significantly later than the spleen.[44, 45] In their discussion, the authors speculated that an adverse drug reaction could have developed a negative immunological effect, owing to the decrease in phagocytic activity of the macrophages with drug inclusions. Several electron microscopy studies have been carried out in both humans and small animals.[40, 46] The results showed crystalloid cavities with polygonal shapes with delimiting membranes in the cytoplasm. These empty spaces were remainders of drug deposits washed away during the sample preparation involving a series of extensive alcohol dehydration steps. Meanwhile, no one has directly characterized whether clofazimine inclusions are pure drug crystals or complexes with other endogenous materials in the body.

In terms of cellular uptake and response to clofazimine, just as the reticular endothelial systems are the immunological outposts in the body that would take care of atypical stress, e.g. parasitic invasion,[41] we hypothesized that cells would have a similar subcellular functionality that would respond to the exposure to poorly soluble compounds. As clofazimine is a weakly basic drug (pKa = 8.5), it could first accumulate within acidic compartments through an ion-trapping mechanism, in which protonation decreases the drug molecule's permeability across the lipid bilayers.[47] However, as the protonated form of the molecule still continues to favor partitioning within the lipid phase significantly (logD = 6.59 at pH 5, predicted by MarvinSketch, ChemAxon, Appendix A), cells may need to counteract the random partitioning of clofazimine which otherwise

would change the biological lipid membranes' fluidity and compromise their function. So far, no transporter mechanism has been shown to efflux the clofazimine out of cells, and the drug molecules have seemed to accumulate in subcellular compartments.

A previous study from our group has reported that the lipophilic compound chloroquine (logP = 4.63) did not reach a steady state concentration during subcellular drug accumulation, and the concentration continued to increase.[48] Such an un-saturable phenomenon was partly caused by drug induced phospholipidosis,[49-51] a phenomenological malfunction in cells in clearing phospholipids, which results in a significant accumulation of phospholipids in cytoplasm that could be detected with electron microscopy[52] and confocal Raman imaging.[48] In addition to *a priori* knowledge, that clofazimine has been reported to precipitate in cells,[40, 41] we could trace the vibrantly red clofazimine with transmitted microscopy and explore subcellular accumulation phenomena. Therefore, we sought to investigate the physicochemical and biological nature of clofazimine precipitation in MDCK cells (Madin-Darby Canine Kidney epithelium) and Balb/c mice in order to address whether clofazimine can crystallize inside the cells.

1.4 Biological response against poorly soluble, lipophilic xenobiotics

Several exogenous substances are known to accumulate and cause pigmentation *in vivo*,[53-55] and sometimes reveal similar empty cavities under microscopy.[22, 23] For example, some heavy metals and drugs are reported to induce hyperpigmentation by deposition into different parts of the body and photochemically react with ultraviolet light to cause color changes.[56] In the case of poorly soluble paraffin wax, it was reported to

accumulate and induce inflammatory changes in the liver and mesenteric lymph nodes of Fischer-344 rats, but not in Sprague-Dawley rats.[57] Histochemical analysis in Fischer-344 rats showed the development of splenomegaly, liver microgranulomas, and Kupffer cells with lysosomal, polyhedral cavities under electron microscopy. These reports indicate that accumulation of foreign substances can trigger different immunological responses and related chronic inflammation involving phagocytes depending on biological contributions of the species. Therefore, in addition to the physicochemical characterization, we sought to investigate any pathophysiological changes that are induced upon clofazimine administration and *in vivo* precipitation or aggregation formation. Understanding the physiological basis of this phenomenon could provide the cellular and microscopic underpinnings of the atypical pharmacokinetic behavior of such poorly soluble drugs focused by the current research investments in the pharmaceutical industry.

1.5 References

1. Buxton, I. L.; Benet, L. Z., Chapter 2. Pharmacokinetics: The Dynamics of Drug Absorption, Distribution, Metabolism, and Elimination. In *Goodman & Gilman's The Pharmacological Basis of Therapeutics*, 12 ed.; Brunton, L. L.; Chabner, B. A.; Knollmann, B. C., McGraw-Hill: New York, **2011**.

2. FDA *Critical Path Opportunities Report* U.S. Department of Health and Human Services Food and Drug Administration: March, **2006**; 1-37.

3. DiMasi, J. A.; Hansen, R. W.; Grabowski, H. G. The price of innovation: new estimates of drug development costs. *J Health Econ* **2003,** *22*, (2), 151-85.

4. PricewaterhouseCoopers *Pharma 2020: Virtual R&D Which path will you take?*; **2008**.

5. van de Waterbeemd, H.; Gifford, E. ADMET in silico modelling: towards prediction paradise? *Nat Rev Drug Discov* **2003,** *2*, (3), 192-204.

6. Loew, L. M.; Schaff, J. C. The Virtual Cell: a software environment for computational cell biology. *Trends Biotechnol* **2001,** *19*, (10), 401-6.

7. Amidon, G. L.; Lennernas, H.; Shah, V. P.; Crison, J. R. A theoretical basis for a biopharmaceutic drug classification: the correlation of in vitro drug product dissolution and in vivo bioavailability. *Pharm Res* **1995,** *12*, (3), 413-20.

8. Benet, L. Z.; Broccatelli, F.; Oprea, T. I. BDDCS Applied to Over 900 Drugs. *AAPS J* **2011**, DOI:10.1208/s12248-011-9290-9.

9. Cuperlovic-Culf, M.; Barnett, D. A.; Culf, A. S.; Chute, I. Cell culture metabolomics: applications and future directions. *Drug Discovery Today* **2011,** *15*, (15-16), 610-621.

10. Reichl, S.; Kolln, C.; Hahne, M.; Verstraelen, J. In vitro cell culture models to study the corneal drug absorption. *Expert Opinion on Drug Metabolism & Toxicology* **2011,** *7*, (5), 559-578.

11. Semlin, L.; Schafer-Korting, M.; Borelli, C.; Korting, H. C. In vitro models for human skin disease. *Drug Discovery Today* **2011,** *16*, (3-4), 132-139.

12. Wu, C. Y.; Benet, L. Z. Predicting drug disposition via application of BCS: transport/absorption/ elimination interplay and development of a biopharmaceutics drug disposition classification system. *Pharm Res* **2005,** *22*, (1), 11-23.

13. Agu, R. U.; Ugwoke, M. I. In vitro and in vivo testing methods for respiratory drug delivery. *Expert Opinion on Drug Delivery* **2011,** *8*, (1), 57-69.

14. Sukardi, H.; Chng, H. T.; Chan, E. C. Y.; Gong, Z.; Lam, S. H. Zebrafish for drug toxicity screening: bridging the in vitro cell-based models and in vivo mammalian models. *Expert Opinion on Drug Metabolism & Toxicology* **2011,** *7*, (5), 579-589.

15. Malkia, A.; Murtomaki, L.; Urtti, A.; Kontturi, K. Drug permeation in biomembranes: In vitro and in silico prediction and influence of physicochemical properties. *European Journal of Pharmaceutical Sciences* **2004,** *23*, (1), 13-47.

16. Balon, K.; Riebesehl, B. U.; Muller, B. W. Drug liposome partitioning as a tool for the prediction of human passive intestinal absorption. *Pharm Res* **1999,** *16*, (6), 882-8.

17. Klopman, G.; Zhu, H. Recent methodologies for the estimation of N-octanol/water partition coefficients and their use in the prediction of membrane transport properties of drugs. *Mini-Rev. Med. Chem.* **2005,** *5*, (2), 127-133.

18. Brouwers, J.; Brewster, M. E.; Augustijns, P. Supersaturating drug delivery systems: the answer to solubility-limited oral bioavailability? *J Pharm Sci* **2009,** *98*, (8), 2549-72.

19. van Hoogevest, P.; Liu, X.; Fahr, A. Drug delivery strategies for poorly water-soluble drugs: the industrial perspective. *Expert Opinion on Drug Delivery* **2011,** *8*, (11), 1481-1500.

20. Han, H.-K.; Amidon, G. Targeted prodrug design to optimize drug delivery. *The AAPS Journal* **2000,** *2*, (1), 48-58.

21. Grases, F.; Costa-Bauza, A.; Garcia-Gonzalez, R.; Payeras, A.; Bassa, A.; Torres, J. J.; Conte, A. Indinavir crystallization and urolithiasis. *Int Urol Nephrol* **1999,** *31*, (1), 23-9.

22. Farge, D.; Turner, M. W.; Roy, D. R.; Jothy, S. Dyazide-induced reversible acute renal failure associated with intracellular crystal deposition. *Am J Kidney Dis* **1986,** *8*, (6), 445-9.

23. Okada, H.; Watanabe, Y.; Kotaki, S.; Ikeda, N.; Takane, H.; Kanno, Y.; Sugahara, S.; Ban, S.; Nagata, M.; Suzuki, H. An unusual form of crystal-forming chronic interstitial nephritis following long-term exposure to tosufloxacin tosilate. *Am J Kidney Dis* **2004,** *44*, (5), 902-7.

24. Roy, L. F.; Villeneuve, J. P.; Dumont, A.; Dufresne, L. R.; Duran, M. A.; Morin, C.; Jobin, J. Irreversible renal failure associated with triamterene. *Am J Nephrol* **1991,** *11*, (6), 486-8.

25. Daudon, M.; Jungers, P. Drug-induced renal calculi - Epidemiology, prevention and management. *Drugs* **2004,** *64*, (3), 245-275.

26. Hesse, A.; Siener, R. Current aspects of epidemiology and nutrition in urinary stone disease. *World J Urol* **1997,** *15*, (3), 165-71.

27. Yarlagadda, S. G.; Perazella, M. A. Drug-induced crystal nephropathy: an update. *Expert Opinion on Drug Safety* **2008,** *7*, (2), 147-158.

28. Pascual, E. Management of crystal arthritis. *Rheumatology* **1999,** *38*, (10), 912-916.

29. Barry, V. C.; Belton, J. G.; Conalty, M. L.; Denneny, J. M.; Edward, D. W.; O'Sullivan, J. F.; Twomey, D.; Winder, F. A new series of phenazines (rimino-compounds) with high antituberculosis activity. *Nature* **1957,** *179*, (4568), 1013-5.

30. Barry, V. C.; Conalty, M. L. The Antimycobacterial Activity of B 663. *Lepr Rev* **1965,** *36*, 3-7.

31. O'Connor, R.; O'Sullivan, J. F.; O'Kennedy, R. The pharmacology, metabolism, and chemistry of clofazimine. *Drug Metab Rev* **1995,** *27*, (4), 591-614.

32. Atkinson, A. J., Jr.; Sheagren, J. N.; Rubio, J. B.; Knight, V. Evaluation of B.663 in human leprosy. *Int J Lepr Other Mycobact Dis* **1967,** *35*, (2), 119-27.

33. Desikan, K. V.; Ramanujam, K.; Ramu, G.; Balakrishnan, S. Autopsy findings in a case of lepromatous leprosy treated with clofazimine. *Lepr Rev* **1975,** *46*, (3), 181-9.

34. Mansfield, R. E. Tissue concentrations of clofazimine (B663) in man. *Am J Trop Med Hyg* **1974,** *23*, (6), 1116-9.

35. Sukpanichnant, S.; Hargrove, N. S.; Kachintorn, U.; Manatsathit, S.; Chanchairujira, T.; Siritanaratkul, N.; Akaraviputh, T.; Thakerngpol, K. Clofazimine-induced crystal-storing histiocytosis producing chronic abdominal pain in a leprosy patient. *Am J Surg Pathol* **2000,** *24*, (1), 129-35.

36. Banerjee, D. K.; Ellard, G. A.; Gammon, P. T.; Waters, M. F. Some observations on the pharmacology of clofazimine (B663). *Am J Trop Med Hyg* **1974,** *23*, (6), 1110-5.

37. Barry, V. C.; Buggle, K.; Byrne, J.; Conalty, M. L.; Winder, F. Absorption, distribution and retention of the riminocompounds in the experimental animal. *Ir J Med Sci* **1960,** *416*, 345-52.

38. Levy, L. Pharmacologic studies of clofazimine. *Am J Trop Med Hyg* **1974,** *23*, (6), 1097-109.

39. Schaad-Lanyi, Z.; Dieterle, W.; Dubois, J. P.; Theobald, W.; Vischer, W. Pharmacokinetics of clofazimine in healthy volunteers. *Int J Lepr Other Mycobact Dis* **1987,** *55*, (1), 9-15.

40. McDougall, A. C. Electron microscope studies of the antileprosy drug B663 (clofazimine; Lamprene). *Int J Lepr Other Mycobact Dis* **1974,** *42*, (1), 1-12.

41. McDougall, A. C.; Horsfall, W. R.; Hede, J. E.; Chaplin, A. J. Splenic infarction and tissue accumulation of crystals associated with the use of clofazimine (Lamprene; B663) in the treatment of pyoderma gangrenosum. *Br J Dermatol* **1980,** *102*, (2), 227-230.

42. Beshensky, A. M.; Wesson, J. A.; Worcester, E. M.; Sorokina, E. J.; Snyder, C. J.; Kleinman, J. G. Effects of urinary macromolecules on hydroxyapatite crystal formation. *J Am Soc Nephrol* **2001,** *12*, (10), 2108-16.

43. Feng, P. C.; Fenselau, C. C.; Jacobson, R. R. A new urinary metabolite of clofazimine in leprosy patients. *Drug Metab Dispos* **1982,** *10*, (3), 286-8.

44. Conalty, M. L.; Barry, V. C.; Jina, A. The antileprosy agent B.663 (Clofazimine) and the reticuloendothelial system. *Int J Lepr Other Mycobact Dis* **1971,** *39*, (2), 479-92.

45. Conalty, M. L.; Jackson, R. D. Uptake by reticulo-endothelial cells of the rimino-phenazine B.663(2-P-chloroanilino-5-P-chlorophenyl-3: 5-dihydro-3-isopropyliminophenazine). *Br J Exp Pathol* **1962,** *43*, 651-4.

46. Belaube, P.; Devaux, J.; Pizzi, M.; Boutboul, R.; Privat, Y. Small bowel deposition of crystals associated with the use of clofazimine (Lamprene) in the treatment of prurigo nodularis. *Int J Lepr Other Mycobact Dis* **1983,** *51*, (3), 328-30.

47. de Duve, C.; de Barsy, T.; Poole, B.; Trouet, A.; Tulkens, P.; Vanhoof, F. Lysosomotropic Agents. *Biochemical Pharmacology* **1974,** *23*, (18), 2495-531.

48. Zheng, N.; Zhang, X.; Rosania, G. R. Effect of phospholipidosis on the cellular pharmacokinetics of chloroquine. *J Pharmacol Exp Ther* **2010,** *336*, (3), 661-71.

49. Alakoskela, J. M.; Vitovic, P.; Kinnunen, P. K. Screening for the drug-phospholipid interaction: correlation to phospholipidosis. *ChemMedChem* **2009,** *4*, (8), 1224-51.

50. Hostetler, K. Y.; Reasor, M.; Yazaki, P. J. Chloroquine-induced phospholipid fatty liver. Measurement of drug and lipid concentrations in rat liver lysosomes. *J Biol Chem* **1985,** *260*, (1), 215-9.

51. Reasor, M. J.; Hastings, K. L.; Ulrich, R. G. Drug-induced phospholipidosis: issues and future directions. *Expert Opin Drug Saf* **2006,** *5*, (4), 567-83.

52. Dake, M. D.; Madison, J. M.; Montgomery, C. K.; Shellito, J. E.; Hinchcliffe, W. A.; Winkler, M. L.; Bainton, D. F. Electron microscopic demonstration of lysosomal inclusion bodies in lung, liver, lymph nodes, and blood leukocytes of patients with amiodarone pulmonary toxicity. *Am J Med* **1985,** *78*, (3), 506-12.

53. Ming, M. E.; Bhawan, J.; Stefanato, C. M.; McCalmont, T. H.; Cohen, L. M. Imipramine-induced hyperpigmentation: four cases and a review of the literature. *J Am Acad Dermatol* **1999,** *40*, (2 Pt 1), 159-66.

54. Treister, N. S.; Magalnick, D.; Woo, S. B. Oral mucosal pigmentation secondary to minocycline therapy: report of two cases and a review of the literature. *Oral Surg Oral Med Oral Pathol Oral Radiol Endod* **2004,** *97*, (6), 718-25.

55. Hashimoto, K.; Wiener, W.; Albert, J.; Nelson, R. G. An electron microscopic study of chlorpromazine pigmentation. *J Invest Dermatol* **1966,** *47*, (4), 296-306.

56. Granstein, R. D.; Sober, A. J. Drug- and heavy metal-induced hyperpigmentation. *J Am Acad Dermatol* **1981,** *5*, (1), 1-18.

57. Griffis, L. C.; Twerdok, L. E.; Francke-Carroll, S.; Biles, R. W.; Schroeder, R. E.; Bolte, H.; Faust, H.; Hall, W. C.; Rojko, J. Comparative 90-day dietary study of paraffin wax in Fischer-344 and Sprague-Dawley rats. *Food Chem Toxicol* **2010,** *48*, (1), 363-72.

Chapter 2

Molecular Imaging of Intracellular Drug-Membrane Aggregate Formation

2.1 Abstract

Clofazimine is a lipophilic antibiotic with an extremely long pharmacokinetic half-life associated with the appearance of crystal-like drug inclusions, *in vivo*. Here, we studied how clofazimine accumulates inside cells in the presence of supersaturating, extracellular concentrations of the drug (in the range of physiological drug concentrations). Based on a combination of molecular imaging, biochemical analysis and electron microscopy techniques, clofazimine mass increased inside cells *in vitro*, over a period of several days, with discrete clofazimine inclusions forming in the cytoplasm. These inclusions grew in size, number and density, as long as the drug-containing medium was replenished. With Raman confocal microscopy, clofazimine's spectral signature in these inclusions resembled that of amorphous clofazimine precipitates and was unlike that of clofazimine crystals. Additional experiments revealed that clofazimine first accumulated in mitochondria, with ensuing changes in mitochondrial structure and function. In turn, the degenerating organelles coalesced, fused with each other and condensed to form prominent drug-membrane aggregates (dubbed autophagosome-like

drug inclusions or "ALDIs"). Like clofazimine, it is possible that intracellular drug-membrane aggregate formation is a common phenomenon underlying the reported phenotypic effects of other small molecule drugs with similar physicochemical properties.

2.2 Introduction

Intracellular drug targeting can be useful to minimize drug toxicity and maximize efficacy. Nevertheless, the sequestration of drugs within intracellular organelles can also affect pharmacokinetics and pharmacodynamics after systemic delivery[1-3]. Among several known organelle sequestration mechanisms, ion-trapping of drugs within acidic compartments, i.e. lysosomes, has been most extensively studied[4, 5]. Protonation of weakly basic molecules leads to increased solubility and decreased membrane permeability, and promotes retention within lysosomes and endosomes. In the case of lipophilic cations, the electrical potential present across the inner membrane of mitochondria drives accumulation of membrane permeant lipophilic cations into this organelle [1, 3, 6, 7]. Beyond transmembrane pH gradients (i.e. lysosomotropism) and electrical potentials (i.e. mitochondriotropism), interactions of chemical agents with intracellular membranes could directly promote drug accumulation. To study this phenomenon, the FDA approved antibacterial drug clofazimine was selected as a model compound. Clofazimine is highly lipophilic and possesses and unusually long pharmacokinetic half-life of up to 70 days [8] associated with extensive accumulation of the drug in the body[9].

Although clofazimine's low solubility has been suspected to be responsible for its atypical pharmacokinetics, the mechanism by which drug accumulates intracellularly is

not known[8-12]. To study this, we decided to pursue a cell-based approach to determine whether clofazimine forms intracellular precipitates or crystal-like deposits in Madin Darby Canine Kidney (MDCK) cells, *in vitro*. MDCK cells were selected because they are considered a robust in vitro assay system for drug transport studies. While these cells originated from the epithelia of the distal renal tubules, they are also used as a model to study the passive diffusive component of intestinal drug absorption[2] and to study drug bioaccumulation associated with ion-trapping[13] and phospholipidosis[3, 14]. Taking advantage of clofazimine's red color, the drug's absorbance, fluorescence, and biodistribution properties could be readily measured. In addition, Raman spectral imaging and electron microscopic examination were performed to reveal the mechanism of clofazimine's intracellular accumulation: the formation of organelle-derived, intracellular drug-membrane aggregates.

2.3 Materials and Methods

Chemicals. Reagents were purchased from Sigma-Aldrich (St. Louis, MO), unless otherwise indicated.

Drug mass measurement. MDCK (CCL-34^{TM} ATCC, Manassas, VA) cells were maintained with DMEM plus 10 % FBS (Gibco® 10082), 10 % non-essential amino acid (Gibco® 11140 from Invitrogen, Carlsbad, CA), and with 10 % penicillin/streptomycin (Gibco® 15140) in a 37°C 5% CO_2 incubator. For experiments, MDCK cells were incubated with clofazimine solutions: clofazimine-containing medium was made by diluting 10 mM clofazimine stock (in DMSO) into DMEM plus 5 % FBS immediately before adding to cells (clofazimine added to cell culture medium without FBS formed

amorphous precipitates, but in 5% FBS no visible precipitates formed due to drug binding to serum proteins). For clofazimine mass measurements, cells were detached using Trypsin-EDTA (Gibco® 15050), resuspended in 0.1 M citric acid/ 0.1 M trisodium citrate buffer (pH 5) and counted with hemocytometer. Equal number and volume of cells were transferred to 96-well plates and dissolved with 100 µl ATCC detergent (American Type Culture Collection, 30-1010K). The clofazimine absorbance at 495 nm was measured with a plate reader (Synergy-2, Biotek Instruments, Winooski, VT) and mass was calculated with the aid of a standard curve generated separately.

LC/MS analysis of intracellular clofazimine. Analysis of clofazimine's chemical stability was performed for samples treated with drug-containing media (10 µM or 0 µM), and for pure drug (1 µg/ml). For extraction, samples were resuspended in methanol to dissolve and extract the drug, and then centrifuged at 15,000g for 10 minutes to remove insoluble components. Analysis was performed with HPLC (Agilent1200, Zorbax RX-C18 column) coupled to a mass spectrometer (Applied Biosystems QTRAP 3200) eluted with H_2O:acetonitrile gradient (Analyst1.4, Applied Biosystems). Full scanning of total ion current (TIC) from 200 to 800 of the reference drug sample revealed intact clofazimine 473.2 and two ion transition fragments of 431.2 and 429.2 (*m/z*). For treated cells, multiple reaction monitoring (MRM) was performed, scanning for 44 common metabolic transformations of the intact molecule and the two fragments of 431.2 and 429.2 *m/z*.

Light and fluorescence microscopy. Cells on cover glasses were cultured with clofazimine-medium for the indicated times. For cellular lipid staining, 1 µg/ml Nile red was added for 2 hours. MTR staining was carried out with or without CFZ in media with

150 nM of MTR (from 10 mM DMSO stock solution) incubated for 45 minutes. After incubation, cover glasses were washed twice with DPBS and inverted onto glass slides for visualization on Olympus 51X upright epifluorescence/polarization microscope equipped 100× objective (1.40 NA, PlanApo oil emersion), cross polarizers, U-MWIBA3 (eGFP) for green U-MWG2 (rhodamine) filter cube for red channel, and an Olympus DP-70 color camera. Images were acquired using DP controller 3.1.1.267 under same exposure settings.

Transmission Electron Microscopy. Samples were processed as previously described [15] and imaged with a Philips CM-100 at magnifications from ×2,600 to ×130,000. Objects from pictures of cells taken during triplicate experiments were counted and scored for each category (with 6 to 10 individual cells analyzed per sample).

Mitochondrial respiration measurement. Mitochondrial respiration was measured using Seahorse XF24 Extracellular Flux Analyzer (Seahorse Bioscience Inc., North Billerica, MA) equipped with optical sensors that measure oxygen and protons in the extracellular media[16]. Briefly, 24 hours before the measurement, 50,000 cells were seeded onto wells of XF24 cell culture microplates (V7, Seahorse Bioscience) with 150 µl DMEM, and additional 100 µl was added after 4 hours when cells attached firmly. After 24 hours, cells were washed and pre-incubated with bicarbonate-free media (DMEM base XF Assay Medium, Seahorse Bioscience 100965) in 37 $^{\circ}$C incubator without CO_2 control. Injection cartridge (Seahorse Bioscience 100840) was pre-incubated with calibration media 24 hour-prior to the assay and four different injection ports were loaded with following compounds containing 20 µM BSA with 10 fold concentrate of the drugs in media: CFZ (100 µM, port A), oligomycin (10 µM, port B), FCCP (carbonyl

cyanide *p*-trifluoromethoxyphenylhydrazone, 30 µM, port C), and Antimycin A (15 µg/ml, port D). After automated calibration of the sensors, at pre-determined time points, O_2 level was measured and OCR (oxygen consumption rate) was calculated from the depleting oxygen level and data were analyzed using algorithm described by the manufacturer[17]. For plotting drug effects, OCR measurements for each well were subtracted by the internal, baseline OCR obtained for that same well, based on the measurement made before injecting any drug (arbitrarily set to the 27th minute read after cells equilibrate in the instrument).

Confocal Raman microscopy. Cover glasses were inverted on glass slides, and sealed with nail polish. The glass slides were then frozen in liquid N_2 and kept at less than -20°C until microscopic analysis using a WITec alpha300R instrument equipped with a CCD camera, a UHTS300 Raman spectrometer and with a 10 mW power 532 nm doubled Nd:YAG laser (WITec GmbH©, Germany). For the analysis of clofazimine signal, a 2nd order polynomial was fitted to the raw data for background fluorescence subtraction, and the remaining signal was filtered with median-2 filter (WITec project 2.00 software).

Lipid analysis. Cells were prepared on 10 cm-diameter dish and incubated with media containing either 10 µM or 0 µM of clofazimine for 36 hours. Cells were trypsinized, counted and kept frozen until analysis at the Lipidomics lab at Michigan Metabolomics and Obesity Center. Lipids were extracted using methanol:chloroform (2:1) solution and isolated with thin layer chromatography (TLC Silica gel 60, E.Merck). Chloroform:methanol:acetic acid:water (100:40:12:4) was used as mobile phase and TLC bands were scraped off and weighed for neutral lipid and phospholipid species, while phospholipid species (lyso phosphatidylcholine, phosphatidic acid, phosphatidyl choline,

phosphatidyl ethanolamine, phosphatidyl serine, phosphatidyl inositol, sphingomyelin, cardiolipin) were quantified according to the inorganic phosphorous assay[18]. For each lipid species, reference standards were purchased from Sigma. The experiments were independently repeated three times and the results analyzed with the Student's T-test.

Mitochondria isolation and clofazimine partitioning. Mitochondria were isolated using a commercial kit (MITOISO1, Sigma) from approximately 10^8 cells and homogenized with rotating motor (200 rpm, >50 times) in 4 – 5 ml volume of Extraction Buffer A (E2778 Sigma) followed by centrifugation at 1,000g for 5 min, and then at 11,000g for 10 min. After the enrichment procedure, a small brown-white color pellet comprised of enriched mitochondria was verified using the JC-1 accumulation assay, following the kit's instructions. To measure CFZ binding to isolated mitochondria, 5 μM CFZ solution was made in Storage Buffer (S9689 Sigma), which contains ATP/ADP and DTT in potassium buffer to sustain the mitochondrial respiration, then added to the isolated mitochondria. The mix was vortexed until homogenous, then centrifuged at 11,000g for 10 min. Clofazimine that was bound to the pellet, that remained dissolved in the liquid, or that was absorbed to the sides of the tube were extracted with MeOH. MeOH extracts were cleared by after centrifugation at 11,000g for 10 min. The mass of clofazimine in each fraction was determined from the concentration of clofazimine in the extracts, using the absorbance plate reader, with the aid of a standard curve. The mass of clofazimine remaining in the supernatants was determined by adding the mass of clofazimine that adsorbed to the sides of the centrifuge tube to that which remained dissolved in the liquid.

Image processing. For display, images were digitally enhanced and overlaid using Photoshop®. For control vs. experimental comparisons within the same figure, contrast and brightness settings were similarly adjusted.

2.4 Results

2.4.1 Biochemical Analysis and Transmitted Light Microscopy Reveal Intracellular Clofazimine Inclusion Formation

Clofazimine accumulated intracellularly upon incubation with cells (Figure 1A). Based on the calculated single cell volume of 1.6 pL[5], cellular concentration approximated 4 mM. However, concentration in the extracellular medium was 10 μM, mostly in protein-bound form (SI. 1), which is within range of serum concentrations *in vivo*[19]. We observed a rapid increase of cell-associated drug mass within minutes after the start of incubation, followed by a continuous, gradual increase that continued for as long as the cells were maintained in the clofazimine-containing medium (Figure 1B). To determine if intracellular clofazimine was metabolized, we performed LC/MS chemical analysis of intracellular clofazimine in cells incubated with or without 10 μM clofazimine in culture medium for 90 hours. Intracellular clofazimine was present intact with no major metabolites detected (SI. 2).

Within the first 12 hours of clofazimine accumulation, small and scattered clofazimine inclusions in the cytoplasm formed nanometer-sized bright red speckles, visible with transmitted light illumination. After 24 hours or longer, inclusions grew in size, ranging from 1 to 2 μm in length, and assumed irregular shapes and heterogeneous red color. They continued growing in size for as long as the extracellular medium was

replenished with fresh, clofazimine-containing medium (Figure 1B, 120 hours). The size, shape and color of the inclusions were consistent with previous report in mouse lung macrophages[10]. Intracellular clofazimine accumulation was reversible. After clofazimine-treated cells were transferred to drug-free medium, the efflux half-life was between 2 and 3 hours, with some red inclusions remaining visible even after 6 hours of efflux. At these concentrations, clofazimine incubation inhibited cell growth and intracellular drug mass accumulation was proportional to the drug concentration in the medium (SI. 3).

2.4.2 Fluorescence microscopy yields evidence that large clofazimine inclusions form from condensation and aggregation of smaller vesicles.

In buffer, dilute clofazimine solutions (< 10 μM) fluoresce under 450 nm illumination (528 nm emission), but more concentrated solutions result in fluorescence quenching (SI. 4). With epifluorescence microscopy, we found small intracellular inclusions were fluorescent at those wavelengths (460 – 495 nm excitation, 515 – 550 nm emission), but that the larger, redder inclusions apparent at later time points did not fluoresce (arrow, Fig 1C). We inferred that clofazimine first accumulated in the small fluorescent vesicles, and then became increasingly concentrated in the larger, red (but nonfluorescent) inclusions.

The larger clofazimine inclusions were brightly stained with Nile Red (NR), a highly lipophilic, neutral fluorophore that is commonly used as cellular lipid stain. This suggested that the larger clofazimine inclusions were enriched in a hydrophobic component. Without clofazimine, cells showed significantly lower NR staining which bleached very quickly, without evidence of organelle-associated NR staining. However, measurement of total cellular lipid, neutral lipid and various phospholipids did not reveal

statistically significant alterations in lipid mass or relative contents after clofazimine treatment (data not shown). Thus, while the growth of clofazimine inclusions was associated with increased NR staining and photostability, there were no measurable changes in lipid profiles.

2.4.3 Chemical imaging yields evidence of clofazimine aggregates but no evidence of intracellular crystals.

To investigate whether intracellular clofazimine inclusions were formed by crystallization of clofazimine, cells were analyzed with polarization microscopy. Birefringence from intracellular clofazimine inclusions was not detectable (SI. 5). With confocal Raman microscopy[20, 21], clofazimine-treated cells exhibited a fluorescence signal (Figure 2A) superimposed on a drug-specific vibrational Raman signal (Figure 2B). Clofazimine fluorescence (Figure 2C) and Raman signals (Figure 2D) was localized almost exclusively to the cytoplasm, mostly in discrete spots in the perinuclear region corresponding to the red clofazimine inclusions observed by transmitted light microscopy (Figure 1).

Clofazimine's vibrational signal (Figure 2D, in the region between 1100 and 1600 cm^{-1}) overlapped with the overall fluorescence signal. After subtracting the fluorescence signal, different parts of the cells exhibited similar Raman spectra, only varying in intensity (Figure 2E). The strongest vibrational signals came from the punctate foci in the perinuclear region (Figure 2E 2, 4, 6, 7, and 8). In contrast, regions inside the nucleus and at the cell periphery lacked Raman signal (Figure 2E 1, 3, and 5). Again, the specific Raman chemical signal of clofazimine corresponded to the distribution of red inclusions observed with transmitted light microscopy (Figure 1).

As a reference, the vibrational Raman spectra of untreated cells (negative control; Figure 2Fa) and the vibrational spectra of crystalline and amorphous clofazimine precipitates in various buffers (positive controls; Figure 2Fb – h) were compared to the Raman spectra of clofazimine-treated cells. The vibrational spectra acquired from the punctate foci of clofazimine-treated cells (Figure 2Fi) resembled that of positive clofazimine controls (2Fb – h), with signature peaks at 1167, 1255, 1353, and several other peaks between 1406 and 1565 cm^{-1}. In buffer (2Fb – e), peaks at 1298 and 1493 cm^{-1} decreased in intensity, whereas the peak at 1565 cm^{-1} only appeared in association with crystalline clofazimine in pH 5 and 7, indicating vibrational signals of clofazimine are sensitive to the local microenvironment.

Most importantly, the reference spectrum of amorphous clofazimine at pH 5 (Figure 2Fc) resembled that of amorphous clofazimine at pH 3, whereas the spectrum of crystalline in pH 5 (Figure 2Fd) resembled that of crystalline clofazimine at pH 7 (SI. 6). Remarkably, the spectra from drug-treated cells (Figure 2Fi) clearly lacked the peaks of 1436 (*) and 1461 (*) cm^{-1} which were the prominent, signature peaks of crystalline clofazimine. These peaks were absent in amorphous clofazimine aggregates (Figures 2F c and f, bold). Thus, chemical imaging of intracellular drug inclusions also did not yield evidence for the presence of clofazimine crystals.

2.4.4 Transmission electron microscopy reveals an intracellular drug-membrane aggregation pathway, leading to ALDI formation without intracellular crystals.

With TEM, the cytoplasm of control cells appeared normal in morphology (Figure 3A and SI. 7a – c). In comparison, incubation with clofazimine-containing medium for 24

hours induced many dense, osmiophilic multivesicular bodies (MVB) and many other darkly stained, osmiophilic vesicles filled with granular material (Figure 3B and SI. 7g – i). Upon prolonged exposure (10 μM clofazimine for >72 hours), the bulk of cellular membrane content became reorganized into morphologically-distinct and atypical inclusions, many possessing multilamellar membrane features (Figure 3C and SI. 7g – l). These inclusions were highly complex and heterogeneous in their internal structure, resembling autophagosomes[22]. The number, size, location and appearance of these heterogeneous, membranous inclusions corresponded in size, number and distribution to the red clofazimine inclusions observed under transmitted light microscopy (Figures 3D – F and SI. 7j – p). Hence, we inferred these structures corresponded to clofazimine-membrane aggregates, and labeled them autophagosome-like drug inclusion, aldi (SI. 7m – p).

Cytoplasmic object counts from TEM sections of cells exposed to clofazimine containing cell culture media for varying periods of time allowed piecing together a sequence of events leading to aldi formation (Figure 4A and SI. 7). Depending on their apparent size, complexity, density of the internal structure and the time course of appearance, we divided aldis into early (Figure 4B) and late stage (Figure 4C). Based on object counts, aldis accumulated with time, to become the most frequent organelle observed in clofazimine-treated cells (Figure 4D).

2.4.5 Additional structural and functional evidence for a mitochondrial origin of aldis

In TEMs, mitochondria caught our attention, which were prominent in untreated cells but seldom observed in clofazimine-treated cells. We confirmed the number of

intact mitochondria (Figure 4E) decreased significantly upon drug treatment, concomitant with an increase in the number of organelles with morphological features resembling degenerating mitochondria (Figure 4F). Staining cells with a mitochondria-specific, membrane potential-sensitive probe, MitoTracker® Red CMXRos (MTR, Figure 5), revealed that incubation with clofazimine led to mitochondrial membrane depolarization, with diffuse cytoplasmic MTR staining. In untreated cells, normal MTR signal was observed in association with cytoplasmic organelles possessing vermiform appearance, typical for mitochondrial labeling. After clofazimine incubation, MTR background signal in cytoplasm was increased, with fewer organelles showing specific mitochondria morphology. After 21 hours, small clofazimine-containing vesicles (observed using the epifluorescence eGFP channel) corresponded to MTR-labeled mitochondria (observed under rhodamine channel). However, the larger clofazimine inclusions which lacked clofazimine fluorescence did not stain with MTR. Accordingly, we inferred that some of the membranes in aldis could originate from degenerating mitochondria.

Consistent with a mitochondrial origin of these induced, drug-membrane complexes, clofazimine avidly partitioned into isolated mitochondria *in vitro* (Figure 5B). In clofazimine-treated cells, mitochondrial respiratory function was perturbed by clofazimine treatment (Figure 5C). Although basal oxygen level consistently ranged between 132 – 141 mmHg, oxygen consumption rate (OCR) was affected by clofazimine treatment, which reflects a change in mitochondrial respiration responsible for the production of ATP through the reduction of O_2. In positive control experiments, OCR varied in response to the standard pharmacological inhibitors of mitochondrial respiration (Figure 5C, ○): 1) oligomycin inhibited the ATP synthase (complex V), resulting in a

decrease in OCR; 2) carbonyl cyanide *p*-trifluoromethoxyphenylhydrazone (FCCP) disrupted the electrochemical gradient across the mitochondrial membrane, increasing the OCR; and, 3) Antimycin A blocked complex I and III in electron transfer chain, decreasing the OCR. In the experimental conditions, addition of clofazimine (♦) increased the OCR, suggesting a disruption of the proton gradient across the mitochondrial inner membrane, similar to FCCP addition. Furthermore, after clofazimine treatment, the OCR became unresponsive to oligomycin or FCCP, whereas Antimycin remained fully active. This was consistent with clofazimine interfering with the mitochondrial membrane potential, similar to FCCP.

2.5 Discussion

Based on our observations, the intracellular accumulation of clofazimine is accompanied by the formation of massive, intracellular drug-membrane aggregates. Morphologically, these aggregates do not resemble the crystal-like drug inclusions that are observed in patients after months of clofazimine treatment [8-11], but they may be a precursor for such inclusions since similar structures can be also be observed in electron micrographs of clofazimine-treated tissues. Because clofazimine has weakly basic amine groups with reported pKa ranging from 7.87 to 9.11[23], the drug is expected to be protonated and more water soluble in acidic environments. However, the drug is also expected to become deprotonated and less soluble in neutral or alkaline environments, which can lead to the formation of supersaturated solution once the drug is absorbed and distributes throughout the body. It is possible that a lipoprotein carrier could be involved in cellular uptake[24] and that the low pH environment of lysosomes could lead to ion-

trapping[4, 13]. However, based on electron microscopy, the mechanism ultimately responsible for sequestering clofazimine appears to be the formation of aldis: drug-membrane aggregates that resembled autophagosomes in morphology. Biochemical studies with isolated mitochondria revealed that clofazimine accumulates in mitochondria, and functional studies confirmed that clofazimine interacts with mitochondria inside cells, suggesting at least some of the membranes in these aggregates may originate from degenerating mitochondria.

In the continuous presence of clofazimine, the formation of drug-membrane aggregates can destabilize organelle structure and function, inducing membranes to coalesce, fuse and condense, and give rise to aldis. The formation of drug-membrane aggregates can serve as a sink to facilitate the continuous accumulation of clofazimine inside cells, without clofazimine crystals forming intracellularly. With supersaturated clofazimine solutions forming in the gastrointestinal tract, clofazimine can be absorbed into the body and partition into cellular lipids and the phospholipid membranes that form the boundaries of intracellular organelles. Upon prolonged dosing, aldis can accumulate and may serve as an intracellular clofazimine depot. Presumably, aldis may continue to form and grow as long as the drug is not toxic to cells, and the rate of drug-membrane aggregate formation does not exceed the cells' capacity to synthesize new membranes and regenerate its degenerating organelles.

Morphologically, aldis resembled autophagosomes or mitophagosomes [22]. However, aldis lacked the double membrane that normally surrounds autophagosomes. Unlike autophagosomes and mitophagosomes, aldis appeared completely filled with condensed lipid membrane aggregates, instead of the typical, degenerating vesicular

membrane cargo. In the natural degradation of mitochondria (and other organelles) [22, 25, 26], a membrane structure termed phagophore is observed to engulf the degenerating organelle. Later, the mitophagosomes fuse with lysosomes to form autophagolysosomes [22, 25, 26] which degrade the membrane contents for intracellular recycling. Unlike autophagolysosomes or mitophagosomes, aldis appeared to grow continuously by coalescence and condensation. Considering the possibility that aldis were related to multilamellar bodies resulting from phospholipidosis [14, 27], a toxicological phenotype associated with certain classes of lipophilic drugs [28, 29], clofazimine did not lead to a measurable increase in phospholipid levels in MDCK cells.

To conclude, the ability of clofazimine to interact with mitochondria and induce the formation of intracellular drug membrane aggregates may be worth considering not only as a drug side effect, but also in terms of potential therapeutic applications. Indeed, while such phenotypic changes are generally reported as drug side effects, they could also have cytoprotective functions[30, 31]. For example, interaction of clofazimine with mitochondria could be useful to attenuate mitochondrial damage associated with oxidative stress that occurs during ischemia-reperfusion injury [32, 33]. Today, there is an increasing interest in probing drug-membrane interactions as a determinant of the cellular disposition of lipophilic small molecule drugs[6, 34]. Experimental evidence indicates that chloroquine[5] and amiodarone[28, 35] accumulate in association with multilamellar bodies. However, characterizing the formation of drug-membrane complexes within cells has been a challenge. In this context, the ability to use a combination of chemical imaging technologies including Raman, fluorescence, and absorbance to study clofazimine's intracellular disposition, together with the ability to perform electron microscopic

observations on the resulting drug inclusions, constitutes a major advance in terms revealing the appearance of prominent drug-membrane aggregates that result from drug-membrane interactions as they occur within cells.

2.6 Acknowledgements

The project was supported by grant number GM007767 from NIGMS for J.B., and by NIH grant RO1GM078200 to G.R.R. Its contents are solely the responsibility of the authors and do not necessarily represent the official views of NIGMS or NIH. We thank Dorothy Sorenson (TEM, University of Michigan Microscopy and Imaging Analysis Lab), Peng Zou (LC/MS), Dr. Arun K. Das (Michigan Nutrition and Obesity Research Center, NIH grant, DK089503), Katherine Overmyer (Seahorse, Burant Lab), and the engineers and scientists at WITec (Raman confocal microscopy) for technical assistance. We thank Dr. Charles Burant, Dr. Nair Rodriguez-Hornedo, and Dr. David E. Smith for insightful comments.

2.7 Figures

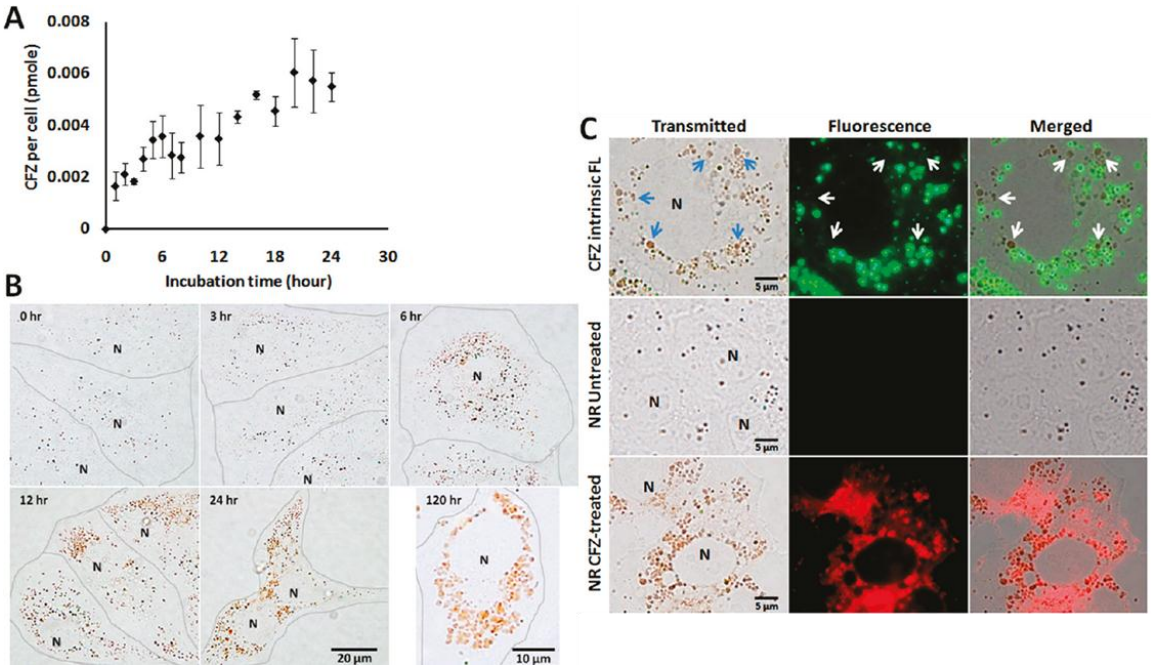

Figure 2-1 Clofazimine accumulation kinetics.

A) Time course analysis of intracellular clofazimine accumulation. (error bars represent the s.e.m., N=3). B) Red intracellular drug inclusions grow in size. Brightfield images were acquired during 0 to 120 hour incubation in 10 µM clofazimine containing 5% FBS-DMEM. Lines were manually drawn to indicate individual cell boundaries. N: nucleus. C) Intrinsic fluorescence of CFZ and Nile Red (NR) staining of control and drug-treated cells. Cells were incubated with CFZ containing DMEM for 24 hours and imaged with the standard eGFP (green) and rhodamine (red) fluorescence filter set. Arrows point to large clofazimine inclusions lacking green fluorescence (whereas small inclusions are visibly fluorescent). Nile Red staining (NR) of CFZ treated vs. untreated samples were acquired and displayed under the same exposure settings, showing significantly greater NR fluorescence in association with clofazimine inclusions.

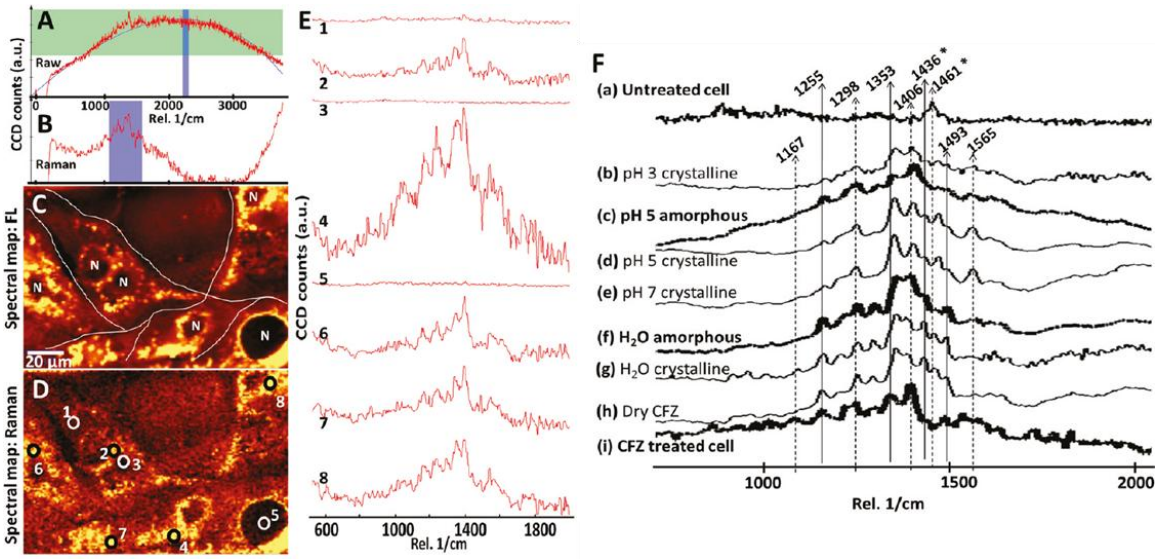

Figure 2-2 Confocal Raman imaging of clofazimine-treated cells.

A) Polynomial fitting of a representative, raw spectral scan acquired from a clofazimine treated cell. B) Background subtracted Raman vibrational spectra from A. C) The spectral intensity map of a selected fluorescence spectral region (2199 – 2296 cm^{-1}), highlighted in blue in panel A. D) The spectral map of the selected, background subtracted, Raman spectral region (1100 – 1600 cm^{-1}), highlighted in blue in panel B. E) spectra of various regions of in D (1: cytosol, 2: perinuclear region, 3: center of the nucleus, 4: perinuclear region; 5: center of the nucleus; 6-8: various punctate cytoplasmic foci. F) Representative, fluorescence-subtracted Raman spectra of untreated MDCK cells (a); clofazimine precipitates in different buffer solutions (b – g); dry clofazimine crystals (h); and, drug-treated cells (i). The intensity is in arbitrary units, normalized to the same scale. 1436 and 1461 cm^{-1} (*) are vibrational peaks that are prominent in crystalline clofazimine but almost absent the amorphous clofazimine (bold line).

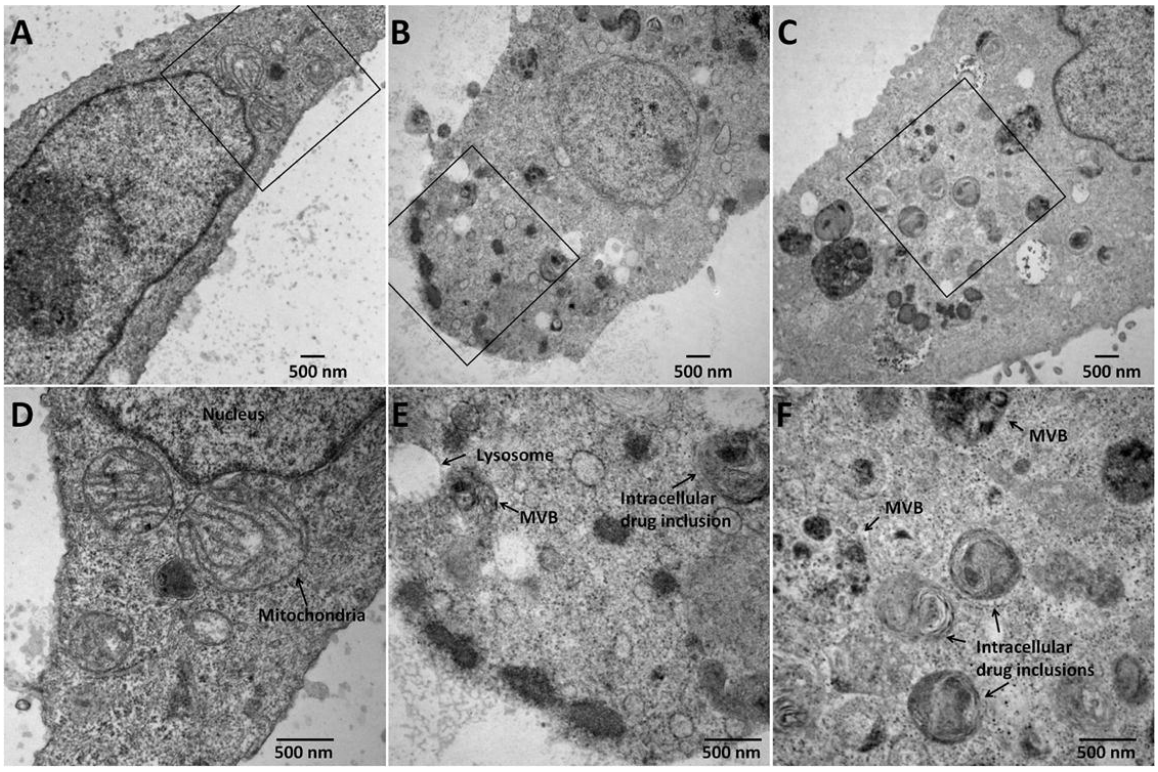

Figure 2-3 TEM images of treated cells

A) Control cell (vehicle-only with 5% FBS-DMEM after 24 hr treatment); and cells incubated with 10 μM clofazimine for 24 hr (B) or 87 hr (C). D, E, and F are zoom-in of boxed regions in A, B, and C, respectively. Cytoplasmic objects were categorized into autophagosome-like drug inclusions (aldis) if they did not show characteristic features of the typical organelles, while exhibiting lipid-rich (lamellar or vesicular) internal structures stained with osmium tetroxide.

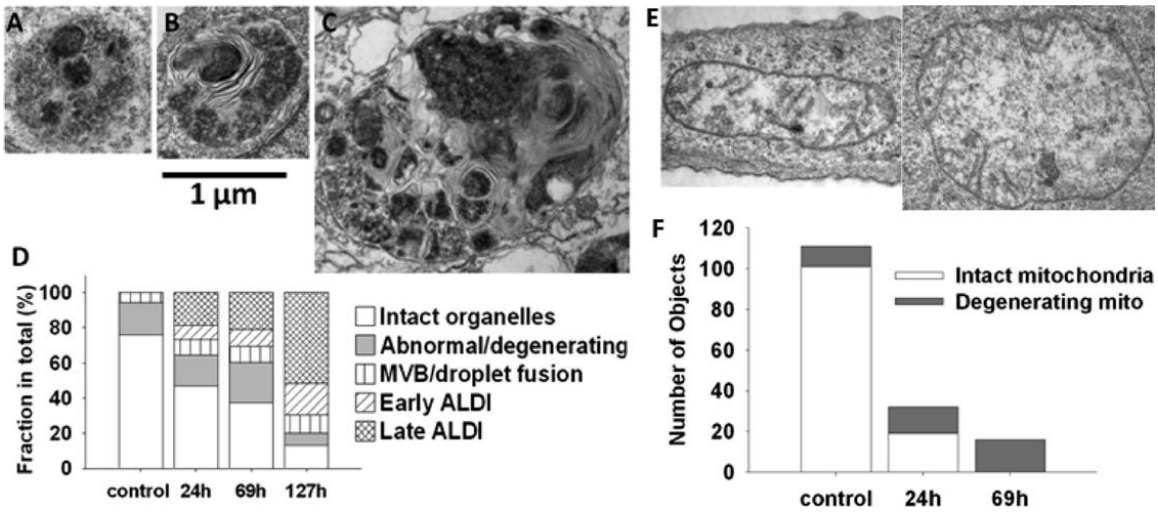

Figure 2-4 Temporal analysis of ALDI biogenesis and mitochondria degeneration.

A) Representative image of osmiophilic and granular multivesicular body that appears during the first 24 hr incubation. B) Early aldi, showing internal lamellae and heterogeneous appearance C) More complex aldi representative of those that appeared at latter time points. D) Measured frequency of different organelles, at various time points after beginning of clofazimine incubation. E) TEM images of abnormal/degenerating mitochondria in clofazimine treated cells. F) Frequency of normal vs. degenerating mitochondria changes during drug treatment. For TEM organelle counts, morphological features were manually scored from 6 or more cells.

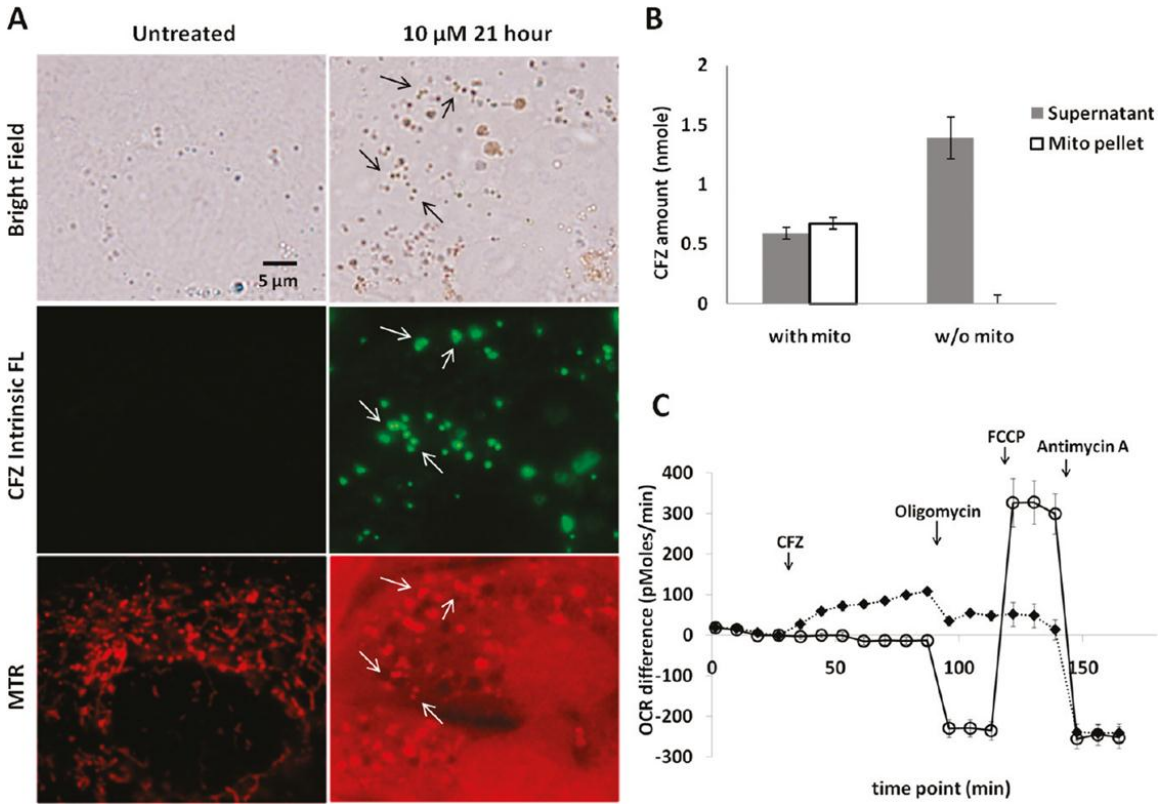

Figure 2-5 Clofazimine associates with mitochondria, followed by dissipation of the mitochondrial membrane potential.

A) MitoTracker Red (MTR) staining of untreated vs. clofazimine treated cells. Arrows at 21 hr treatment indicate clofazimine fluorescence (green channel) colocalized with functional mitochondria (labeled with MTR signal in red channel). However, the larger (older) clofazimine inclusions do not stain with MTR. (B) Clofazimine binds to isolated mitochondria. As a control, the same experiment was repeated with storage buffer alone and no mitochondria (w/o mito). Under control conditions, clofazimine signal was not detected in the pellet after centrifugation. Error bar represents standard deviation from representative experiment. Student's T-test show statistically significant differences in both supernatant and pellet ($p<0.05$; N=2). C) Oxygen consumption rate (OCR) differences of clofazimine-treated cells (♦) vs. control cells (○). Various inhibitors of mitochondrial respiration were sequentially applied in the presence or absence of clofazimine at pre-determined time points, as indicated in x-axis. The OCR difference was calculated as the measured OCR level minus the baseline OCR level (at the 27th minute). Error bars indicate s.e.m; N=3 (the error bar may be smaller than marks). Statistical significance for each treatment was tested comparing the last data point before vs. the new treatment's last data point: 4th point vs. 11th point for clofazimine effect, 11th vs. 14th for oligomycin, 14th vs. 17th for FCCP, and 17th vs. 20th for Antimycin A. For every treatment, $p < 0.05$.

2.8 Supporting Information Available

This material is published in *Molecular Pharmaceutics* and supporting information figures SI. 1 – SI. 7 are available in the Appendix B.

2.9 References

1. Rajendran, L.; Knolker, H. J.; Simons, K. Subcellular targeting strategies for drug design and delivery. *Nat Rev Drug Discov* **2010,** *9*, (1), 29-42.

2. Zhang, X.; Shedden, K.; Rosania, G. R. A cell-based molecular transport simulator for pharmacokinetic prediction and cheminformatic exploration. *Mol Pharmaceutics* **2006,** *3*, (6), 704-16.

3. Zheng, N.; Tsai, H. N.; Zhang, X.; Rosania, G. R. The Subcellular Distribution of Small Molecules: From Pharmacokinetics to Synthetic Biology. *Molecular Pharmaceutics* **2011**, DOI:10.1021/mp200092v.

4. de Duve, C.; de Barsy, T.; Poole, B.; Trouet, A.; Tulkens, P.; Vanhoof, F. Lysosomotropic Agents. *Biochemical Pharmacology* **1974,** *23*, (18), 2495-531.

5. Zheng, N.; Zhang, X.; Rosania, G. R. Effect of phospholipidosis on the cellular pharmacokinetics of chloroquine. *J Pharmacol Exp Ther* **2010,** *336*, (3), 661-71.

6. Balaz, S. Modeling kinetics of subcellular disposition of chemicals. *Chem Rev* **2009,** *109*, (5), 1793-899.

7. Horobin, R. W.; Trapp, S.; Weissig, V. Mitochondriotropics: A review of their mode of action, and their applications for drug and DNA delivery to mammalian mitochondria. *Journal of Controlled Release* **2007,** *121*, (3), 125-136.

8. Banerjee, D. K.; Ellard, G. A.; Gammon, P. T.; Waters, M. F. Some observations on the pharmacology of clofazimine (B663). *Am J Trop Med Hyg* **1974,** *23*, (6), 1110-5.

9. Atkinson, A. J., Jr.; Sheagren, J. N.; Rubio, J. B.; Knight, V. Evaluation of B.663 in human leprosy. *Int J Lepr Other Mycobact Dis* **1967,** *35*, (2), 119-27.

10. Conalty, M. L.; Barry, V. C.; Jina, A. The antileprosy agent B.663 (Clofazimine) and the reticuloendothelial system. *Int J Lepr Other Mycobact Dis* **1971,** *39*, (2), 479-92.

11. Sukpanichnant, S.; Hargrove, N. S.; Kachintorn, U.; Manatsathit, S.; Chanchairujira, T.; Siritanaratkul, N.; Akaraviputh, T.; Thakerngpol, K. Clofazimine-

induced crystal-storing histiocytosis producing chronic abdominal pain in a leprosy patient. *Am J Surg Pathol* **2000,** *24*, (1), 129-35.

12. McDougall, A. C. Electron microscope studies of the antileprosy drug B663 (clofazimine; Lamprenel). *Int J Lepr Other Mycobact Dis* **1974,** *42*, (1), 1-12.

13. Goldman, S. D.; Funk, R. S.; Rajewski, R. A.; Krise, J. P. Mechanisms of amine accumulation in, and egress from, lysosomes. *Bioanalysis* **2009,** *1*, (8), 1445-59.

14. Reasor, M. J.; Hastings, K. L.; Ulrich, R. G. Drug-induced phospholipidosis: issues and future directions. *Expert Opin Drug Saf* **2006,** *5*, (4), 567-83.

15. Chen, V. Y.; Posada, M. M.; Blazer, L. L.; Zhao, T.; Rosania, G. R. The role of the VPS4a-exosome pathway in the intrinsic egress route of a DNA-binding anticancer drug. *Pharmaceutical Research* **2006,** *23*, (8), 1687-1695.

16. Ferrick, D.; Neilson, A.; Beeson, C. Advances in measuring cellular bioenergetics using extracellular flux. *Drug Discov Today* **2008,** *13*, (5-6), 268-74.

17. Gerencser, A. A.; Neilson, A.; Choi, S. W.; Edman, U.; Yadava, N.; Oh, R. J.; Ferrick, D. A.; Nicholls, D. G.; Brand, M. D. Quantitative microplate-based respirometry with correction for oxygen diffusion. *Anal Chem* **2009,** *81*, (16), 6868-78.

18. Bartlett, G. R. Phosphorus assay in column chromatography. *J Biol Chem* **1959,** *234*, (3), 466-8.

19. O'Connor, R.; O'Sullivan, J. F.; O'Kennedy, R. The pharmacology, metabolism, and chemistry of clofazimine. *Drug Metab Rev* **1995,** *27*, (4), 591-614.

20. Chernenko, T.; MatthaÌˆus, C.; Milane, L.; Quintero, L.; Amiji, M.; Diem, M. Label-Free Raman Spectral Imaging of Intracellular Delivery and Degradation of Polymeric Nanoparticle Systems. *ACS Nano* **2009,** *3*, (11), 3552-3559.

21. Keren, S.; Zavaleta, C.; Cheng, Z.; de la Zerda, A.; Gheysens, O.; Gambhir, S. S. Noninvasive molecular imaging of small living subjects using Raman spectroscopy. *Proc Natl Acad Sci U S A* **2008,** *105*, (15), 5844-9.

22. Eskelinen, E. L. Maturation of autophagic vacuoles in Mammalian cells. *Autophagy* **2005,** *1*, (1), 1-10.

23. Wan, H.; Holmen, A. G.; Wang, Y.; Lindberg, W.; Englund, M.; Nagard, M. B.; Thompson, R. A. High-throughput screening of pKa values of pharmaceuticals by pressure-assisted capillary electrophoresis and mass spectrometry. *Rapid Commun Mass Spectrom* **2003,** *17*, (23), 2639-48.

24. Morrison, N. E.; Marley, G. M. Clofazimine binding studies with deoxyribonucleic acid. *Int J Lepr Other Mycobact Dis* **1976,** *44*, (4), 475-81.

25. Fader, C. M.; Colombo, M. I. Autophagy and multivesicular bodies: two closely related partners. *Cell Death Differ* **2009,** *16*, (1), 70-8.

26. Yang, Z.; Klionsky, D. J. Eaten alive: a history of macroautophagy. *Nat Cell Biol* **2010,** *12*, (9), 814-22.

27. Alakoskela, J. M.; Vitovic, P.; Kinnunen, P. K. Screening for the drug-phospholipid interaction: correlation to phospholipidosis. *ChemMedChem* **2009,** *4*, (8), 1224-51.

28. Reasor, M. J. Influence of a pre-existing phospholipidosis on the accumulation of amiodarone and desethylamiodarone in rat alveolar macrophages. *Res Commun Chem Pathol Pharmacol* **1991,** *72*, (2), 169-81.

29. Reasor, M. J.; McCloud, C. M.; Beard, T. L.; Ebert, D. C.; Kacew, S.; Gardner, M. F.; Aldern, K. A.; Hostetler, K. Y. Comparative evaluation of amiodarone-induced phospholipidosis and drug accumulation in Fischer-344 and Sprague-Dawley rats. *Toxicology* **1996,** *106*, (1-3), 139-47.

30. Pallet, N.; Bouvier, N.; Legendre, C.; Gilleron, J.; Codogno, P.; Beaune, P.; Thervet, E.; Anglicheau, D. Autophagy protects renal tubular cells against cyclosporine toxicity. *Autophagy* **2008,** *4*, (6), 783-91.

31. Sarkar, S.; Perlstein, E. O.; Imarisio, S.; Pineau, S.; Cordenier, A.; Maglathlin, R. L.; Webster, J. A.; Lewis, T. A.; O'Kane, C. J.; Schreiber, S. L.; Rubinsztein, D. C. Small molecules enhance autophagy and reduce toxicity in Huntington's disease models. *Nat Chem Biol* **2007,** *3*, (6), 331-8.

32. Korde, A. S.; Pettigrew, L. C.; Craddock, S. D.; Maragos, W. F. The mitochondrial uncoupler 2,4-dinitrophenol attenuates tissue damage and improves mitochondrial homeostasis following transient focal cerebral ischemia. *J Neurochem* **2005,** *94*, (6), 1676-84.

33. Shao, H.; Li, J.; Zhou, Y.; Ge, Z.; Fan, J.; Shao, Z.; Zeng, Y. Dose-dependent protective effect of propofol against mitochondrial dysfunction in ischaemic/reperfused rat heart: role of cardiolipin. *Br J Pharmacol* **2008,** *153*, (8), 1641-9.

34. Balaz, S.; Lukacova, V. Subcellular pharmacokinetics and its potential for library focusing. *J Mol Graph Model* **2002,** *20*, (6), 479-90.

35. Lee, P.; Kirk, R. G.; Reasor, M. J. X-ray microanalysis of cultured alveolar macrophages with phospholipidosis. *Exp Mol Pathol* **1993,** *58*, (2), 96-104.

Chapter 3

Expansion and Structural Reorganization of Macrophages Mediate the Massive Redistribution and Retention of Clofazimine upon Long Term Administration

3.1 Abstract

The antibacterial clofazimine is a poor solubility and high lipophilicity drug, possessing a pharmacokinetic half-life greater than 70 days. Here, we have studied the biodistribution of clofazimine in mice fed with clofazimine mixed diet and discontinuation for 16 wks. Various organs were collected at different time points for biochemical and histological analyses.

Clofazimine was sequestered in cytoplasmic compartment within the cells of the liver, lungs and lymphatic organs, but not in the kidneys or brain. Most interestingly, drug content measured in abdominal fat at 3 wks was significantly greater than 8 wks of treatment, while other organs exhibited greater accumulation after the prolonged treatment. Such redistribution of clofazimine from fat to other organs was suspected to result from the role of macrophages extracting the drug from circulation, which in turn leads to an efflux from the fatty tissues, redirecting the molecules into a more stable form of intracellular sequestration.

Inside macrophages, these drug inclusions grew in size and number. Moreover, macrophage numbers increased and the spleen expanded in size and mass more than threefold, suggesting concomitant inflammatory response. Upon discontinuation of clofazimine administration, the drug was cleared out at different efflux patterns from various organs, yet was mostly retained in the spleen.

In conclusion, the sequestration of lipophilic, poorly soluble drug molecules into specialized cytoplasmic inclusions within an increased number of macrophages impacts the biodistribution of clofazimine upon prolonged dosing. The results demonstrate how changes in organ mass and volume as well as the changes in drug interaction with cellular and subcellular compartments can exert a major effect on systemic pharmacokinetic parameters.

3.2 Introduction

Poorly soluble, lipophilic antibacterial clofazimine exerts an extremely long half-life up to 70 days.[1] This effect is mainly due to the drug disposition in the cells within the body instead of more common elimination from the body such as renal or hepatic clearance.[2] Pathologically, such deposition is related to dark purple pigmentation associated with congestion in the small intestine upon months of administering high doses (300 – 400 mg daily), causing abdominal pain and malabsorption in patients, and in some cases splenic infarction requiring removal of the organ.[3]

Although several investigators have studied the pharmacology and pharmacokinetics of clofazimine administered in patients and in animals,[1, 4] there has been a lack of understanding about how the drug distributes and what are the cellular and

microscopic mechanisms by which bioaccumulation occurs. We hypothesize that subcellular level compartmentalization and sequestration observed *in vitro* would affect whole body distribution; therefore, pharmacokinetic parameters such as plasma half-life and drug disposition *in vivo* may be affected. We took advantage of clofazimine's lipophilicity (logP > 7, Appendix A) and its distinctive red color to detect the accumulation, which did not follow classical pharmacokinetics models in which an elimination process, such as hepatic metabolism or renal excretion, plays a major role in lowering plasma concentration.[5] Importantly, such an atypical case study can further be applied to investigate the pharmacokinetic behavior of other poorly soluble, lipophilic drugs lacking distinctive optical signals, which are in other words not readily detectable in terms of bioaccumulation and adverse effects.

From earlier studies in our group, we identified liver microgranulomas[6] to be one of the significant accumulation sites within drug treated mice.[7] They were the result of the chronic inflammation response created by the collection of macrophages around the blood vessels of mice at washout phase, for which the drug diets were replaced by drug-free food after 8 wks of feeding. The microgranulomas were associated with macrophage marker F4/80 and developed fibrosis stained by Masson's trichrome which is an indicator of the chronic damage on the tissue component of the liver. Since the clofazimine-like drug inclusions (CLDIs) and drug contents were localized in particular organs but not in others, we hypothesized that such sequestration could function as a detoxification, isolation mechanism of the poorly soluble irritant. In fact, studies on insoluble paraffin[8] or bacterial infections[9] have suggested that the macrophages can function as a defensive mechanism of anti-inflammatory process.

Here, we generate a more detailed pharmacokinetic distribution map of clofazimine among major organs and plasma, and a combined microscopic analysis to show the atypical, multiscale, redistribution phenomena in mice. The conclusion suggests that the large volume of distribution in non-compartmental pharmacokinetics may result in from the sequestration mechanism of the lipophilic drug.

3.3 Materials and Methods

Animal experiment. Mice (4-5 wk male Balb/c) were purchased from Jackson lab (Bar Harbor, Maine) and acclimatized for 2 wks in the university specific pathogen free animal facility. All animal care and experimental procedures complied with approved protocol by University of Michigan Committee of Use and Care of Animals. Mice were divided into two groups, fed with drug with powder food (drug was pre-dissolved to 3 mg/ml of sesame oil, mixed at 0.01% oil to food (0.03% drug to chow)) or with oil mixed food (vehicle only control) served in ceramic jar placed on the cage floor. Clofazimine was purchased from Sigma-Aldrich (C8895, St. Louis, MO), and sesame oil (Roland, China or Shirakiku, Japan) was purchased from local grocery store. An average 25g mouse consumed about 3g of food per day, half of them spilled on the cage floor and wasted. Assuming oral bioavailability to be 50% in average,[10] approximately 20 mg/kg was daily intake and 10 mg/kg was clofazimine daily absorption.

Biochemical analysis of clofazimine in tissues. At predetermined time points organs were collected and kept in -20°C after CO_2 euthanasia and blood collection through cardiac puncture. Tissue (0.05 – 0.1 g/ml water) was homogenized with Tissumizer (Tekmar®, Cincinnati, OH) and 100 µl of sample was mixed with same volume of 5N

NaOH than extracted with 300 µl dichloromethane twice in a bath sonicator.[11] After centrifuged at 2000g for 10 minutes to collect dichloromethane layer, the solvent was evaporated at 40°C and reconstituted in MeOH for absorbance to be measured at 490 nm by Synergy-2 plate reader (Biotek Instruments, Winooski, VT). Concentration was calculated from the standard curve generated by spiking drug solution into a tissue extract from vehicle-only treated sample. Average extraction yield was 60 – 80% for other organs except abdominal fat which was around 100% recovery.

CLDI isolation. CLDI purification was done using the protocol previously reported.[7] In brief, two 8 wk treated spleens and an 8 wk treated liver homogenates was diluted in distilled water (0.025 – 0.05 g/ml) and sonicated for 30 minutes, then centrifuged (100g for 1 min). Supernatants were resuspended in 0.125% Trypsin-EDTA solution (Gibco) and kept at 37°C for 1 hour, followed by another centrifugation at 100g to remove large cell debris. The drug inclusions in supernatant were then pelleted by centrifugation (21,000g × 1 min), and resuspended in water for analyses. Protein content was determined with the BCA assay (Pierce 23227, Thermo Scientific) and clofazimine content was determined spectrophotometrically. For protein assay, equal volume of 5% SDS solution was mixed with the samples and the protein content was measured following the BCA kit instructions. The yield of triplicate run was averaged to result in 10-fold purification.

Plasma concentration determination. Multiple samples of collected blood were let clot at room temperature and centrifuged at 7000g for 5 minutes and supernatants were submitted to LC-MS core at Michigan Nutrition and Obesity Research Center. 20 µl of sample was extracted with 60 µl of acetonitrile for 10 minutes at 4°C with intermittent

vortexing. After centrifugation at 15,000 rpm at 4°C, the supernatant was injected into Agilent 1200 RRLC coupled to 6410 Triple Quad LC/MS. Xbridge C18 column (2.5 µ, 2.1mm ID × 10 mm long, Waters) was used. Mobile phase: A = 5 mM ammonium acetate, adjusted to pH 9.9 with ammonium hydroxide; B = acetonitrile. Flow rate = 0.35 ml/min, linear gradient from 50 to 100% B over 1.5 min; hold 100% for 1.5 min, return to 50% B and re-equilibrated for 2.5 min. Mass spectrometer source condition: 325°C, gas flow 10 L/min, nebulizer 40 psi, capillary 4000V, positive ion mode. MS acquisition parameter: MRM mode, transition 1:473.1 to 431.1, dwell time 400 ms, fragmentor 180, collision energy 40; transition 2: 473.1 to 429.1, dwell time 100 ms, fragmentor 180, collision energy 40.

CLDI contents were intact clofazimine. Using the LC/MS methods and equipment setting in the above, the content from three different tissue extracts were confirmed to be the same as the positive control, clofazimine in acetonitrile, which showed elusion time of 3.374 min. Triplicates of one liver sample and two spleens were eluded at the same time 3.374 min, and the extraction yield was 90% in average, demonstrating comparable amount of drug concentration from the biochemical analysis above. This finding was consistent with other reports demonstrating the compound found in drug treated mice were intact using thin layer chromatography[12] and laser microprobe mass analysis (LAMMA)[13] which used laser to evaporate crystal-like drug inclusion in spleen and detected clofazimine using a mass spectrometer.

Mouse perfusion fixation for EM. Blood was collected from euthanized mice and washed by perfusing 5 – 6 ml of 0.1M Sorensen's buffer at 2.5 ml/min rate injected to left ventricle and egressed to vena cava. Then, 5 ml of Karnovsky's fixative (3%

paraformaldehyde, 2.5% glutaraldehyde, 0.1 M Sorensen's buffer, pH 7.4) was infused to result in stiffening of the corps, and turning organ colors to pale pink. Immediately after perfusion, organs were taken out for either paraffin fixation or TEM sample preparation.

Tissue cryo-fixation or paraffin fixation for immunohistochemistry. Cryosection of organs embedded in OCT (Tissue-Tek® 4583, Sakura) were carried out using Leica 3050S cryostat, and samples were sectioned to 10 μm thicknesses, placed onto glass slide with a drop of glycerol and covered with #1.5 cover glass. Paraffinization of the perfusion fixed organ and heat mediated antigen retrieval were carried out in histology lab at Pathology Cores of Animal Research (PCAR), Unit for Laboratory Animal Medicine (ULAM) at the University of Michigan. Routine H&E and Masson's trichrome staining, as well as immunohistochemistry of F4/80 (1/100 dilution, ab6640, abcam®), αSMA (1/200, ab5694, abcam®), vWF (1/500, ab7356, Millipore), CD21 (1/200, ab75985, abcam®), CD3T (1/300, RM-9107S, Thermo Scientific) were carried out using Horse Radish Peroxidase and intelliPATH FLX DAB chromogen (IPK5010, Biocare Medical, Concord, CA).

Transmission Electron Microscopy. Immediately after perfusion fixation, the organs kept in fixative were diced into pieces smaller than 1 mm in each dimension, and they were preserved in the glass vial with the fixative stored at 4°C. After rinsing three times with Sorensen's buffer, diced tissues were stained with 1% osmium tetroxide in 0.1M Sorensen's buffer and washed three times in Sorensen's buffer. Dehydration was carried out with graded ethanol/water series (50, 70, 90, and two changes of 100%) for 15 min each. After transitioning through three changes of propylene oxide, tissues were infiltrated with Epon resin (Electron Microscopy Sciences), and then polymerized at

60°C for 24 h. The blocks were then ultramicrotome sectioned to 70 nm thicknesses and mounted on copper EM grid (Electron Microscopy Sciences) which were post-stained with uranyl acetate and lead citrate before TEM imaging with Philips CM-100. Images were recorded digitally using a Hamamatsu ORCA-HR camera system operated by AMT software (Advanced Microscopy Techniques Corp., Danvers, MA). Magnifications: ×2,600 to ×256,000.

Transmitted light, polarization (PL) and fluorescence microscopy (FL). Olympus 51X upright epifluorescence/polarization microscope equipped with 100× objective (1.40 NA, PlanApo oil emersion), cross polarizers, and an Olympus DP-70 color camera was used. For fluorescence channel, U-MWIBA3 (eGFP) filter cube for the green, U-MWG2 (rhodamine) filter cube for red channel were used. Images were acquired using DP controller 3.1.1.267 under the same exposure settings. For display purposes, images were digitally enhanced using Microsoft® PowerPoint and Adobe Photoshop®. For control vs. experimental comparisons within the same figure, contrast and brightness settings were adjusted to same extent.

3.4 Results

3.4.1 Skin pigmentation starts within 1 wk followed by organ pigmentation caused by drug accumulation

Physiological changes in clofazimine treated mice indicated low levels of drug toxicity. Although the extent of weight gain was different, the body weight increased during 8 wks of treatment and further increased after the discontinuation of the treatments with powder food mixed with either drug-in-oil (treated) or oil-only (control) (Fig 1A).

The skin and hair discoloration was visible during the first wk of treatment and was further darkened as the treatment was continued (Fig 1B). After 8 wks of treatment, when drug-food was replaced with a drug-free, normal diet (washout phase), the redness of the outer skin and hair did turn pale; however, the previously-treated group remained pink and distinguishable for a couple of months compared to the control group.

Upon anatomical inspection, significant but heterogeneous pigmentation was observed throughout the organs (Fig 1C). The lungs, pericardium and diaphragm surrounding the chest cavity had marked spots of black discolored punctate while the liver and spleen showed homogeneous pigmentation into dark purple or black. The oracle and heart did not seem to be affected. Notably, the size and mass of the mesenteric lymph node and spleen had increased, suggesting absorption of the drug through the intestinal lymphatic system, and subsequent inflammatory response had developed in conjunction with splenomegaly similar to pathogen invasion[8] or irritation of poorly soluble substances[7] in the blood stream. The ileum first developed dark purple to black coloration over the course of 3 wks of treatment but as treatment was continued the change further progressed to the jejunal area upward. In visual inspection of isolated jejunal and ileal sections, patches of pigmentation were observed along the outer walls of the intestine, contrasted by the minimal changes in the duodenum and stomach even after 18 wks of treatment. The mesenteric lymph node and all other lymph nodes inspected (superficial cervicals, deep cervicals, mediastinal, axillary, brachial, thymus, pancreatic sheet, linguinal, lumbar, sciatic, and caudal) turned dark black throughout, suggesting a significant crystal-like drug deposition within the lymphatic tissues. The omental fat and abdominal fat turned bright orange in color from the beginning of the first wk and

remained orange throughout 8 wks of treatment, indicating that the partitioning into fat had reached saturation early on. Also, the orange color revealed that the partitioned drugs within the fatty tissues were in unionized state, whereas clofazimine aggregation and precipitation in other organs had dark red or black pigmentation as observed for the drug powder suspended in buffers with various pHs.[5, 13] Interestingly, the skin isolated from the abdominal section itself did not seem to be much different in color, which also corresponds to the earlier observation that most deposits are localized at the subcutaneous layer underneath the skin and causing overall reddish discoloration.[4] Bones seemed to be clean except the tip of the femurs demonstrating a black pigmentation. The nervous system such as the brain, spinal cord, and sciatic nerve from the back leg appeared clean. The pancreas and kidney did not show much difference in color provided the lymphatic cover or renal capsule was removed. These sheet-like tissues consisted mostly of adipose tissue with macrophages that would be responsible for partial pigmentation along the viscera.

3.4.2 Development of splenomegaly

The increase in spleen mass was statistically significant compared to the changes in the kidney which is one of the mildly, or minimally, affected organs (Fig 1D). The spleen mass did not change from that of the control mice (no drug, oil mixed powder food) during the first 3 wks of treatment. However, continued drug treatment to either 8 wks or 18 wks resulted in 3.2- and 5.2-fold increase in weight. The increase was also significant in washout phase after treatment (WO) which is the period after 8 wks discontinuation of the drug food feeding. The WO spleen weight continued to increase by 20%, meanwhile the body weight increased only by 3.5% and the kidney remained

constant throughout the dosing. Significant increase in spleen mass and size indicates there is an anti-inflammatory response associated with clofazimine treatment.

3.4.3 Transmitted light microscopy revealed differential distribution of crystal-like drug inclusions among various organs

After isolation of the organs, the tissues were inspected either by wet-mount or by the 10 μm-cryosections on the slide glass. The 8 wk treatment sample of the lung parenchyma revealed heterogeneous distribution of red colored drug deposits, and there were two distinctive populations: ALDI (autophagosome-like drug inclusions)[13] and CLDI (crystal-like drug inclusions)[7] as previously reported (Fig 2A). The ALDIs have subcellular organelle-like features that are fluorescent in eGFP but do not polarize light due to lack of a regular, structural organization.[13] However, the CLDIs have distinguished optical features that can rotate the polarized light and appear brightly birefringent (Fig 2B), as well as fluoresce under the standard rhodamine channel as previously reported from our group.[7] While the size of an ALDI does not measure more than 2 μm, that of a CLDI can range from 5 to 20 μm in length. Notably, the distribution pattern in the kidney for these drug inclusions appeared to be dependent on the histological section. For example, the kidney medulla showed a broad staining of orange color along the tubular cells similar to that demonstrated by our previous investigation: presence of ALDIs and the absence of the CLDI in Madin-Darby dog kidney epithelial cells. In contrast to the medulla, the cortex of the same kidney near a glomerulus (GM) appeared clean without such broad staining, but rather was associated with a small number of CLDIs around the blood vessels (V). In the jejunum and ileum, the CLDIs were only associated with the lamina propria of villi, suggesting that the enterocytes were

free from accumulation (Fig 2E). Meanwhile the drug deposition was concentrated in the walls of the intestine. The mesenteric lymph nodes at the 8th wk appeared swollen and were filled with countless aggregations of CLDIs comprised of individual, needle-like structures (Fig 2F). Interestingly, they were scattered around the germinal center (GC), whereas the follicles seemed to be clean and the lymphocytes within these regions were free of drug inclusions. A similar observation was recorded in the spleen at the 3rd wk (Fig 2G) and 8th wk (Fig 2H), where the progression of CLDI aggregations was observed around the germinal centers. From the liver, we found the progression of CLDI distribution changed from a scattered pattern across the section at the 3rd wk (Fig 2I) to a more concentrated and localized pattern around the blood vessels at the 8th wk (Fig 2J). The hepatocytes lacked the CLDIs, and therefore we suspected that endothelium, fibroblasts or Kupffer cells would be responsible for the drug sequestration and CLDI formation that is absent in other cell types. The CLDIs could be isolated through trypsinization of tissue homogenates followed by the series of differential centrifugation, and resulted in a removal of more than 95% of protein contents. The tissue unbound CLDIs, collectable through centrifugation, were a maximum 91% (average 50 ± 36%). On average, 10-fold purification could be achieved for further biochemical and physicochemical analysis.[7]

3.4.4 TEM image analysis

As particular tissue accumulated the poorly soluble clofazimine differently from other organs, transmitted electron microscopy was implemented to investigate whether specific types of cells were involved in the drug inclusion formation. In the lungs of 4.5 wk treated mice, we found that only parenchymal macrophages showed CLDI cavities,

where needle-like structures with empty space were preserved after extraction of the drug during the sample preparation (Fig 3A). The macrophages also contained significant amount of ALDIs, which are round and osmiophilic objects with concentrated lipidic membranes as described previously.[13] In the section of the kidney from 8.5 wk treated mice (Fig 3B), we found, although it was rare, the peritubular macrophages (M) contained cytoplasmic CLDI cavities. However, the neighboring tubular cells (T) consisting of the epithelium of renal tubules contained only ALDIs in their cytoplasm as demarcations, with comparable ultrastructure to what was found *in vitro* of MDCK cultures.[13] Generally, macrophages are hard to find in the kidneys; however, macrophage infiltrations are reported to be a common immunological response induced by nephrotoxic reagents (e.g., cyclosporine).[14]

In the jejunal submucosa of a 4.5 wk treated mouse (Fig 3C) and in the spleen of 8.5 wk treated mouse (Fig 3D), a significant number of macrophages appeared with CLDI cavities and ALDIs. Alongside, there was a distinct population of cells absent of neither ALDIs nor CLDIs. The cells had small cytoplasm with rounded nuclei, indicating they are lymphocytes, and this observation was consistent with the absence of the red CLDI population around the lymphoid follicles of the lymph nodes or spleen seen under light microscopy (Fig 2F-H).[15] For the CLDI cavities in macrophages, we could draw a structural morphology of CLDIs that assumed a polyhedral in shape, having 4 to 7 facets once they appear thicker than 1 to 2 μm in widths. When smaller, these CLDI cavities seemed to exist more as bundles of needles juxtaposed sideways.

In the liver of 4.5 wk treated mice (Fig 3E), the marked development of CLDIs were observed over a specific region around the hepatocytes identified by the

characteristic, round nucleus and biliary ducts (H). In contrast to the hepatocytes, which remained unaffected by the drug treatment, a couple of macrophage-like cells (M), presumably Kupffer cells, were aggregating into a colony showing CLDI development. Electron micrographs of samples after prolonged treatment to 8.5 wks (Fig 3F) have shown a palpable increase of the number and size of the CLDI cavities, and these increases were comparable to those that were measured from the isolated CLDIs in our previous study.[7] The expansion of macrophage population in the liver was localized around the blood vessels, and they were developing in the inner regions of the endothelium, suggesting that they were progressing towards the pathological condition referred as microgranulomas.[6]

3.4.5 Biodistribution changes along the course of drug treatment

Colorimetric assessments of drug content within various tissues were carried out to investigate the differential accumulation and biodistribution in relation to what was observed in the microscopic analysis. In terms of drug concentration, the extracted contents were normalized by the weight of wet tissue and plotted to demonstrate the relative concentrations between 3 wk treatment, 8 wk treatment, and washout (WO, 8 wks of drug-free diet after the 8 wks of treatment) (Fig 4A). During the 8 wks of treatment, the drug concentrations in the spleen, liver, and small intestine (jejunum and ileum) had dramatically increased more than 15 fold from that of the 3rd wk. More captivatingly, contents in fat within this period had decreased to about 38% despite the continued treatment. Such a reversed trend could be explained by redistribution of the drug from the adipose tissues to spleen or liver where the delayed accumulations occur as a solid mass. While concentration in the spleen did not change from 8th wk to washout,

concentration in the liver showed marked decrease to 25%, suggesting a different retention mechanism is present in the spleen, a similar pattern having been observed previously in human patients.[1] Since the major elimination route for this metabolically stable drug has been suggested to occur through biliary clearance followed by fecal excretion,[4, 16] we reasoned that the effective decrease of the liver content may result from closer biliary access which the spleen lacks. Presumably, the drug deposits in the spleen must be dissolved into plasma in order to be transferred to the bile; therefore, the poorly soluble drug accumulated in the spleen would accompany a prolonged retention with possibly a longer plasma half-life.

Since the total drug content in an organ is dependent on the total weight of the particular tissue, the drug concentration was converted to drug mass (Fig 4B) for the four major accumulation organs by multiplying either the measured weight (for spleen and intestine) or the reported values from the literature (for liver and fat, provided by Jackson Laboratory). Within the 8th wk samples of spleen, liver, jejunum/ileum, and fat, approximately 13 mg of total drug mass was found, which corresponded to 83% of the total drug consumed, assuming 50% bioavailability after a 20 mg/kg/day dose. Although the concentrations measured in the liver were lower than those of the spleen, the larger weight and volume of the liver made it the largest storage compartment, since it reserved up to 6 mg of CFZ during the 8 wks of treatment. Assuming fat to be 16% of the body weight (Jackson Laboratory), the drug mass in the fat at the 8th wk apparently had decreased to 1/3 from that of the 3rd wk which had more than 3 mg of CFZ. Also, the CFZ content in the jejunum and ileum (Fig 4A) changed over the course of treatment in contrast to the duodenum content (Fig 4C) or to that of the large intestine (not shown)

which accompanied no detectable pigmentation. The jejunum revealed secondary dark-purple pigmentation that started from the lower portion of the ileum and progressed upstream of the small intestine but did not advance to the duodenal portion. The distinctive coloration boundaries had stopped at 7 ± 0.4 cm point after the stomach at the 8th wk of treatment. By multiplying the total weight of the jejunum and ileum (30 ± 0.7 cm, 1.3 ± 0.1 g), the drug mass within the portion averaged about 3 mg. Meanwhile, the concentration in the lungs peaked at 8 wks of treatment and cleared out relatively quickly to 25%, and the duodenum as well as kidney remained clean throughout the course of treatment (Fig 4C).

3.4.6 Plasma concentration reflects the drug content in adipose tissue

The plasma concentration was measured to investigate pharmacokinetics and the relationship between various organs among which the drug contents were distributed (Fig 4D). Interestingly, the plasma concentration revealed a similar trend to that of the fat rather than other highly perfusive organs such as the liver. The measured plasma concentrations were within a comparable range to previously reported values, 2.6 – 7 μM, measured in animals and humans, the plasma concentration decreased for higher doses and for longer treatments.[1, 17] Similarly, the current study shows higher concentration in the 3rd wk and then a decrease during the course of treatment and in the washout phase. Such dynamic interplay between dose strength and duration is thought to be owing to the fast partitioning between the plasma and adipose tissues prior to formation of crystal-like drug inclusions in the spleen, liver, or jejunum. We reasoned that since the drugs in adipose tissues exist as neutral, orange in color, and lipid-soluble form, it would be easier for the molecules to be transported elsewhere by plasma, whereas sequestered solid mass

in other tissues would face an energy barrier –thermodynamic solubility– in order to leave the depository, therefore resulting in a directionality to the drug redistribution.

3.4.7 Macrophages form the crystal-like drug inclusions

As the CLDIs were shown to be distributed in an organ-specific manner, we sought to determine whether there was any cell specificity in tissues with immunohistochemical staining. In the liver, we found the progression of the microgranulomas during the 6 wks of treatment and even at the washout phase (Fig 5). Macrophages were positively stained with the macrophage-specific antibody F4/80 after feeding mice with oil-diet (6wk Oil) or clofazimine-diet (6wk CFZ). Staining of the developing microgranulomas with F4/80 at 6wk CFZ appeared slightly larger than the individual, diffusely existing Kupffer cells seen in the vehicle only sample (Oil), indicating that more macrophages were recruited upon continued dosing. The clofazimine treatment accompanied fibrosis as the same microgranulomas were stained with Masson's trichrome (MTS). In the control sample, the MTS, α-smooth muscle actin (SMA) or endothelial cell marker (von Willebrand Factor, vWF) staining did not show any sign of fibrosis or involvement of muscle cell or endothelium. In the higher magnification, small microgranulomas (arrow) were enlarged to reveal the cytoplasmic scars or empty cavities where the CLDIs were removed by organic solvents during the immunostaining. At this stage, cells were positively stained with F4/80 and were developing fibrotic tissue; however, there was no involvement of muscle or endothelial cells. It is noteworthy, that at the washout phase, microgranulomas were localized around the blood vessels (triangles), and possibly more around the hepatic arteries than the central veins which in general appear as much larger and loosened structures.[15] This

suggests that the neutrophil augmentation from the circulation onto the existing microgranulomas is more likely than the local macrophage proliferation.[9]

In the villi of the jejunum, we did not find any changes in the population of any particular type of cell (Fig 6A). The F4/80 positive macrophage level was comparable between the treated and untreated sample of lamina propria. CD21 (follicular dendritic cell marker) and CD3 (early T cell marker) staining did not show any significant differences between the samples. The submucosa of intestinal walls were mostly deposited with macrophages; however, due to variability between the samples and sections, we could not make any quantitative observation.

Similar to that which was seen in the TEM analysis, the kidney cortex section showed an increased level of macrophage infiltration around the glomerulus and peritubular regions. The F4/80 (Fig 6B, triangle), α-smooth muscle actin (SMA) and von Willebrand Factor (vWF) staining indicated the macrophage infiltrated next to the blood vessels, indicating kidney inflammation.[14]

As the spleen was most concentrated with CLDIs, we investigated the distribution pattern of different cells around the germinal center, where lymphocytes were concentrated and isolated from the surrounding sinus through which blood is filtered (Fig 7). The untreated sample revealed a clear distinction between the F4/80 positive macrophages, CD21 positive follicular dendritic cells, and CD3 positive early T cells. In the 6 wk treated mouse spleen, an equivalent region to the control section did show a similar pattern. Notably, the CLDI cavities were identified to show empty cytoplasm (triangle), and they were only localized at the periphery of the germinal centers which themselves appeared normal. The macrophage marker (F4/80 and CD21) stained only in

a diffuse manner for CLDI positive cells, suggesting possible cell necrosis. However, they were in close proximity to a large number of F4/80 positive cells for possible augmentation. Consistent with the TEM image analysis and previous report,[3] we concluded that the macrophage distribution and recruitment determines the site-specific localization of the drug deposits, and therefore the drug content in a certain tissue; in other words, lymphatic tissues will accumulate and sequester more drugs.

3.5 Discussion

As a lipophilic compound is generally assumed to partition into fatty tissues to exert a larger volume of distribution, an earlier pharmacokinetics study of clofazimine demonstrated that fat is the main storage compartment for a short period of time.[2] In that study, drug absorption and distribution were monitored in mice for either 1 or 5 days after a daily dose of 40 mg/ml through oral gavage. The drug contents in the lungs, spleen, and liver peaked at 6 hours, followed by a sharp decrease and then remained at minimal level until another dose was given. However, the contents in fat increased consistently over a 24 hour period, which kept on increasing with each daily treatment throughout the 5 days of treatment. These observations imply that fat can extract lipophilic molecules from the plasma and highly perfusive organs, and therefore plays a significant role in the drug distribution within 5 days. In the current study, we demonstrated that a longer term administration of clofazimine involves another level of physiological factors, that the expansion and structural reorganization of tissue-macrophages significantly affect the distribution and retention of the poorly soluble, lipophilic drug.

In terms of systemic pharmacokinetics, the formation of atypical, intracellular drug inclusions of clofazimine was linked to lowering the plasma concentration by a sequestration mechanism that is different from common elimination processes such as drug metabolism or renal excretion. In addition, the volume of the spleen increased as it sequestered a more significant amount of the drug in the process. Similarly, liver microgranulomas was a response of the body to an idiosyncratic drug reaction, driving the majority of the clofazimine into inert, solid forms and serving as a storage compartment for the drugs en masse. Altogether, these results challenge the pharmacokinetic models assuming compartments with constant volumes and homogeneous tissue composition.

The microgranulomas development also indicated that macrophages can recognize irritants at the molecular level and sequester them within the cytoplasmic compartment, which would trigger a positive feedback to recruit more macrophages. It was expected to see some necrosis within the center of the microgranulomas, as highly active macrophages would end up accumulating more materials, and therefore mechanical stress could eventually kill the cells. However, additional layers of macrophages summoned by pre-existing layers can further extract and isolate clofazimine from the systemic circulation. In the same context, the progression of splenomegaly without significant change of concentrations during the washout phase suggests ongoing recruitment of macrophages for further isolation of the drug. Chronic irritation and macrophages' anti-inflammatory response caused fibrosis, similar to the cases of poorly soluble substances persisting and retention due to resistance to macrophagic metabolism.[8]

At the 8th wk of treatment, the spleen could contain the poorly soluble clofazimine more than 1% of the organ weight. Such a massive accumulation in the form of solid matter advocates for the physiological nature of a large volume of the distribution, which is a conceptual volume to represent total amount of drug in the body assuming a constant plasma concentration. As a matter of fact, the drug sequestration in the macrophage is responsible for the biodistribution of the poorly soluble, lipophilic drug.

3.6 Acknowledgements

The project was supported by grant number GM007767 from NIGMS for J.B., and by NIH grant RO1GM078200 to G.R.R. Its contents are solely the responsibility of the authors and do not necessarily represent the official views of NIGMS or NIH. J.B. was supported by American Foundation for Pharmaceutical Education. We thank Dorothy Sorenson (MIL, Univ. of Michigan), Paula Arrowsmith (PCAR, Univ. of Michigan) and Dr. Gerald Hish (ULAM, Univ. of Michigan) for technical support. This work utilized the Core Services supported by grant DK089503 of NIH to the University of Michigan. We thank Dr. Charles Burant, Dr. Nair Rodriguez-Hornedo, and Dr. David E. Smith for insightful comments.

3.7 Figures

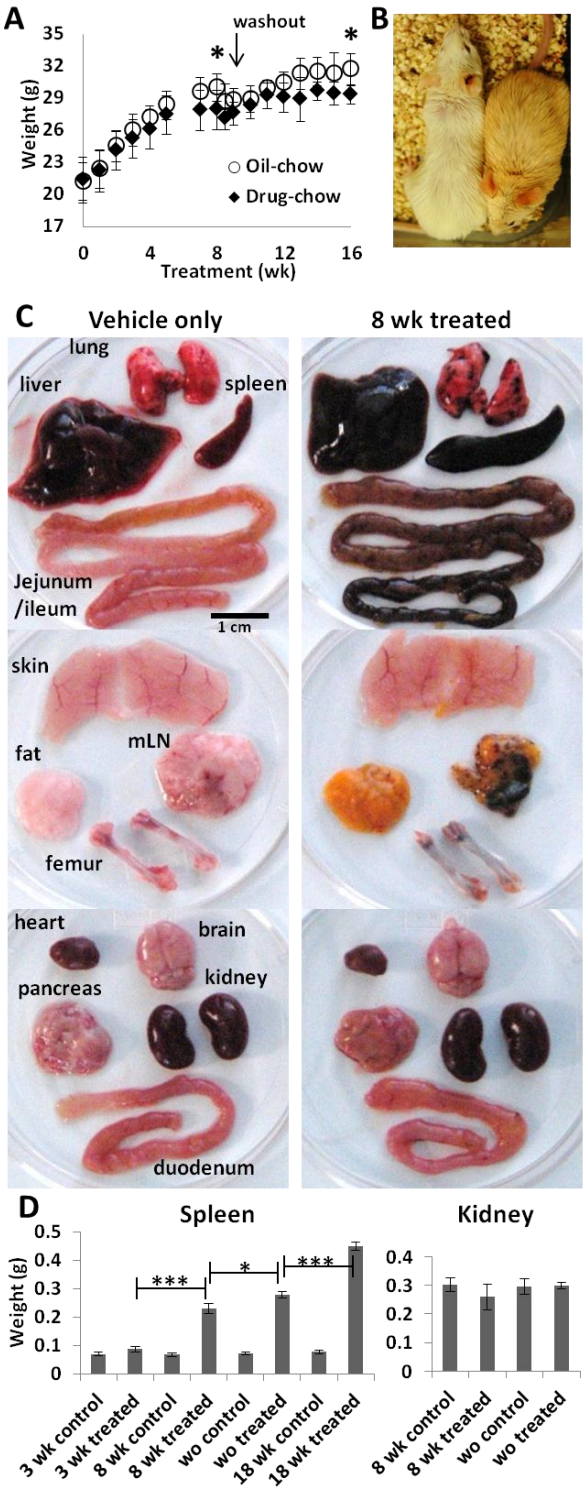

Figure 3-1 Pigmentation in CFZ treated mice

(**A**) Body weight monitored for 8 wks of treatment followed by additional 8 wks of washout period by feeding drug-free, regular diet. Weight gains for the 16 wks in each groups were statistically significant (*, $p<0.05$). (**B**) Skin and hair discoloration to pink was apparent at 8 wk treatment (right) compared to the mouse treated with vehicle-only diet (left). (**C**) Significant pigmentation was observed on the lungs, liver, spleen, jejunum, ileum, and msenteric lymph node (mLN). Mild, orange color pigmentation was observed in the hypodermis of the skin, abdominal fat, omental fat attached to mesenteric lymph node, and tips of femurs. The color of the heart, brain, pancreas, kidney and duodenum remained unchanged. (**D**), 8 wk drug treatment induced splenomegaly, which even further increased during washout period (WO) compared to the controls (drug-free diet) or 3rd wk of treatment. In contrast, mass change of the kidney was insignificant. Statistical significance: *, $p<0.05$, and ***, $p<0.001$, S.E.M. $n = 4 – 6$, ANOVA (analysis of variance).

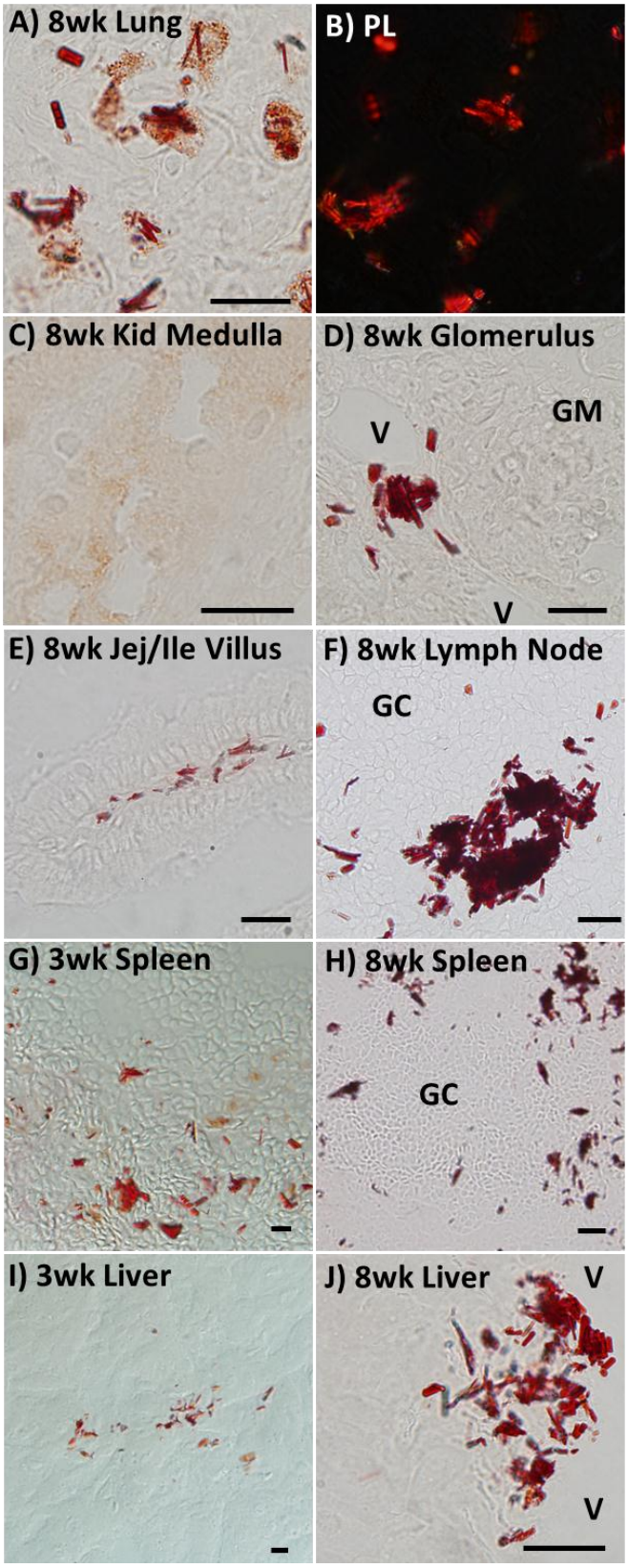

Figure 3-2 Frozen section of organs from drug treated mice

(**A**) 8 wk treated lung parenchyma showed distinct, vibrant red drug inclusions. (**B**) CLDIs were birefringent under polarized light, while smaller, autophagosome-like drug inclusions did not. (**C**) 8 wk treatment affected kidney medulla without CLDIs. (**D**) Glomerulus (GM) in the cortex region of the same kidney. (**E**) 8 wk treated jejunal/ileal section is shown. CLDIs in the lamina propria of intestinal villus, enterocytes were clean. (**F**) 8wk treated mesenteric lymph node with significant and heterogeneous distribution around the germinal center (GC). (**G** and **H**) Spleens with CLDI development. (**I** and **J**) Liver developed CLDIs from scattered (3 wk) to localized (8 wk) pattern around the vessel region (V). Scale bars = 20 µm.

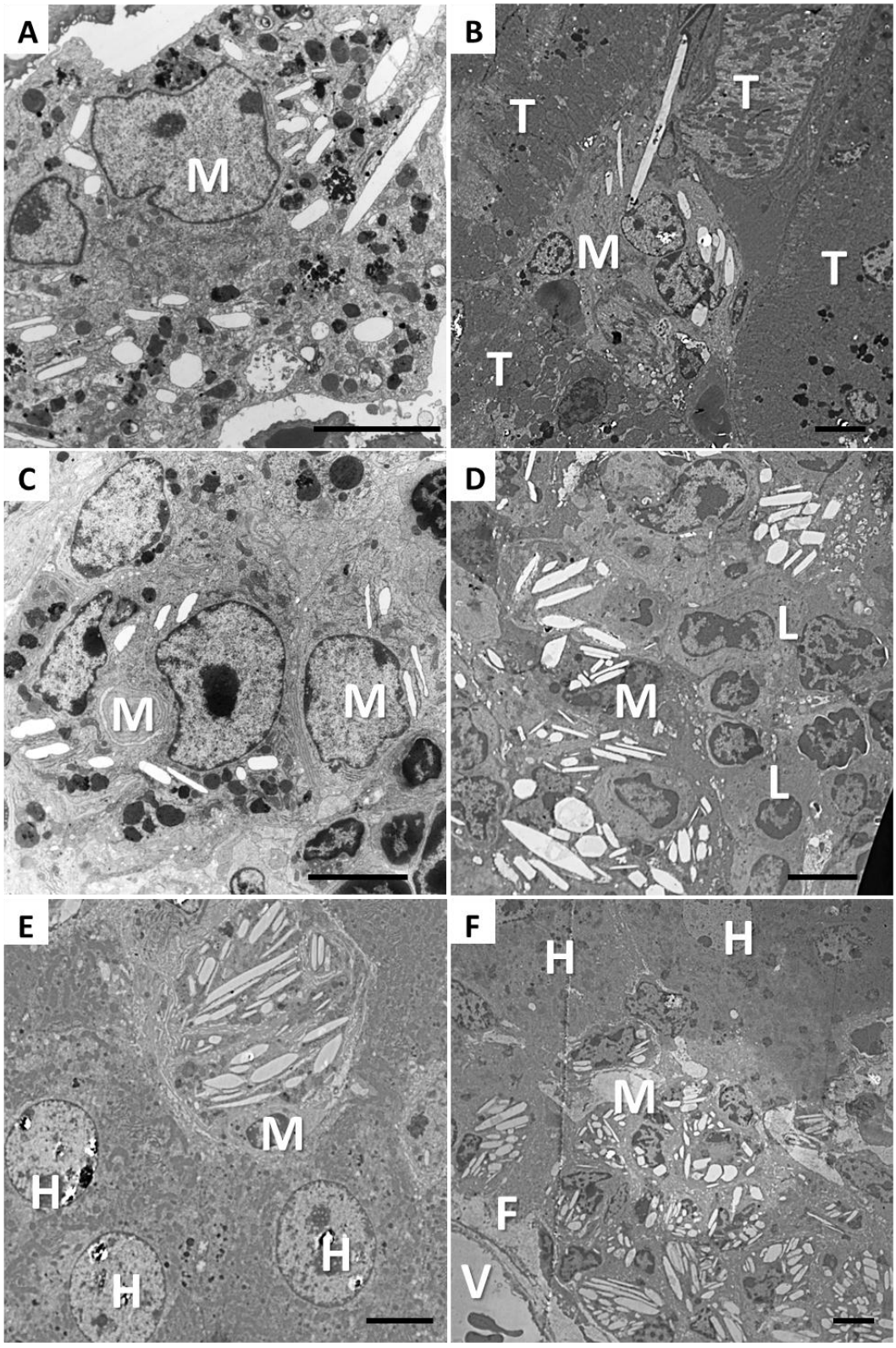

Figure 3-3 TEM images of affected organs showing different types drug inclusions associated with unique histological features.

(**A**) 4.5 wk treated lung parenchyma macrophages (M) with cytoplasmic inclusions bodies. While autophagosome-like drug inclusions (ALDIs) were preserved, CLDIs were shown as empty cavities as they were washed out. (**B**) 8.5 wk treated kidney tubular region with numerous renal tubules (T) were shown. In peritubular region, a group of macrophages appeared with CLDI cavities in the cytoplasm. (**C**) 4.5 wk treated mice jejunal submucosa showed a number of macrophages with ALDIs and CLDIs. (**D**) 8.5 wk treated spleen showed significant amount of CLDI cavities associated presumably with macrophages. Lymphocytes (L) with small cytoplasm and round nuclei did not have CLDI cavities. (**E**) 4.5 wk treated liver showed a number of Kupffer cells with CLDI cavities surrounded by hepatocytes (H). (**F**) 8.5 wk treated liver developed a significant size of microgranulomas around the blood vessel. Fibrocytes (F) were separating the endothelium from the macrophages in microgranulomas. Scale bars = 5 μm.

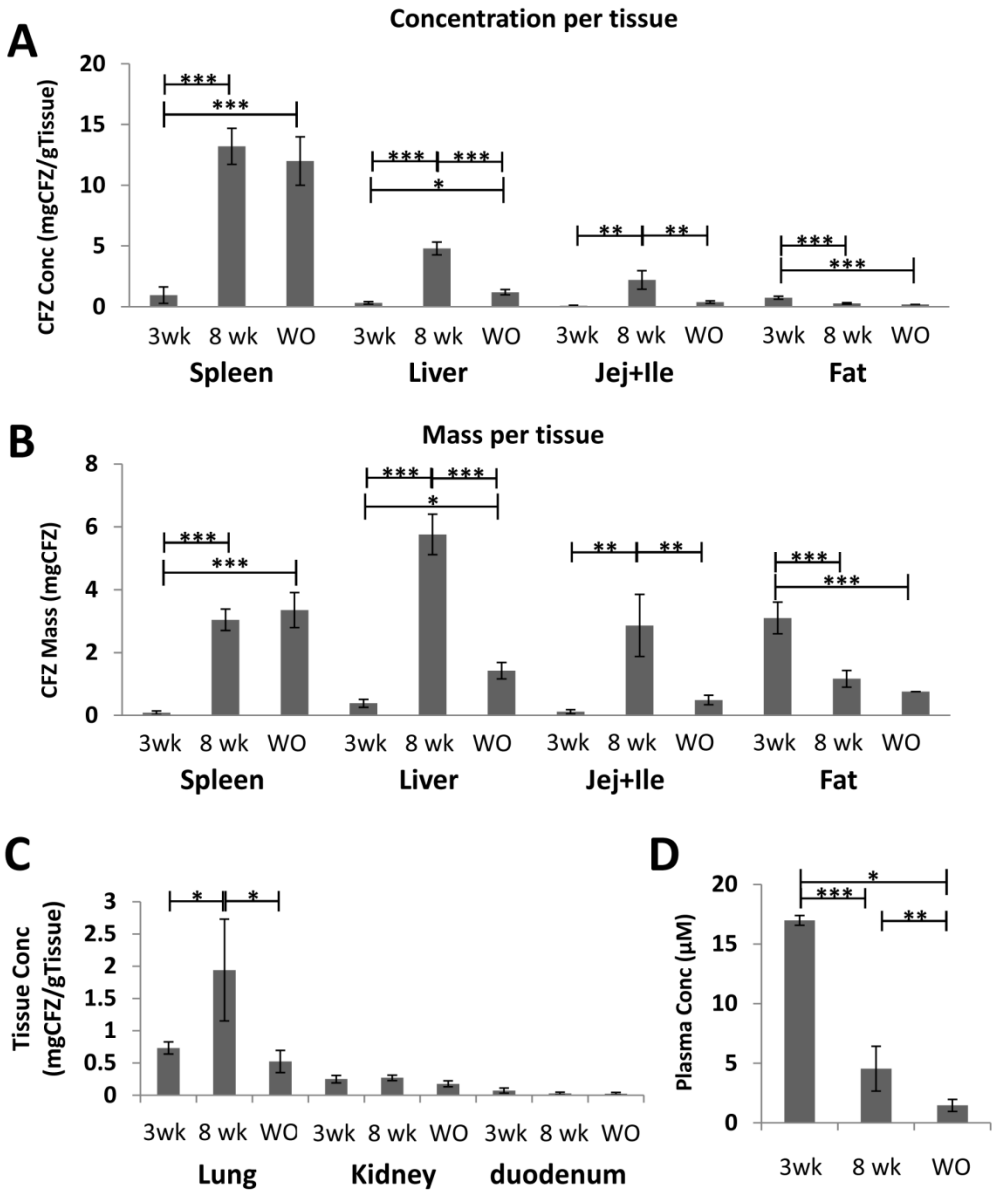

Figure 3-4 CFZ content analysis in various organs.

(**A**), Concentration of CFZ per gram of the spleen, liver, intestinal segments from the jejunum to ileum, and fat after 10 mg/kg mice daily absorption. Total drug mass in these organs (**B**) were obtained by multiplying total weight of the respective organs. (**C**), The lungs have developed a significant accumulation between 3wk and 8 wk, which was effectively cleared out during the washout phase (WO). The kidney and duodenum show no difference between the treatments. (**D**), CFZ concentration measured in plasma which peaked at earlier point of treatment decreased significantly during further treatment and washout phase. (*, $p<0.05$, ** $p<0.01$, ***, $p<0.001$, S.E.M, N = 4 – 6 by ANOVA)

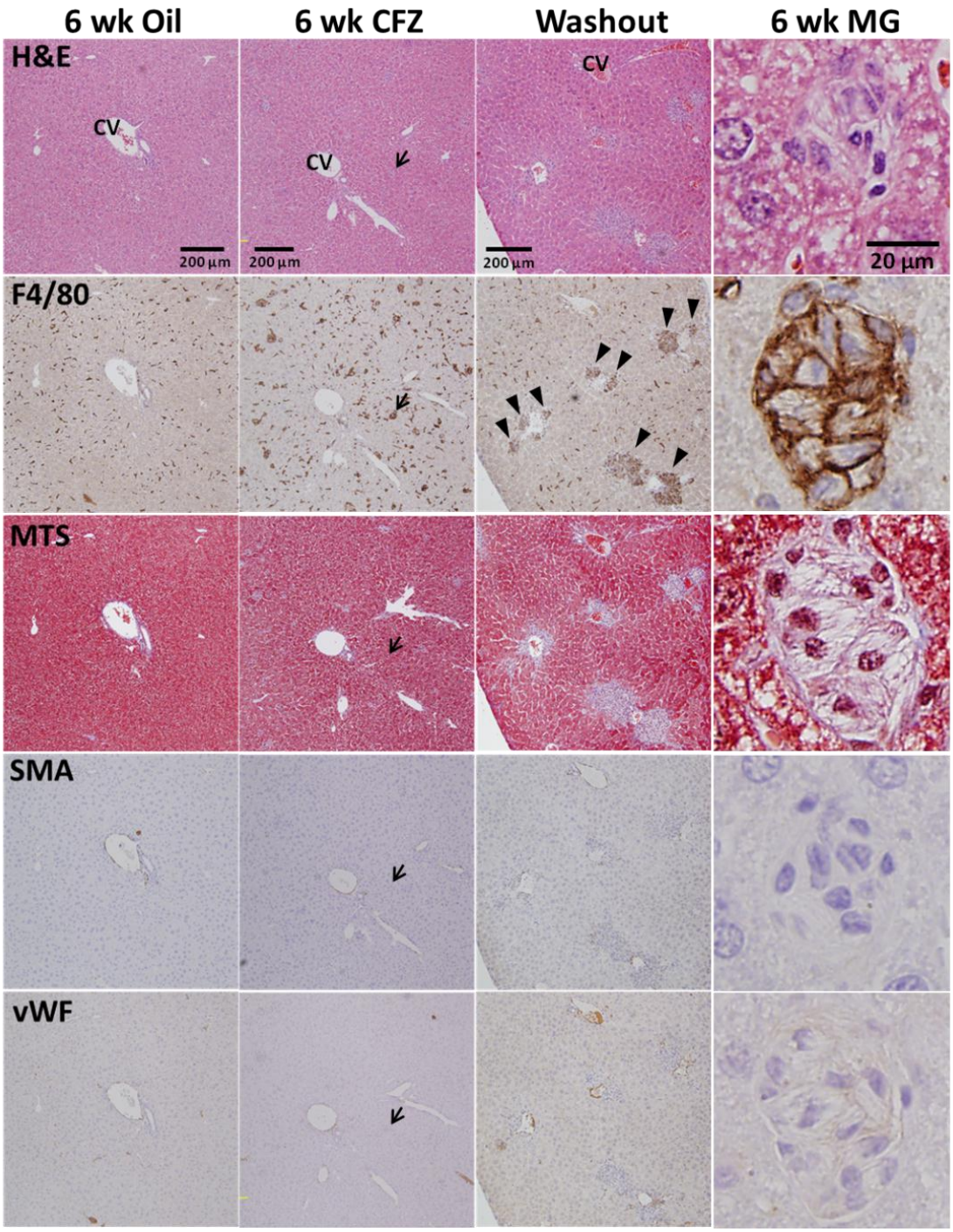

Figure 3-5 Liver microgranulomas developed to sequester CFZ as CLDIs.

Regions around the blood vessels underwent a structural transformation as drug treatment lasted as well as during the washout phase. Macrophage distribution by the F4/80 staining showed the scattered distribution of Kupffer cells developing into small colonies evenly distributed throughout the section. However, larger colonies of microgranulomas (triangles) developed with fibrosis (MTS) at region around the vessels (vWF). Higher

magnification images indicated the microgranulomas (arrow) were actually comprised of macrophages that contained a significant number of CLDIs in cytoplasm shown by the cavities. There was no involvement of muscle tissue indicated by α-smooth muscle actin staining (SMA)

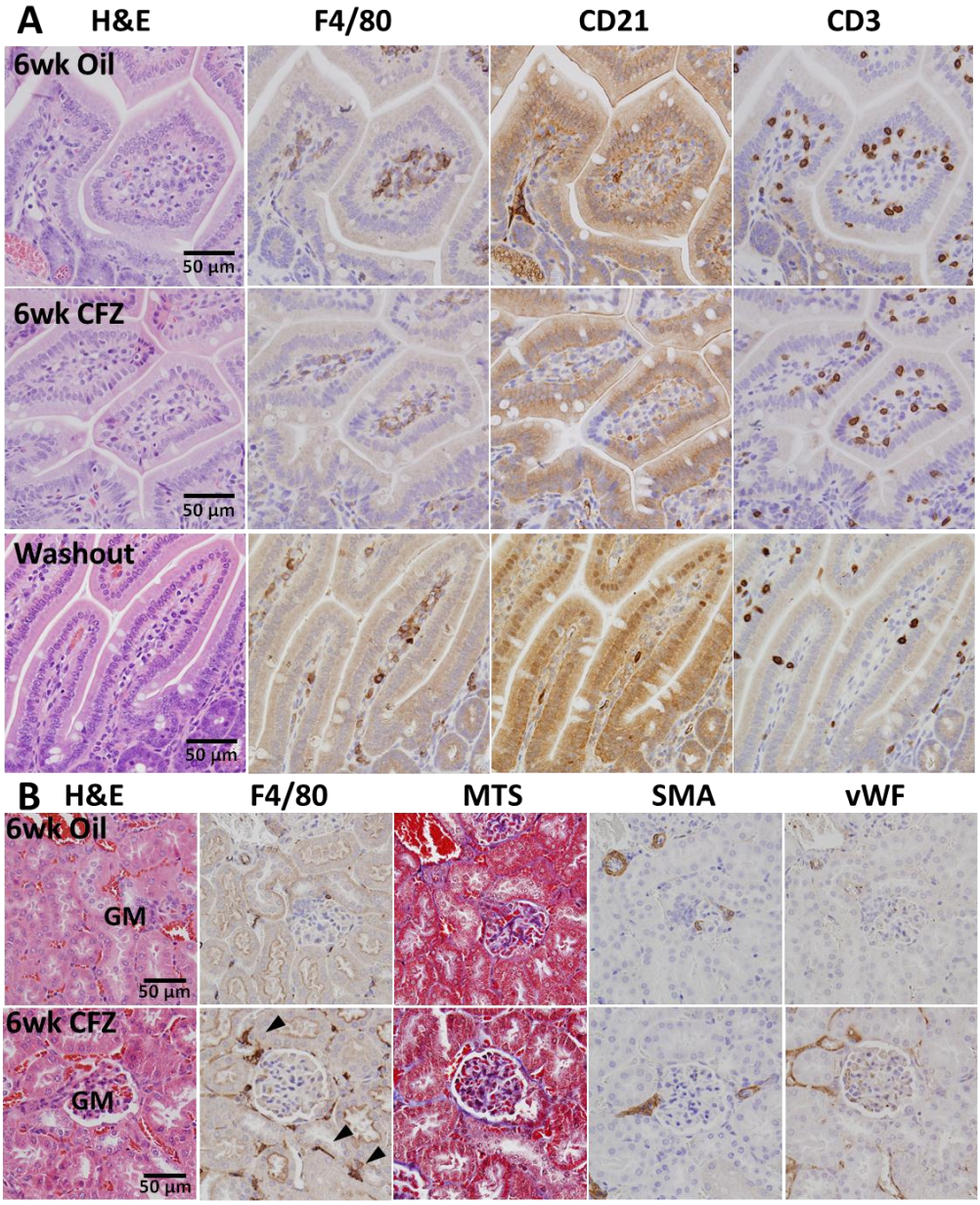

Figure 3-6 Immunostaining for 6 wk treated mice jejunum and kidney.

(**A**), jejunal sections of 6 wk treated mice are shown. Macrophage marker F4/80, dendritic cell marker CD21 or T cell marker CD3 did not show much difference between control, 6 wk treated, and washout of jejunal villi. (**B**) In the kidney with 6 wk of drug treatment, macrophages that are normally absent had infiltrated around the glomeruli. Masson's trichrome staining (MTS), α-smooth muscle actin (SMA), or von Willebrand factor (vWF) did not show much difference other than structures around the blood vessels.

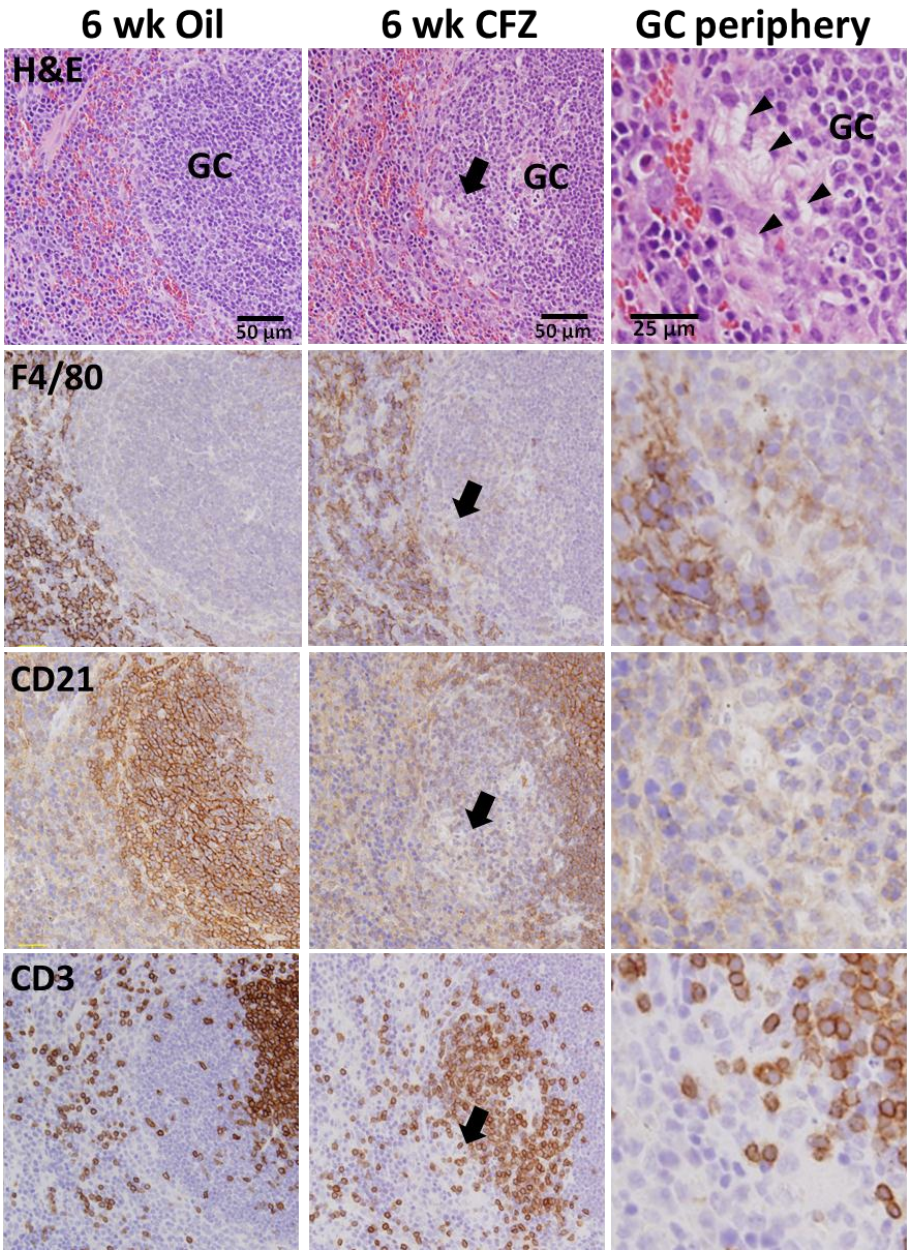

Figure 3-7 Spleen revealed a specific region that localized CLDIs

In contrast to the control, CFZ treated mice spleen developed a significant CLDI storing region around the germinal centers (GC) that are rich in lymphocytes and lymphoblasts. On the periphery of this region, there were a significant number of cells with cytoplasmic CLDI cavities.

3.8 References

1. Banerjee, D. K.; Ellard, G. A.; Gammon, P. T.; Waters, M. F. Some observations on the pharmacology of clofazimine (B663). *Am J Trop Med Hyg* **1974,** *23*, (6), 1110-5.

2. Barry, V. C.; Buggle, K.; Byrne, J.; Conalty, M. L.; Winder, F. Absorption, distribution and retention of the riminocompounds in the experimental animal. *Ir J Med Sci* **1960,** *416*, 345-52.

3. McDougall, A. C.; Horsfall, W. R.; Hede, J. E.; Chaplin, A. J. Splenic infarction and tissue accumulation of crystals associated with the use of clofazimine (Lamprene; B663) in the treatment of pyoderma gangrenosum. *Br J Dermatol* **1980,** *102*, (2), 227-230.

4. Mansfield, R. E. Tissue concentrations of clofazimine (B663) in man. *Am J Trop Med Hyg* **1974,** *23*, (6), 1116-9.

5. Levy, L.; Randall, H. A study of skin pigmentation by clofazimine. *Int J Lepr Other Mycobact Dis.* **1970,** *38*, (4), 404-416.

6. Williams, G. T.; Williams, W. J. Granulomatous inflammation--a review. *Journal of Clinical Pathology* **1983,** *36*, (7), 723-733.

7. Baik, J.; Rosania, G. R. Cytoplasmic Construction of Supramolecular Structures with Organelle- and Crystal-like Features. *submitted to Pharm Res* **2011**.

8. Griffis, L. C.; Twerdok, L. E.; Francke-Carroll, S.; Biles, R. W.; Schroeder, R. E.; Bolte, H.; Faust, H.; Hall, W. C.; Rojko, J. Comparative 90-day dietary study of paraffin wax in Fischer-344 and Sprague-Dawley rats. *Food Chem Toxicol* **2010,** *48*, (1), 363-72.

9. Jenkins, S. J.; Ruckerl, D.; Cook, P. C.; Jones, L. H.; Finkelman, F. D.; van Rooijen, N.; MacDonald, A. S.; Allen, J. E. Local macrophage proliferation, rather than recruitment from the blood, is a signature of TH2 inflammation. *Science* **2011,** *332*, (6035), 1284-8.

10. Wishart, D. S.; Knox, C.; Guo, A. C.; Cheng, D.; Shrivastava, S.; Tzur, D.; Gautam, B.; Hassanali, M. DrugBank: a knowledgebase for drugs, drug actions and drug targets. *Nucleic Acids Research* **2008,** *36*, (suppl 1), D901-D906.

11. Venkatesan, K.; Deo, N.; Gupta, U. D. Tissue distribution and deposition of clofazimine in mice following oral administration with or without isoniazid. *Arzneimittelforschung* **2007,** *57*, (7), 472-4.

12. Aplin, R. T.; McDougall, A. C. Identification of crystals of the rimino-phenazine compound B663 (Lamprene: clofazimine) in mouse spleen macrophages by thin layer chromatography and mass spectrum analysis. *Experientia* **1975,** *31*, (4), 468-9.

13. Baik, J.; Rosania, G. R. Molecular Imaging of Intracellular Drug-Membrane Aggregate Formation. *Molecular Pharmaceutics* **2011**, DOI:10.1021/mp200101b.

14. Guo, S.; Wietecha, T. A.; Hudkins, K. L.; Kida, Y.; Spencer, M. W.; Pichaiwong, W.; Kojima, I.; Duffield, J. S.; Alpers, C. E. Macrophages are essential contributors to kidney injury in murine cryoglobulinemic membranoproliferative glomerulonephritis. *Kidney Int* **2011**, DOI:10.1038/ki.2011.249.

15. Rhodin, J. A., *An Atlas of Histology*. Oxford University Press: New York, **1975**; 55-64.

16. O'Connor, R.; O'Sullivan, J. F.; O'Kennedy, R. The pharmacology, metabolism, and chemistry of clofazimine. *Drug Metab Rev* **1995,** *27*, (4), 591-614.

17. Levy, L. Pharmacologic studies of clofazimine. *Am J Trop Med Hyg* **1974,** *23*, (6), 1097-109.

Chapter 4

Cytoplasmic Construction of Supramolecular Structures with Organelle- and Crystal-like Features

4.1 Abstract

Eukaryotic cells naturally possess a limited repertoire of evolutionarily-conserved organelles and cytoskeletal elements. To endow cells with a new structural element, we fed mice with a supramolecular structure-forming molecule: a cell-permeant, highly-insoluble, antibacterial drug clofazimine. Clofazimine was mixed with powder diet and fed to Balb/c mice for 2 months, followed by drug-free diet. At predetermined time points, various organs were collected for biochemical analysis and microscopic imaging, including polarization, fluorescence, and electron microscopy. After absorption, clofazimine accumulated in macrophage-like cells, where intracellular drug-membrane complexes transformed into functionally-integrated structural elements. These "polyhedrosomes" were birefringent red needles with the internal structure of planar stacks of membranes at the core, forming elongated, faceted prisms. Meanwhile, the harvested macrophages with polyhedrosomes could adhere and migrate on the plastic culture dish, and could release the structure-forming molecule upon illumination. Physicochemical properties showed that the polyhedrosomes were unlike pure drug

crystals or other cellular organelles. They burst in distilled water or when heated, and disintegrated in alkaline media. We demonstrate how artificial structural elements with organelle- and crystal-like features can be constructed within the cytoplasm of mammalian cells *in vivo*.

4.2 Introduction

Low concentrations of exogenous chemical agents are normally used in pharmaceutical science experiments to probe different aspects of cell physiology by activating or inhibiting specific receptors or enzymes. Nevertheless, we decided to investigate a previously unexplored dimension of chemical biology: the possibility of using small molecule chemical agents as physical building blocks to endow cells with new structural and functional features. For this purpose, we used clofazimine, a highly cell-permeant, non-toxic antibiotic[1-4] approved for clinical use to treat leprosy and other inflammatory diseases.[2, 4, 5] It dissolves in acidic solutions, or in DMSO, and becomes virtually insoluble in aqueous media at neutral or alkaline pH.[6] Therefore, in the gastrointestinal tract after oral administration, clofazimine can form supersaturated solutions when it passes from the acidic pH of the stomach to the more alkaline pH of the intestine. During the absorption and distribution, the drug can possibly form complexes with intracellular membranes leading to a significant subcellular drug accumulation as suggested in the previous study with MDCK cells exposed to supersaturating concentrations of the drug for 5 days.[6] In light of these observations, we decided to investigate the supramolecular structures that form upon long-term, continuous administration of clofazimine *in vivo*.

4.3 Materials and Methods

Animal experiments and perfusion fixation for TEM imaging. The University of Michigan Committee of Use and Care of Animals approved all animal studies and procedure. Mice (4-5 wk male Balb/c, Jackson lab, Maine) were fed with drug with powder diet (3 mg/ml clofazimine (Sigma, C8895) in sesame oil, mixed at 0.01% oil to food). Blood was collected from euthanized mice and carcasses were fixed by perfusing 0.1M Sorensen's buffer and Karnovsky's fixative (3% paraformaldehyde, 2.5% glutaraldehyde) infused to left ventricle and let egressed to vena cava (2.5 ml/min). Tissues were minced smaller than 1 mm in each dimension followed by TEM sample preparation and imaging.[6] Control mice were fed with 0.01% oil to food, and wash out mice were fed drug- and oil-free diet.

Biochemical analysis of clofazimine in tissues. At predetermined time point mice were euthanized using CO_2, and blood was removed through cardiac puncture. Next, the organs were collected, washed in cold DPBS, and kept at -20°C until further analysis. Tissue (0.05 – 0.1 g/ml water) was homogenized with Tissumizer (Tekmar®, Cincinnati, OH), extracted with dichloromethane twice and the solvent was evaporated.[7] For measurement, clofazimine was redissolved in methanol and its absorbance was measured at 490 nm. Concentration was calculated using as standard curve generated by spiking extracted tissue of the control (vehicle-only treated) mice with known amounts of drug. Extraction yield was 60 – 80%.

Immunohistochemistry. Tissues were perfusion fixed as described above, paraffin-embedded and stained with the standard H&E and Masson's trichrome technique. Horse Radish Peroxidase and intelliPATH FLX DAB chromogen kit (IPK5010, Biocare

Medical, Concord, CA) was used for F4/80 (1/100, ab6640, abcam®), α-SMA (1/200, ab5694, abcam®), and vWF (1/500, ab7356, Millipore) antibody staining. All staining was performed by the Pathology Core for Animal Research (PCAR) in the Unit for Laboratory Animal Medicine (ULAM) at the University of Michigan.

Freeze-fracture freeze-etch EM. Unfixed liver was collected after exsanguination, kept in 4°C, and shipped overnight to the Heuser lab at Washington University (St. Louis) for freeze-etch EM analysis, as reported previously[8] with minor modifications. In brief, the sample was quickly frozen against a copper block, cooled with liquid helium using slam freezer and kept in liquid nitrogen. The sample was fractured with Balzers 400 nitrogen cooled vacuum evaporator and freeze-etched for 2 min at -100°C. Rotary replica was generated with 2 nm platinum and backed with 10 nm carbon film support. It was cleaned with chromo-sulfuric cleaning solution (Fisher Scientific, cat# SC88) for 12 hours and rinsed with DI water. The sample was picked up on formvar coated grids for viewing on a JEOL 1400 electron microscope with AMT camera.

Primary cell isolation and culture. 4% Brewer's thioglycollate medium was prepared sterile as described.[9] A 2 ml volume of solution was injected IP. Cells were collected 4 days later using cold DPBS. Bone marrow macrophages were flushed out from mice femurs using a fine needle syringe with DPBS.[10] Cells from spleen and lymph nodes were collected by mincing small tissue using a cell strainer with 100 μm mesh size. Cells were seeded in tissue culture plates and kept 7 days in 37°C, 5% CO_2 with DMEM supplemented with 10% FBS, Pen/Strep, and non-essential amino acids.

Polyhedrosome isolation. Tissue homogenate was sonicated for 30 minutes, centrifuged (100g for 1 min) to remove large cell debris. Supernatant was resuspended in 0.125%

Trypsin-EDTA solution (Gibco) and kept at 37°C for 1 hour, followed by centrifugation at 100g to remove large cell debris. The drug inclusions in supernatant were then pelleted by centrifugation (21,000g for 1 min), and resuspended in water. Protein content was determined with the BCA assay (Pierce 23227, Thermo Scientific) and clofazimine content was determined spectrophotometrically as described above. For protein assay, equal volume of 5% SDS solution was mixed with the samples and the protein content was measured following the BCA kit instructions.

Powder X-ray diffraction of clofazimine crystals and isolated polyhedrosomes. PXRD of dried samples of isolated polyhedrosomes and 8 wk treated (or control) mouse tissue homogenate were carried out with benchtop Rigaku Miniflex X-ray diffractometer (Danvers, MA). CuKα radiation (λ = 1.54 Å), tube voltage = 30 kV, tube current = 15 mA. Data were collected at 2 theta from 2.5 to 40 at a continuous scan at the rate of 2.5°/min. Diffractograms of triclinic and monoclinic form of clofazimine crystals were imported from Cambridge Structural Database (CSD) and positive control for clofazimine crystals was obtained from the powder from the bottle.

4.4 Results

For long term, continuous administration, mice were fed with powdered chow supplemented with the structure-former clofazimine, *ad libitum.*[4, 7, 11, 12] This resulted in a daily intake of approximately 20 mg/kg, well below clofazimine's LD50 and comparable to the human daily dose of 4.3 mg/kg.[13] As in humans,[13] the skin of the Balb/c mice gradually turned red after three wks (Fig. 1a). Otherwise, the treated animals gained weight and behaved similarly to their untreated counterparts (Fig. 1b).

From 3 to 8 wks of dietary supplementation, biodistribution analysis revealed a steady state accumulation of clofazimine in the kidney, muscle, heart, and brain (Fig. 1c). However, continuous, non-steady state accumulation occurred in the spleen, liver, lymph nodes, bone marrow, intestine and lungs. In the spleen, the mass of structure-former almost reached 1% of the wet organ weight (Fig. 1c). After discontinuation, the skin of the drug-diet treated mice gradually returned to a paler color over a period of two months. Some organs, like the kidneys, gradually lost most of the structure-former. However, clofazimine concentration only decreased by 76% and 73% in liver and lung respectively, while changes in concentration in the spleen were statistically insignificant, indicating a specific retention mechanism (Fig. 1c).

In vivo, clofazimine accumulated in tissues in metabolically intact form.[3, 11] Examination of unfixed, frozen tissue sections by transmitted light microscopy revealed dark, ruby red and crystal-like drug inclusions present in all organs exhibiting continuous accumulation and retention of the drug (Fig. 1d). They were most numerous in spleen and lymph nodes, followed by liver, small intestine and lungs. In treated mice, splenomegaly (mass increase by >3.4 fold (N=5), $P<0.01$; t-test) and swollen mesenteric lymph nodes were observed.[14] In contrast, tissues achieving steady state levels of clofazimine lacked drug inclusions. At 3 wk treatment, the inclusions were 2.2 ± 0.78 (SD) μm in width and 3.9 ± 2.6 μm in length. At 8 wk treatment, the individual inclusions were only slightly more elongated to 6.0 ± 3.6 μm ($P<0.01$) but increased in numbers. Thus, the growth of drug inclusions was constrained by the size of the cells. After treated mice were switched to a clofazimine-free, regular diet for two months (Fig.

1c, wash), the drug inclusions were still prominent in those organs that retained clofazimine (e.g., spleen).

In the liver, only macrophage-like cells appeared to contain inclusions (Fig. 1e), and surrounding hepatocytes clearly lacked them. Cells with drug inclusions formed small clusters resembling microgranulomas, which are normally formed by liver macrophages under stress (Fig. 1f, M).[15] These clusters were adjacent to blood vessels (Fig. 1f, V). Cells in these clusters expressed the F4/80 antigen (macrophage marker; Fig. 1f) which are also labeled the Kupffer cells. The cell clusters were embedded in extracellular matrix (Masson's trichrome staining, MTS; Fig. 1f) and they did not stain with von Willebrand factor (endothelial cell marker, vWF; Fig. 1f) or α-smooth muscle actin (smooth muscle marker, αSMA; Fig. 1f).

In the jejunum, drug inclusions were absent in the enterocytes, and were prominent in cells of the lamina propria and the lymphatic regions of the muscularis mucosae. As in the liver, these cells stained positively with the F4/80 marker but lacked staining with the vWF and αSMA. Together with the accumulation of clofazimine and retention in spleen and lymph nodes, these results indicated the special role of immune cells at the sites of deposition.

Due to the extraction procedure used for sample preparation, intracellular drug inclusions in liver and spleen generally appeared as empty, elongated cavities. Nevertheless, in the macrophage-like cells of the intestine the inclusions were not extracted (Fig. 2a). Since their supramolecular features did not resemble any other known subcellular structures, we dubbed these structures "polyhedrosomes". They were osmiophilic, elongated and polyhedral in shape, and bounded by a lipid bilayer (Fig. 2b).

In addition, there were other atypical organelles with heterogeneous granular bodies merging with elongated polyhedrosome-like structures or with multilamellar bodies merging with amorphous granular bodies (Fig. 2c).

The regular, internal membrane organization of polyhedrosomes was evident at higher magnifications. As seen in medial cross-sections cut along the long axis of the structure (Fig. 2d and 2e), polyhedrosomes possessed a multilamellar core comprised of planar sheets separated by parallel array of clear "channels" spaced 18 nm apart, and aligned parallel to the long axis of the structure (Fig. 2g and 2f). In some regions, the polyhedrosome structure appeared as a lattice with periodic structural elements repeating every 10 or 18 nm (Fig. 2e and 2f).

Transversal cross-sections cut perpendicularly to the long axis (Fig. 2h) revealed the multilamellar core comprised of planar stacks of alternating black and white membranes of 10 nm thickness (Fig. 2i). The core was surrounded by concentric lamellae of cortical, multilayered membranes. The entire structure was bounded by an outermost membrane bilayer (Fig. 2h). The multilayered membrane that filled the entire structure seemed to be comprised of stacks of trilayer membranes present in all the elongated polyhedrosomes, as well as in the transitional structures (Fig. 2c). This trilayer membrane consisted of a thick, dark osmiophilic band at the center (Fig. 2j, arrows) flanked by two thinner osmiophilic bands on either side (Fig. 2j, triangles). A clear, 5 nm layer separated the central band and the flanking bands. In the polyhedrosome core, the trilayer membranes were separated by a regular, 5 nm clear layer that was continuous with membrane-free regions (Fig. 2h, *).

In order to gain structural information on the un-extracted sample without using organic solvent, freeze-fracture freeze-etch electron microscopy (FEEM) was implemented on the unfixed liver of a 6 wk treated mouse (Fig. 2l and m). Consistent with the results from TEM study, FEEM showed a three-dimensional, planar, multilamellar organization at the core of the polyhedrosomes, with no evidence of lateral organization along the plane of each layer. The polyhedrosomes were surrounded by a double membrane (Fig. 2l and m, blue and purple) with protein-like structural features similar to those present in the other cellular membranes in the cytoplasm of the cell (green).

Remarkably, this multilamellar structure was unlike any other membrane organizations formed by intracellular membranes or previously reported forms of isolated phospholipids reconstituted in aqueous medium.[16] Also, the membrane-bound polyhedral structure possessing such an atypical supramolecular architecture was distinct from any other organelles, cytoskeletal or supramolecular architecture naturally present in mice macrophages.[16]

To study the newly formed intracellular structures polyhedrosomes in greater detail, bone marrow macrophages (BMM) were isolated from femurs, and peritoneal macrophages (PM) were elicited by intraperitoneal injection of 4% thioglycollate.[9] These cells attached and spread on tissue culture plastic (Fig. 3a). The polyhedrosomes of the elicited macrophages resembled those *in vivo*. Peritoneal macrophages containing the polyhedrosomes were observed to migrate out from clusters onto the tissue culture plastic (Fig. 3b) indicating the cells were alive and remained functional despite the inclusions. In contrast to the toxic effect reported in previous study with MDCK cells,[6] the

polyhedrosomes seemed to be compatible with macrophages, as numerous intact mitochondria were observed.

Interestingly, with peritoneal macrophages isolated *in vitro*, illuminating polyhedrosomes with 490 nm light induced release of structure-former (Fig. 3c). Soon after illumination, the structure-former's fluorescence filled the cell. Upon continued illumination, the fluorescence diffused to the neighboring cells (Fig. 3c), indicating perturbation of the crystal-like drug inclusions is possible via optical stimulus.

When live cells were plated on tissue culture plastic, polyhedrosomes maintained their shape and size. Outside cells, polyhedrosomes gradually transformed into irregular, rhomboidal shapes resembling typical clofazimine crystals, which grew larger than the cells in length: from 9.7 ± 3.1 μm (day 0) to 15 ± 4.7 μm (day 7) (Fig. 3d). Nevertheless, intracellularly retained polyhedrosomes were highly regular in shape. They appeared rigid and did not bend when cells were detached and rounded up in suspension (Fig. 3e). Generally, cells contained one, two or more polyhedrosomes of similar length as bundles.

To further examine the characteristics of polyhedrosomes, we decided to compare their physicochemical properties directly to pure clofazimine crystals.[17-21] In contrast to polyhedrosomes, clofazimine crystals were highly irregular in shape and size (Fig. 4a). They fluoresced in the standard, green (eGFP) channel and in the red (Cy3) channel of the epifluorescence microscope. These properties did not change when they were placed in water and heated to 100 °C, placed in 1N NaOH or trypsinized.

For comparison, polyhedrosomes were isolated by mincing and disaggregating spleens with 0.125% trypsin-EDTA, ultrasonicating them for one hour after passing them through a cell strainer. Polyhedrosomes were the only microscopic structure remaining

visibly intact, and could be further purified through step-wise centrifugation as described in the methods section. Isolated polyhedrosomes were immediately resuspended in 10% sucrose and the structure was stable for more than 3 months stored in -20°C. The calculated clofazimine content within isolated polyhedrosomes were normalized by protein content, and content analysis indicated that the purification process enriched as much as 16-fold for 8 wk treated spleen homogenate. Greater than 90% of the total clofazimine mass in the homogenates were recovered in the polyhedrosome fraction, while 95% of proteins were removed. The isolated polyhedrosomes were birefringent, and appeared dark, ruby red in color and needle-like in appearance. Unlike control clofazimine crystals, they were homogenous in shape and size, and polarized light as a single birefringent domain. They did not fluoresce in the green eGFP channel, yet they were brightly fluorescent in the red Cy3 channel (Fig. 4b).

Unlike clofazimine crystals, isolated polyhedrosomes were highly responsive to the environment. Upon exposure to distilled water (Fig. 4c), they burst into smaller birefringent globules which aggregated into large masses and became fluorescent in the green eGFP channel. Upon treatment with 1N NaOH (Fig. 4d), polyhedrosomes underwent localized changes in structure: parts of the elongated polyhedrosomes fragmented and transformed to the green eGFP fluorescent form. Other polyhedrosomes treated in this manner became fluorescent at the tips (arrows). Isolated polyhedrosomes in suspension disintegrated when heated to 100°C for 15 minutes (Fig. 4e). When heated, they turned yellow, became fluorescent in the green eGFP channel, and burst into small globules that remained attached without aggregating to each other. Polyhedrosomes remained largely intact after 0.125 % trypsin-EDTA treatment for 1 hr (Figure 4f).

Based on powder X-ray diffraction of isolated polyhedrosomes (Fig. 4g), a single peak was observed at a small diffraction angle. The absence of diffraction peaks at higher angles was consistent with the liquid crystal-like organization of polyhedrosomes observed by EM (Fig 2).

4.5 Discussion

The ability of clofazimine to induce the formation of highly organized, liquid crystal-like multilamellar structures inside the cells of a mammalian organism is quite remarkable. The organelle-like membrane organization of the polyhedrosomes is an indication that the intracellular membrane organization of mammalian cells is not under strict genetic control. Instead, the results indicate the organization of intracellular membranes can be chemically manipulated with structure-forming molecules like clofazimine, in a manner that had not been previously observed in nature or in test tubes.[22] More importantly, the formation and growth of polyhedrosomes were constrained to the cytoplasm of macrophage-like cells, indicating that such a structure is a product of the cells' biosynthetic machinery interacting with the structure forming molecule in a very specific manner.

We hypothesize that the formation of polyhedrosomes reflects local differences in complex biological processes regulating organelle and cell membrane organization, homeostasis, and cell survival, rather than being purely a result of local differences in the pharmacokinetics and biodistribution of the structure forming molecule. That polyhedrosomes are only associated with a specific cell type is evidence that the formation of such a structure is under epigenetic control. Indeed, although they are

present in different organs of the body, polyhedrosomes are always associated with macrophage-like cells. A local expansion of the macrophage-like cell population was observed in association with microgranulomas formation in the liver, and the splenomegaly phenotype. This suggests that specific macrophage cell growth and differentiation signaling pathways determine the organ accumulation and tissue distribution patterns of polyhedrosomes.

Our results demonstrate that a highly stimulus-responsive, organelle-like supramolecular structure can be constructed through the massive accumulation of an insoluble, structure-forming small molecule within the cells of an animal. Polyhedrosomes possess features of liquid crystals, but their size, shape, distribution, and molecular structure is under biological control. Unlike the natural organelles of eukaryotic cells and unlike inert clofazimine crystals,[6, 23] the distinctive physical, chemical and biological properties of polyhedrosomes sets them in a class of their own. They are most akin to a solid-state, living cell-based micro-device, and they should be genetically tractable and evolvable.

4.6 Acknowledgements

Grant support from GM007767 (to J.B.), and RO1GM078200 (to G.R.R.). Above contents are sole responsibilities of authors, and do not represent the official views of NIH. J.B. was supported by American Foundation for Pharmaceutical Education. We thank Dorothy Sorenson (MIL, Univ. of Michigan), Paula Arrowsmith (PCAR, Univ. of Michigan), Dr. Gerald Hish (ULAM, Univ. of Michigan), and Dr. Robyn Roth (Heuser

lab, Washington Univ., St. Louis) for technical support. We thank Dr. Charles Burant, Dr. Nair Rodriguez-Hornedo, and Dr. David E. Smith for helpful suggestions.

4.7 Figures

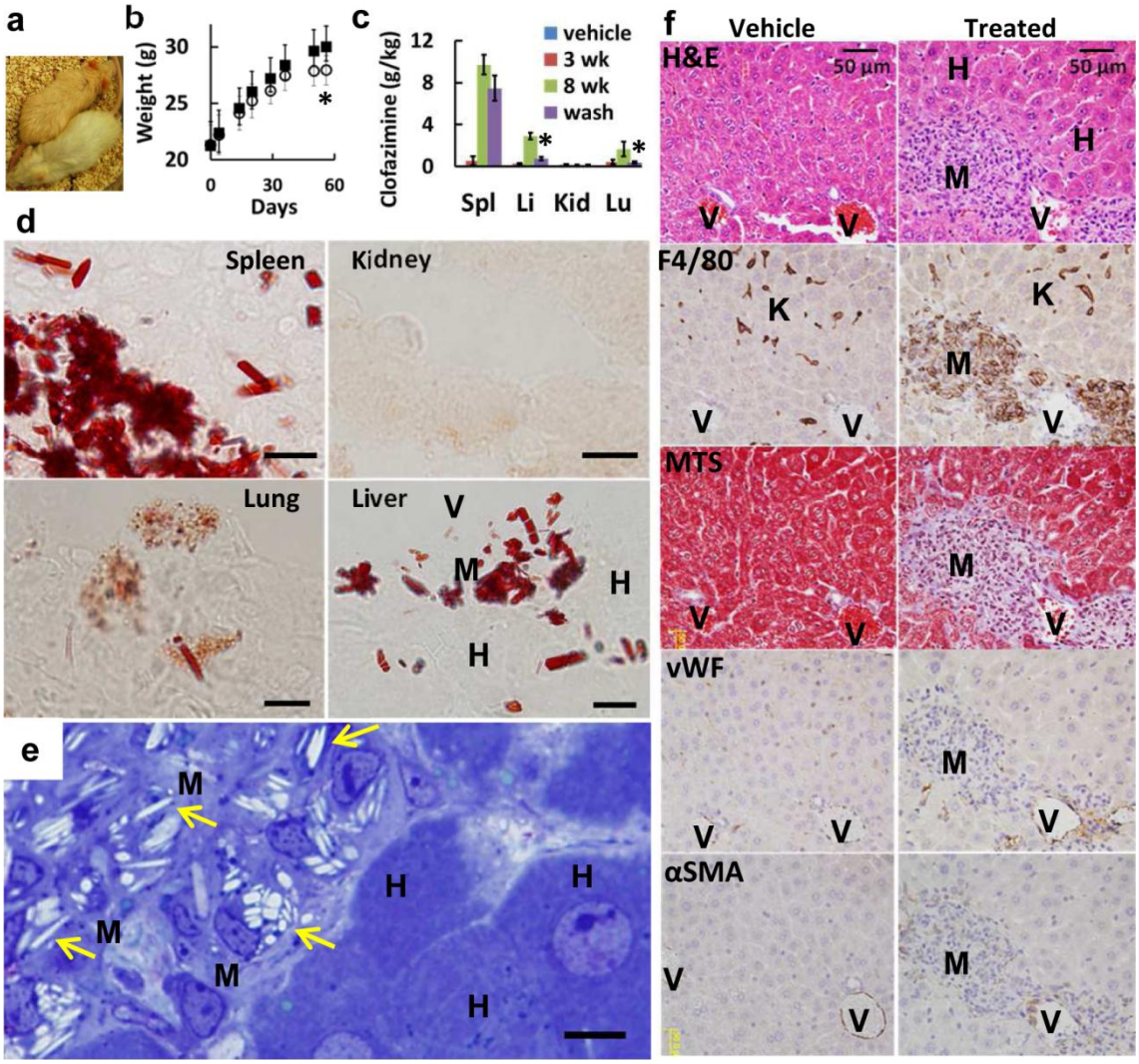

Figure 4-1 Clofazimine inclusions formed in macrophage-like cells *in vivo*.

(**a**) Mice fed with the structure-former for 3 wks (upper) showed reddish pigmentation visible in the ear, tail, and skin when compared to mice treated with vehicle only (lower). (**b**) Weight gains in mice fed with and without structure-former were comparable (n = 40, ■, vehicle; ○, treated; *, $P<0.01$, Student's T-test). (**c**) Biochemical analysis of various organs revealed differences in the accumulation and retention of the structure-former upon wash out (*, $P<0.01$, n = 5 per group, ANOVA). (**d**) Ruby red inclusions appeared in frozen sections of spleen, lung and liver, but not in kidneys of 8 wk drug-diet. H, hepatocyte; V, blood vessel; M, microgranulomas. (**e**) Intracellular inclusions were extracted in perfusion-fixed liver upon EtOH-dehydration and staining with toluidine blue. Arrows indicate needle-like cavities remaining after extraction. (**f**) Histological sections revealed cellular changes in liver of mice fed with the structure-former. H&E,

F4/80 (macrophage), Masson's trichrome staining (MTS, collagen fibers), von Willebrand factor (vWF, endothelium) and alpha-smooth muscle actin (αSMA). K, Kupffer cells. Scale bar = 10 μm unless indicated otherwise.

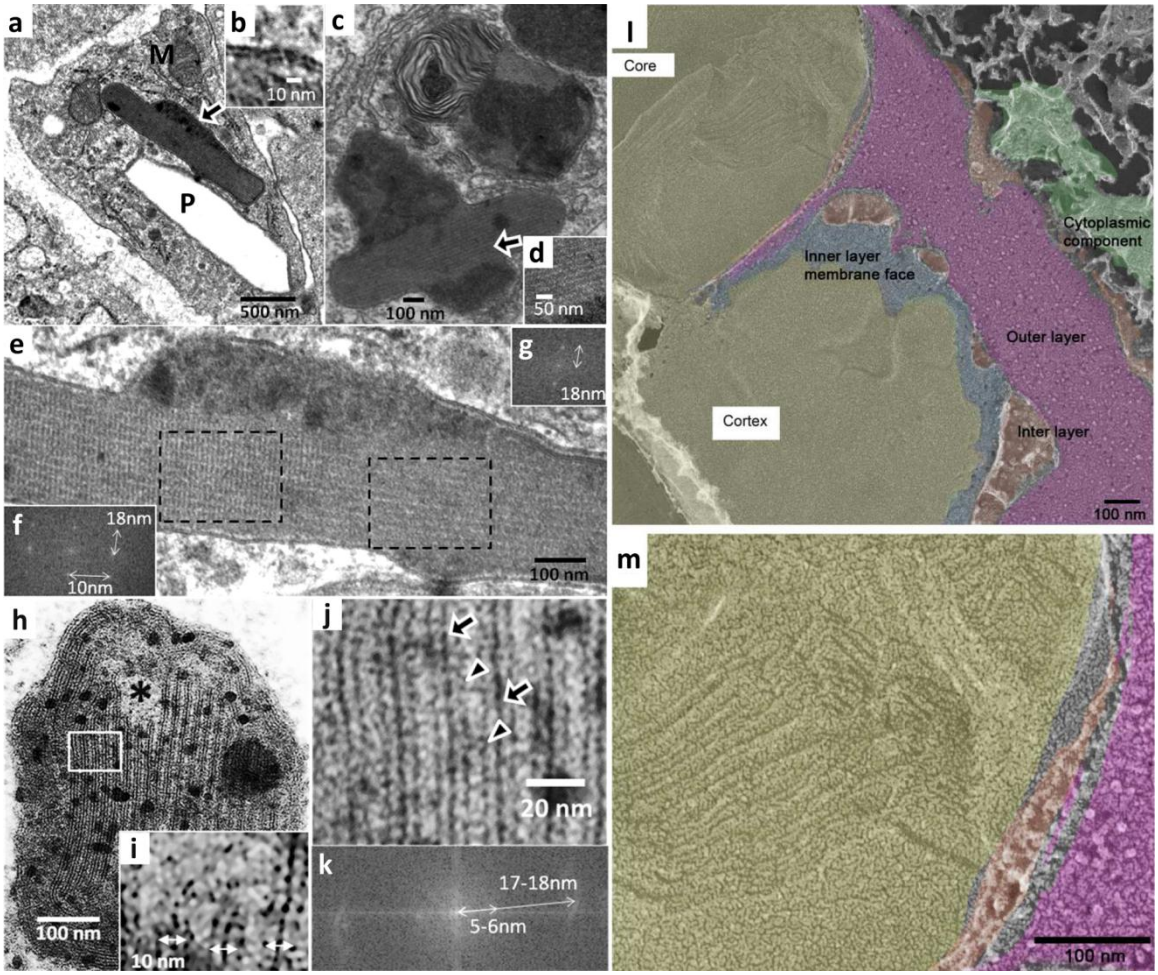

Figure 4-2 TEM analysis revealed the internal structure of polyhedrosomes.

(**a**) Intact polyhedrosomes were observed in the cells of the lamina propria of 8.5 wk treated mouse jejunum. P, extracted polyhedral cavities. M, mitochondria. Arrow: atypical structure, magnified in panel b. (**b**) Polyhedrosomes were delimited by a lipid bilayer. (**c**) Polyhedrosomes appeared to form from heterogeneous granular domains transforming into a lamellar structure (arrow, magnified in **d**), observed in 4.5 wk treated jejunum. (**e**) Zoomed image of the polyhedrosome from (a) showed the lattice-like lamellar structure. (**f**) and (**g**), Fast Fourier Transform confirmed the regular, periodic structure of polyhedrosomes. (**h**) Transversal cross section of polyhedrosomes from 8.5 wk jejunum showed an internal organization of parallel bands and some amorphous regions indicated by (*****). (**i**) Zoomed image revealed the trilayer membrane of 10 nm in width separated by inter-laminar spaces continuous with amorphous region. (**j**) Zoomed image of rectangle in (h), showing trilayer membrane structure comprised of a central dark band (arrows) flanked by a pair of less prominent, dark bands (triangles) on either side. The central band and flanking bands are separated by clear 5 nm space. The trilayer membranes were regularly spaced and formed planar stacks, with the central bands exhibiting the 18 nm spacing observed with FFT (**k**). (**l**) Unfixed liver of 6 wk treated mouse was processed with FEEM analysis. The polyhedrosome was wrapped by double membrane (blue and purple) which was surrounded by cytoplasmic components

(green). The inner cortex and core showed a multilayered organization with no evidence of lateral molecular ordering (**m**).

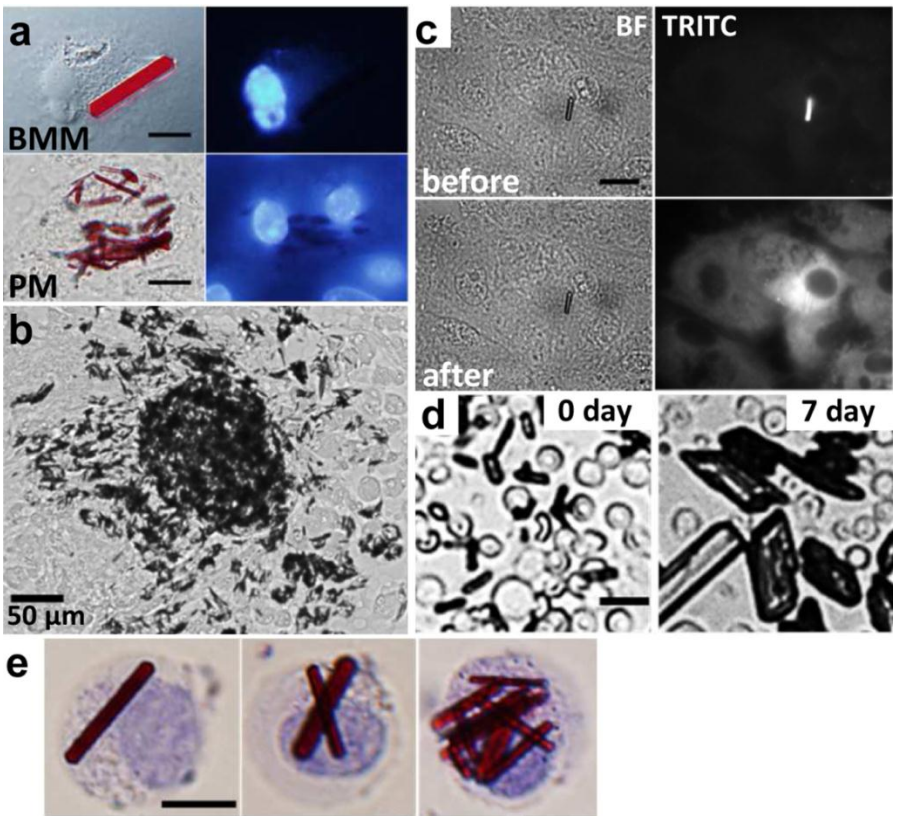

Figure 4-3 Macrophages containing intracellular polyhedrosomes were collected, plated and studied *in vitro*.

(**a**) Bone marrow macrophage (BMM) and thioglycollate elicited peritoneal macrophages (PM) were obtained from mice fed with structure-former, attached and spread on tissue culture plastic, and were stained with Hoechst 33342 to show nuclei. (**b**) Peritoneal macrophages with polyhedrosomes migrated away from large clusters when plated on tissue culture dishes. (**c**) Blue light triggers structure-former release from polyhedrosomes in peritoneal macrophages, observed in TRITC channel. (**d**) Extracellular polyhedrosomes grew in size and became irregular in morphology, unlike intracellular polyhedrosomes. Red blood cells in the background serve as size markers, for reference. (**e**) Polyhedrosomes inside bone marrow-derived cells in suspension, stained with Trypan Blue. Scale bars = 10 µm unless otherwise indicated.

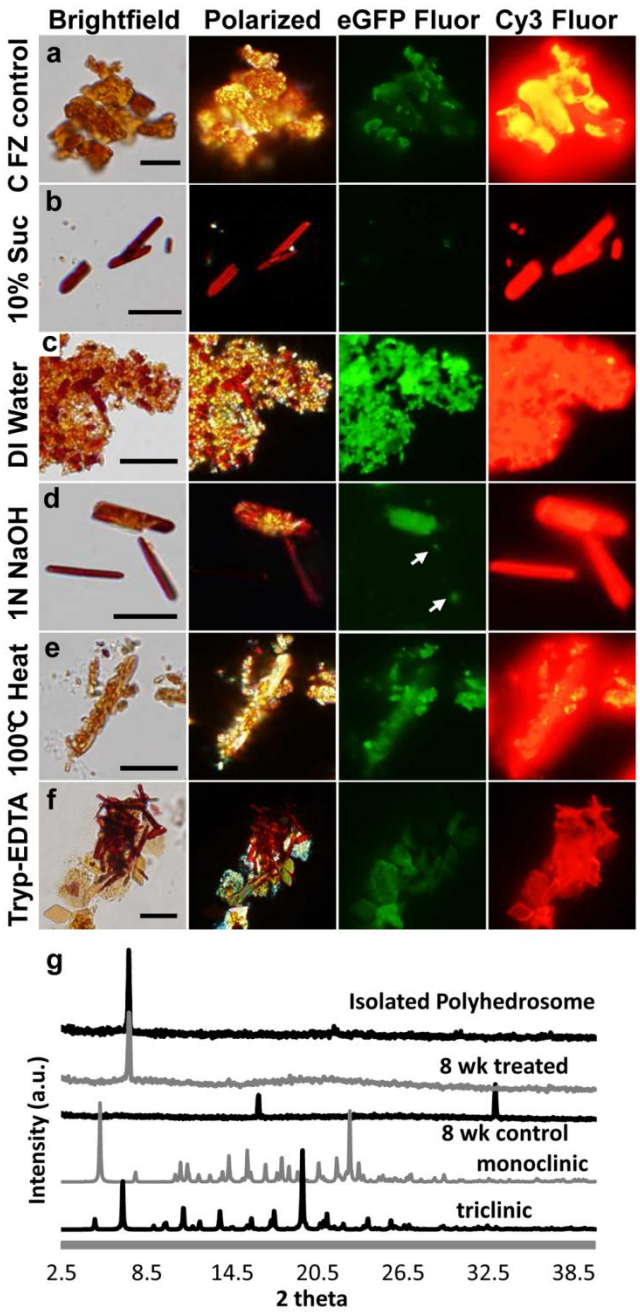

Figure 4-4 Polyhedrosomes respond to stimuli.

Birefringence, fluorescence under eGFP or Cy3 channel showed clofazimine crystals (control, **a**) were unchanged upon different treatments. (**b**) Isolated polyhedrosomes remained intact in isotonic solution of 10% sucrose in water. (**c**) Isolated polyhedrosomes burst and aggregated in distilled water. (**d**) After exposure to 1N NaOH, isolated polyhedrosomes partially disintegrated from different parts. Arrows point to the tips of polyhedrosome that were fluorescent in the green channel. (**e**) After 15 min at 100°C, polyhedrosomes fragmented and changed to a pale orange color. (**f**) Polyhedrosomes remained relatively intact after 30 min sonication and 1 hour trypsin

treatment. Scale bar = 10 µm. (**g**) Powder X-ray diffractogram for isolated polyhedrosomes and 8 wk treated mouse spleen homogenate had single peak at 2 theta = 7.2. Vehicle-treated mouse spleen (8 wk control) and neither of clofazimine crystal polymorphs (monoclinic and triclinic) showed corresponding peaks.

4.8 References

1. Wishart, D. S.; Knox, C.; Guo, A. C.; Cheng, D.; Shrivastava, S.; Tzur, D.; Gautam, B.; Hassanali, M. DrugBank: a knowledgebase for drugs, drug actions and drug targets. *Nucleic Acids Research* **2008,** *36*, (suppl 1), D901-D906.

2. Petri, W. A. J., Drugs for Leprosy. In *Goodman and Gilman's The Pharmacological Basis of Therapeutics*, 11 ed.; Brunton, L. L.; Lazo, J. S.; Parker, K. L., McGraw-Hill: New York, **2006**; 1218-1221.

3. Barry, V. C.; Belton, J. G.; Conalty, M. L.; Denneny, J. M.; Edward, D. W.; O'Sullivan, J. F.; Twomey, D.; Winder, F. A new series of phenazines (rimino-compounds) with high antituberculosis activity. *Nature* **1957,** *179*, (4568), 1013-5.

4. Conalty, M. L.; Barry, V. C.; Jina, A. The antileprosy agent B.663 (Clofazimine) and the reticuloendothelial system. *Int J Lepr Other Mycobact Dis* **1971,** *39*, (2), 479-92.

5. Delhanty, J. D.; Attwood, J.; Wilkie, D. The effect of Lampren on human cells in culture. *Br J Exp Pathol* **1974,** *55*, (1), 13-9.

6. Baik, J.; Rosania, G. R. Molecular Imaging of Intracellular Drug-Membrane Aggregate Formation. *Molecular Pharmaceutics* **2011**, DOI:10.1021/mp200101b.

7. Venkatesan, K.; Deo, N.; Gupta, U. D. Tissue distribution and deposition of clofazimine in mice following oral administration with or without isoniazid. *Arzneimittelforschung* **2007,** *57*, (7), 472-4.

8. Heuser, J. Protocol for 3-D visualization of molecules on mica via the quick-freeze, deep-etch technique. *J Electron Microsc Tech* **1989,** *13*, (3), 244-63.

9. Leijh, P. C.; van Zwet, T. L.; ter Kuile, M. N.; van Furth, R. Effect of thioglycolate on phagocytic and microbicidal activities of peritoneal macrophages. *Infect Immun* **1984,** *46*, (2), 448-52.

10. Racoosin, E. L.; Swanson, J. A. Macrophage colony-stimulating factor (rM-CSF) stimulates pinocytosis in bone marrow-derived macrophages. *J Exp Med* **1989,** *170*, (5), 1635-48.

11. Aplin, R. T.; McDougall, A. C. Identification of crystals of the rimino-phenazine compound B663 (Lamprene: clofazimine) in mouse spleen macrophages by thin layer chromatography and mass spectrum analysis. *Experientia* **1975,** *31*, (4), 468-9.

12. McDougall, A. C. Electron microscope studies of the antileprosy drug B663 (clofazimine; Lamprene). *Int J Lepr Other Mycobact Dis* **1974,** *42*, (1), 1-12.

13. Mansfield, R. E. Tissue concentrations of clofazimine (B663) in man. *Am J Trop Med Hyg* **1974,** *23*, (6), 1116-9.

14. Griffis, L. C.; Twerdok, L. E.; Francke-Carroll, S.; Biles, R. W.; Schroeder, R. E.; Bolte, H.; Faust, H.; Hall, W. C.; Rojko, J. Comparative 90-day dietary study of paraffin wax in Fischer-344 and Sprague-Dawley rats. *Food Chem Toxicol* **2010,** *48*, (1), 363-72.

15. Williams, G. T.; Williams, W. J. Granulomatous inflammation--a review. *Journal of Clinical Pathology* **1983,** *36*, (7), 723-733.

16. Rhodin, J. A., *An Atlas of Histology*. Oxford University Press: New York, **1975**.

17. Atkinson, A. J., Jr.; Sheagren, J. N.; Rubio, J. B.; Knight, V. Evaluation of B.663 in human leprosy. *Int J Lepr Other Mycobact Dis* **1967,** *35*, (2), 119-27.

18. Desikan, K. V.; Ramanujam, K.; Ramu, G.; Balakrishnan, S. Autopsy findings in a case of lepromatous leprosy treated with clofazimine. *Lepr Rev* **1975,** *46*, (3), 181-9.

19. Sukpanichnant, S.; Hargrove, N. S.; Kachintorn, U.; Manatsathit, S.; Chanchairujira, T.; Siritanaratkul, N.; Akaraviputh, T.; Thakerngpol, K. Clofazimine-induced crystal-storing histiocytosis producing chronic abdominal pain in a leprosy patient. *Am J Surg Pathol* **2000,** *24*, (1), 129-35.

20. Mason, G. H.; Ellis-Pegler, R. B.; Arthur, J. F. Clofazimine and eosinophilic enteritis. *Lepr Rev* **1977,** *48*, (3), 175-80.

21. McDougall, A. C.; Horsfall, W. R.; Hede, J. E.; Chaplin, A. J. Splenic infarction and tissue accumulation of crystals associated with the use of clofazimine (Lamprene; B663) in the treatment of pyoderma gangrenosum. *Br J Dermatol* **1980,** *102*, (2), 227-30.

22. Almsherqi, Z. A.; Landh, T.; Kohlwein, S. D.; Deng, Y. Chapter 6: cubic membranes the missing dimension of cell membrane organization. *Int Rev Cell Mol Biol* **2009,** *274*, 275-342.

23. Zheng, N.; Zhang, X.; Rosania, G. R. Effect of phospholipidosis on the cellular pharmacokinetics of chloroquine. *J Pharmacol Exp Ther* **2010,** *336*, (3), 661-71.

Chapter 5

Comparative Study of *In Vivo* Crystal-like Drug Inclusions using Transmitted and Freeze-Etch Electron Microscopy

5.1 Abstract

We present three different types of electron microscopic analysis to characterize the polyhedrosomes, ultrastructural organization of crystal-like drug inclusions (CLDIs). The cryo-electron microscopy (cTEM), transmitted electron microscopy (TEM), and freeze-fracture freeze-etch electron microscopy (FEEM) techniques were implemented to find the cytoplasmic structures resembling polyhedrosomes we have discovered in the tissues of clofazimine treated mice. The cytoplasmic structures found in cTEM and TEM were present in macrophages bound by delimiting membranes which were approximately 20 nm in thickness. Along with empty crystalloid cavities, there were polyhedral osmiophilic structures with polyhedral morphology which resembled CLDIs. Some of the structures contained alcohol-proof, highly organized, lattice-like layers regularly spaced between 6 to 17 nm. Under FEEM, the cytoplasmic organelle revealed planar stacks enclosed by 30 nm thick double membranes which contained pillar-like inter-membrane structures. These supramolecular organizations suggested that the internal lamellae could be some type of lipid component rearranged and compacted into a unique

shape which was controlled by the specific biology of macrophages, rather than the crystallization of pure drug molecules.

5.2 Introduction

Previously we have reported an unusual cytoplasmic structure with crystal- and organelle-like features.[1] These subcellular constructs, which we have named "polyhedrosomes", were formed by the highly permeable and extremely lipophilic (logP > 7) antibacterial drug clofazimine, which accumulated inside the macrophages of mice after oral dosing. The polyhedrosomes were vibrantly red, 10 – 20 nm crystal-like needles with highly homogeneous distribution. Through transmitted electron microscopy (TEM), we found polyhedrosomes' internal structures were highly organized membrane configurations ranging from 5 to 18 nm in which drugs of 1 nm in each dimension were presumably sequestered.

Five decades ago, McDougall performed EM study on the macrophages in clofazimine treated mice and found some structures akin to what we described.[2] The structures he found were empty cavities with membrane outlining, which formed polygonal shapes similar to those of the crystal-like drug inclusions (CLDIs) apparent under transmitted light microscopy. He also observed long, featureless "osmiophilic rods" with 3 – 4 nm internal planes running perpendicular to the long axis flanked by two layers of membranes. Nevertheless, searching for direct evidence of a crystalline structure, he was not able to find any evidence indicating they were crystalline, while he confirmed that the dense bodies were not the result of artifacts, after checking impurity, staining, and possible incomplete alcohol dehydration. Unfortunately, he has not

followed up on his initial report and discussion with the further structural analyses that he originally proposed to conduct.

So far, only a small number of techniques have been applied to characterize these polyhedral, needle-shaped structures embedded in the cytoplasm of a small population within lymphatic organs.[1] Optical, polarization, and fluorescence microscopy inspections allowed for visual differentiation between pure drug crystals and intact CLDIs. Unlike the pure drug, the new constructs were stimulus-responsive, sensitive to osmotic pressure, pH, or temperature for example, indicating they were supramolecular complexes that could be manipulated. Nevertheless, the resolution remains insufficient to probe which molecular entities comprise the assembly.

Brief investigation with electron microscopy in our previous study[1] has suggested that polyhedrosomes are membrane bound lattice structures similar to liquid crystal. Therefore, we decided to further scrutinize the EM images in order to extract as much information as possible and investigate how the lipophilic clofazimine molecules are concentrated and become packed in such a unique way. High magnification electron micrographs from different settings including transmitted and freeze-fracture freeze-etch electron microscopy were acquired and compared in attempt to provide a guideline for experiments to investigate molecular entities of polyhedrosomes. These new findings could be the first step towards building and controlling a new construct in cells.

5.3 Materials and Methods

Animal experiment. Mice (4-5 wk male Balb/c) were purchased from Jackson lab (Bar Harbor, Maine) or Harlan lab (Haslett, Michigan) and acclimatized for 2 wks in the

university specific pathogen free animal facility. All animal care and experimental procedures complied with approved protocol by University of Michigan Committee of Use and Care of Animals. Mice were fed with clofazimine (Sigma C8895, St. Louis, MO) with powder diet (3 mg/ml clofazimine in sesame oil (Shirakiku, Japan), mixed at 0.01% oil to food) or with oil mixed diet (vehicle only) as previously described.[1]

5.3.1 cTEM

Mouse perfusion fixation and sample preparation. After euthanasia, blood was removed through cardiac puncture and washed by perfusing 5 ml of 0.9% saline solution at 2.5 ml/min rate injected to left ventricle and egressed to vena cava. Then, 5 ml of fixative in cacodylate buffer (2% formaldehyde, 2.5% glutaraldehyde in 0.15M cacodylate with 2 mM Ca^{2+}, pH 7.4) was infused. Immediately after perfusion, organs were taken out and cut into pieces to 5 mm in each dimension under 1:10 volume of fixative, stored in cold fixative wrapped around with paper towel and sent out to National Center for Microscopy and Imaging Resources (NCMIR). Tissues were cut into 100 μm thick sections using a vibratome and circular tissue punches were taken from the slices (1.5 mm diameter) and then placed into Leica membrane carriers. These wells were filled with 20% BSA in cacodylate and high-pressure frozen in a Leica EM PACT2 HPF apparatus, stored in liquid nitrogen.

Freeze substitution and imaging. Using Leica AFS2 unit, samples were placed in 0.1% tannic acid in anhydrous acetone at -90°C for 89 hours. Samples were then washed 3 times with acetone at -90°C (30 min each), and placed into 2% OsO_4/0.1% uranyl acetate in acetone (-90°C for 7 hours). They were warmed to -20°C for 14 hour, transferred to 4°C for 2 hours. They were washed in dry acetone at room temperature for 10 min (3

times), placed into series of Durcupan:acetone solution: 25:75 for 3 hours, 50:50 overnight, 75:25 for 4 hours and then 100:0 for overnight. 100% Durcupan was refreshed and left in 60°C oven for 2 days. The membrane carriers were dislodged from Durcupan blocks by cooling liquid nitrogen and 80°C warming, then ultrathin sectioned, placed onto copper 300 mesh grids to post stain with 2% aq uranyl acetate for 10 min followed by Sato lead for 5 min. Imaging was carried out with JEOL 1200EX at 80 kV, recorded onto Kodak 4489 film, developed picture was scanned using a Flextight scanner.

5.3.2 TEM

Mouse perfusion fixation. Blood was collected from euthanized mice and washed by perfusing 5 – 6 ml of 0.1M Sorensen's buffer at 2.5 ml/min rate injected to left ventricle and egressed to vena cava. Then, 5 ml of Karnovsky's fixative (3% paraformaldehyde, 2.5% glutaraldehyde, 0.1M Sorensen's buffer, pH 7.4) was infused to result stiffening of the corps, and organs turn pale pink. Immediately after perfusion, organs were taken out for either paraffin fixation or TEM preparation.

Transmission Electron Microscopy. After perfusion fixation, organs were diced on a dish with 10 fold volume of fixative into pieces smaller than 1 mm in each dimension, and preserved in the glass vial with the fixative at 4°C. After rinsing three times with Sorensen's buffer, tissues were fixed with 1% osmium tetroxide in 0.1M Sorensen's buffer and washed three times in the buffer. Dehydration was carried with graded ethanol/water series (50, 70, 90, and two changes of 100%) for 15 min each. After transitioning through three changes of propylene oxide, tissues were infiltrated with Epon resin (Electron Microscopy Sciences), and then polymerized at 60°C for 24 h. The block was then ultramicrotome sectioned to 30 – 70 nm thickness and mounted on copper EM

grid (Electron Microscopy Sciences) which was post-stained with uranyl acetate and lead citrate before TEM imaging with Philips CM-100. Images were recorded digitally using a Hamamatsu ORCA-HR camera system operated by AMT software (Advanced Microscopy Techniques Corp., Danvers, MA). Magnifications: ×2,600 – ×256,000.

5.3.3 Freeze-fracture freeze-etch EM (FEEM)

Liver FEEM. Fresh liver isolated from 6wk treated mouse was washed in cold DPBS and refrigerated and shipped overnight to the Heuser lab in Washington University at St. Louis for Quick-freeze deep-etch EM analysis performed according to published protocol,[3] with minor modification. 3 × 3 × 1.5 mm thick slices of non-fixed liver were frozen by forceful impact against a pure copper block, cooled to 4°K with liquid helium. Frozen samples were mounted in a Balzers 400 vacuum evaporator, fractured and etched for 2.5 min at -104°C and then rotary-replicated with 2 – 3 nm platinum nanoparticles deposited from a 20° angle above the horizontal, followed by an immediate ~10 nm stabilization film of pure carbon deposited from an 85° angle. Replicated samples were placed into a dish of chromo-sulfuric acid cleaning solution (Fisher Scientific, SC88-500) for overnight. Released replicas were passed through several rinses of distilled H_2O and then picked up on formvar coated copper grids, and photographed with on JEOL 1400 microscope with attached AMT digital camera. Stereo images were obtained using a goniometer stage tilt of ±5° and converted to anaglyph in Photoshop®.

Isolated Crystal-like Drug Inclusions. 25 µl aliquots of purified CLDIs were pipetted onto 3 × 3 mm coverslips, which were chromic-sulfuric acid cleaned, water rinsed and air-dried, just before use. Samples were then quick frozen, fractured and etched as described above. Following platinum/carbon coating, samples were floated on the

surface of a dish containing 52% hydrofluoric acid (VWR, Mallinkrodt #2648). Released replicas were transferred with a glass rod through 3 dishes of distilled H_2O, each containing a loopful of Photo-flo, with a 35 min sit between exchanges. Next, the replicas were floated off onto a dish of chromo-sulfuric acid cleaning solution, where they eventually sank below the surface and sat for one hour. Finally, replicas were passed, by pipet, through several rinses of distilled H_2O and picked up on formvar coated grids for viewing as noted above.

Image processing. For display, images were digitally enhanced and overlaid using Photoshop®. For control vs. experimental comparisons within the same figure, contrast and brightness settings were equally adjusted.

5.4 Results

5.4.1 CLDIs have two distinct domains enclosed by 20 nm bilayers (cTEM)

A perfusion fixed liver from a 6 wk clofazimine treated mouse was refrigerated in cacodylate-base fixative and then freeze-substituted for cryo-electron microscopy (cTEM) as described in the Methods. cTEM photographs showed virtually the same CLDI structures as previously described.[1] They were evident as polyhedral cavities delimited by double membranes in the cytoplasm neighboring with intact organelles such as mitochondria and nucleus (Fig 1). There were two atypical intracellular objects, osmiophilic bodies (*) and CLDI cavities (CC), which seemed to be confined within the same boundary of the double layer with 20 nm in thickness (arrow, Fig 1B). It seemed as if the osmiophilic domains were fusing onto the CC within the same organelle-like compartments, paralleling the CCs (white *) or extending from the tips (black *). This

observation suggests that the separate domains are comprised of different molecular components that react differently to the sample fixation and rigorous processing (Fig 1C and D). The cavities and osmiophilic bodies were consistent with what has been previously described in the literature.[1, 2, 4]

5.4.2 Jejunal villus show polyhedrosomes with 10 – 17 nm spaced lamellae (TEM)

The jejunum of the mouse fed with clofazimine diet for 8.5 wks was perfused with glutaraldehyde containing Karnovsky's fixative as described in the Methods.[1] Under TEM, we found polyhedrosomes containing supramolecular osmiophilic lattice organization, which were not seen in the samples from control mice treated with a vehicle-only diet (Fig 2A). Since the composition of these structures was different from the alcohol washable component that was emptied from ethanol dehydration and resin infiltration, these domains were previously dubbed as "polyhedrosomes (PD)" in order to distinguish them from the CLDIs.[1] Similar to the cTEM images described above, they were bound by 20 nm thick delimiting membranes (Fig 2A inset), which were much thicker, for example, compared to typical membrane structures found in cytoplasm, mitochondrial or plasma membrane. Interestingly, when the PD region is magnified (Fig 2B), a supramolecular structure was revealed with a regular stacks of 10 nm lamellae as analyzed by Fast Fourier Transform (FFT, Fig 2B inset).

Another macrophage found in a different villus contained a neighboring CLDI cavity (CC) and polyhedrosomes of similar size and morphology, which revealed apparent internal structures (Fig 2C). The content in CC was emptied out only leaving a 20 nm outer double layer (Fig 2C1), but one of the polyhedrosomes maintained two

unwashable domains that appeared as a darker amorphous region (Fig 2C2) vs. faintly stained lamellae (Fig 2C3) with 17 nm spacing oriented along the long axis. Notably, some of the CLDI positive cells' cytoplasms had rigid linings or rod-like structures which morphologically resembled the endoplasmic reticulum or Golgi apparatus, located next to the osmiophilic bodies (OB) of polyhedral shape. In a zoomed-in view (Fig 2E), these much darker and thicker linings corresponded to 10 nm tubes flanked by outer tubes akin to structures previously reported.[1, 2]

5.4.3 Stacking pattern of lamellae can vary between polyhedrosomes

In addition to 8.5 wk treatment samples, several polyhedrosome images were collected from mice at washout phase, an 8 wk clofazimine diet followed by 8 wks of drug-free diet for the drug to be cleared out. Although the clofazimine content at this stage in the jejunum decreased significantly, the CLDIs were abundant for ultrastructural study.[1] Under TEM analysis, multiple polyhedral structures were witnessed next to the CLDI cavities (Fig 3A and B) and when these structures were magnified, the internal lattice-like organization was observed (Fig 3C). The individual polyhedrosomes were juxtaposed with each other; however, they had different spacings and intersecting angles as shown in Fig 3PD1 and Fig 3PD2 that ranged from 6 to 10 nm and between 25° to 61°.

The majority of the polyhedrosomes aligned themselves together with CC and assumed polygonal outlines, but occasionally we found transversal sections of the intracellular placement (Fig 4A). One of the polyhedrosomes (*) was magnified to show the stacked layers within hexagonal silhouette (B). When the internal structure was further magnified (C), we found struts layered in two different orientations within a

double membrane bound structure, as represented in FFT. Lattice spacings were about 10 nm apart intersecting at a 55° angle.

In the liver samples of washout phase and 8.5 wk treated mice, multiple domains of CLDIs were observed as described above (Fig 5A and B). Juxtaposed with CC, the osmiophilic bodies (arrows) appeared at 200 – 300 nm in size, and their dark polygonal shapes were limited by the fragmented CLDI membranes. Since the results were comparable to the previous TEM and immunohistochemical analyses from liver microgranulomas, we sought to further investigate the liver samples in 3D.

5.4.4 FEEM shows intact polyhedrosomes in 3 dimension

The freeze-fracture freeze-etch EM technique quickly freezes an unfixed sample and generates a metal replica that can diffract electron beam. A mouse treated with a clofazimine diet for 6 wk was euthanized, exsanguinated, and then the liver was refrigerated for overnight shipment. The sample was frozen in liquid helium to minimize the distortion from water crystals, and fractured under vacuum. After a small fraction of water was sublimated (freeze-etch technique), the samples were shadowed with platinum and carbon nanoparticles which limited the resolution of the acquired images to 2 nm.[5] In the liver, many cytoplasmic components appeared intact, including vesicles and mitochondria filling the background of needle-shaped CLDIs (Fig 6A and B). They were 200 to 400 nm wide, and parts of the long axis were embedded in cytoplasmic material. There were planar layers along the long axis of CLDIs and because these struts were absent in the mitochondrial membranes nearby, they are suggested to be polyhedrosomes, which are CLDIs with internal organization. In some parts of the cells, there were rigid bodies similar to the structure in Fig 2D (Fig 6C), in that they also had outer delimiting

membranes (Fig 6D). In addition, there were vesicles (V) fusing onto the existing rigid, needle-like CLDIs comparable to early investigation with TEMs (Fig 6E and 6F).

Captivatingly, the freeze-fracture method preserved the outer membrane structure and internal stacks of emerging CLDI from the cytoplasm of a liver cell (Fig 7A). They assumed a hexagonal shape covered with the lipid membranes, and inner stacks appeared as a coarse texture that fractured to expose a more diverse pattern than any particular plane as seen earlier in Fig 6A. Also, in close proximity to hexagonal polyhedrosomes, an ER-like rigid body was often juxtaposed for possible fusion (arrow, Fig 7B).

5.4.5 Polyhedrosomes have internal stacks of 6 – 14 nm lamellae and outer membranes connected to cytoplasm

During the fracture, we could visualize a more detailed structure of polyhedrosomes including the internal stacks with different spacing as well as the separation interface between the delimiting double layers (Fig 8A). The rigid body was roughly 500 – 700 nm wide and the outer membrane was peeled away to reveal the texture of the inner membrane that directly contacted the internal material (Fig 8B). They appeared to have compact planes stacked parallel to the x-y plane which were presumably separated due to relatively weak interaction in the z-direction. However, since these stacks were cut unevenly, i.e., fractured in curves, the differences in spacings in FFT analysis did not result in well-defined dots (Fig 8C). Therefore, the measured spacings between the parallel stacks along the long axis ranged between 6 to 14 nm owing to an angled view.

The inner surface of the double layer revealed a cracked texture, dark lining of 10 nm in size (Fig 8D). These features may have resulted from the uneven deposition of

platinum nanoparticles, possibly interacting with the peculiar surface characteristics of what it is masking underneath. The fractured double layer also revealed inter-membrane particles within the separated membranes (arrowhead, Fig 8E). These globular objects were about 12 – 13 nm in size, which were relatively too big for an inter-membrane protein particle, as described in the literature.[5] Notably, the cross section of the double layer was clearly demonstrated at the edge of the unwrapped membrane with approximately 30 nm spacing (Fig 8F). Between the two membranes, there were connecting pillars (arrows) that were 20 nm in height and 12 – 13 nm in width, corresponding to the inter-membrane particles found in Fig 8E.

Almost complete removal of the surrounding bilayers uncovered 3-dimensional geometry of the internal stacks (Fig 9A). The planar structures and elevation of these layers were evident in the upper polyhedrosome. A neighboring structure uncovered of the outer layer showed the membrane morphology similar to that which has been observed. When further zoomed in, the internal lamellae appeared as stacks below the x-y plane, packing normal the z-axis (Fig 9B). As the planar layers were elevated, the upper portion of the section rotated around the y-axis and became angled to the x-y plane.

5.4.6 Isolated CLDIs maintain similar structures but appear larger in size

Using differential centrifugation and sucrose density gradient centrifugation, a significant portion of the CLDIs could be purified to perform further analysis.[1] These structures were mounted on slide glass to be processed for free-etch EM and the results were shown here as distinctive structures among cytoplasmic debris (Fig 10A). Although the structures appear comparable to CLDIs from the liver, they were significantly larger in size, ranging several micrometers in width. This is probably due to the fact that

samples were placed in flat, rather than upright position; therefore the majority of CLDIs were fractured along the long axis, while transversal sections were unlikely to appear. Although the isolation procedure involved a sonication process in order to dissociate cytoplasmic components from the polyhedrosomes, there was evidence of strong adhesion between the vesicle-like structure and the polyhedrosomes (Fig 10B). This was similar to an amorphous domain merging onto crystalline layers as observed in the previous samples. Meanwhile, the multilayered and uneven fracture plane has exposed the internal lamellae of the isolated CLDIs, demonstrating the same structure integration among polyhedrosomes which is distinct from that of any other organelles in cells (Fig 10C).

5.5 Discussion

The structural features of new subcellular construct was recorded using different types of electron microscopy to deduce structural information that would suggest what the composition of polyhedrosomes could be and how they would assemble. Arguably, they were distinct from pure drug crystals as they had multiple domains with internal organization and delimiting double membranes.

We have found that polyhedrosomes contain highly organized internal lamellae with 6 – 17 nm stacks often crossed at angles between 25° and 61°. These layers were often oriented longitudinally along the long axis of the needle-shaped structure, occasionally revealing transversal sections with polyhedral outline. The inner stacks are confined by the delimiting double membranes, 10 – 30 nm in thickness, which could be separated to show the distinctive texture of the inter-membrane space. Within these

spaces, channel-like pillar substructures were seen, through which the inside of the polyhedrosomes seemed to be connected to the surrounding cytoplasm, and once the double layers were separated, they would appear as 12 – 13 nm particles. In addition, we observed vesicles fusing onto the polyhedrosomes, presumably corresponding to a cargo compartment filled with amorphous, cellular materials.

One of the biological membrane organizations that the polyhedrosomes resemble was lyotropic liquid crystalline, whose assembly phase can change depending on the temperature and concentration of its constituents. Several researchers also have reported self-assembled lipid models and biological membrane systems in chemical mixtures, studying them using freeze-fracture electron microscopy.[6-9] For example, Hope et al. reviewed various conditions of phospholipid compositions and reported that a common lipidic bilayer organization could transition into hexagonal H_{II} phase.[7, 9] In such uncommon lipid polymorphism, the components were packed as stacks of cylindrical tubes assembled in a way that the hydrophilic head group of lipids were facing inward to the lumen of 2 nm diameter cylinders.[6] If this structure were fractured in longitudinal section, a distinctive planar structure would appear with varying periodicity from 4 – 15 nm, depending on the lipid composition.[6] When sectioned transversely, it would appear as a hexagonal array, which the polyhedrosome transverse section would resemble to a certain extent. However, it is important to note that the polyhedrosomes we found were different from bundles of cylindrical tubes, and rather it was arranged more as stacks of planes indicating that they are distinct supramolecular structures.

Although we could not come up with a comparable model system, we found that membrane rearrangements could be influenced by manipulating pH, ionic constituents or

protein contents.[6, 9] Tarahovsky et al. tested the electrostatic factor by preparing lipid mixtures of varying molar ratios of anionic and cationic phospholipids, and as a result, found lipidic phases transitioning from lamellar into sponge phase, from sponge to cubic phase, and finally from cubic to inverted hexagonal H_{II} phase.[8] Once the two lipid constituents, EDOPC (1,2-dioleoyl-*sn*-glycero-3-ethylphosphocholine, +1 charge) and cardiolipin (–2 charge), were mixed to 2:1 molar ratio, therefore having a 1:1 charge ratio, the resulting lipidic phase appeared birefringent and became an adhesive gel with a regular spacing of roughly 6 nm. When the charge ratio was increased or decreased by adding smaller or larger amounts of EDOPC, the resulting mixture lost the birefringence while the membrane organization increased the size of the spacing from 10 to 13 nm and eventually lost lattice spacing. These results suggest that a highly organized polymorphic structure could develop from lamellar or amorphous structures as we have witnessed in our study. The lamellar structures in the subcellular drug inclusion were evident, and they often merged onto the existing, mature structures. Since clofazimine has two basic amines, they can become positively charged in acidic organelles, and therefore possibly behave similarly as EDOPC. It is possible that protonated clofazimine molecules interact with cardiolipin, thereby reorganizing the lipidic phase as clofazimine further accumulates and changes the composition ratio in the membranes.

Since the formation of the polyhedrosomes was induced exclusively in macrophages, and hepatocytes or adipocytes were free of the CLDIs, it is reasonable to think that the physiology of macrophages expresses a unique, biological functionality that controls the formation and distribution of the polyhedrosomes. In consistent with kidney medulla epithelium lacking CLDIs or polyhedrosomes, cell types appear to be important

in determining what morphology of a structure they can build: whether they would produce many autophagosome-like drug inclusions corresponding to lamellar to sponge phases, or would alternatively build the highly organized, supramolecular, crystal-like drug inclusions. Even with a continued supply of clofazimine, it seemed that MDCK cells and renal tubular cells in mice were incapable of producing CLDIs, indicating that these cells might be deficient of cardiolipin or equivalent that can hypothetically form complexes with clofazimine.

In summary, we have presented a comparative electron microscopic analysis on clofazimine induced subcellular constructs, polyhedrosomes, for their unique structural organization. By comparing previously studied freeze-fracture membrane model systems, we found that the polyhedrosomes are different from any lipid model systems currently known. However, since some aspects of the polyhedrosomes resemble liquid crystalline or hexagonal arrangements, we suspect important roles of pH and concentration of the co-formers. For future studies, it is recommended to investigate clofazimine-cardiolipin mixtures, and to analyze them with ^{31}P NMR (nuclear magnetic resonance) which is known to be capable of distinguishing the hexagonal H_{II} polymorphism from the common lipid bilayers. In terms of macrophages, it would be beneficial to search for an increased level of cardiolipin or determine if its lipogenesis pathway has been upregulated upon clofazimine treatment.

5.6 Acknowledgements

The project was supported by grant number GM007767 from NIGMS for J.B., and by NIH grant RO1GM078200 to G.R.R. Its contents are solely the responsibility of the

authors and do not necessarily represent the official views of NIGMS or NIH. J.B. was supported by American Foundation for Pharmaceutical Education. We thank Dorothy Sorenson (MIL, Univ. of Michigan), and Dr. Gerald Hish (ULAM, Univ. of Michigan) for technical support. We also thank Dr. Robyn Roth from Heuser lab at Washington University at St. Louis (Department of Cell biology) for freeze-fracture freeze-etch EM, and Dr. Eric Bushong for freeze-substitution and microscopy at the National Center for Microscopy and Imaging Resources (Grant 5P41RR004050 to Mark H. Ellisman). We thank Dr. Charles Burant, Dr. Nair Rodriguez-Hornedo, and Dr. David E. Smith for insightful comments.

5.7 Figures

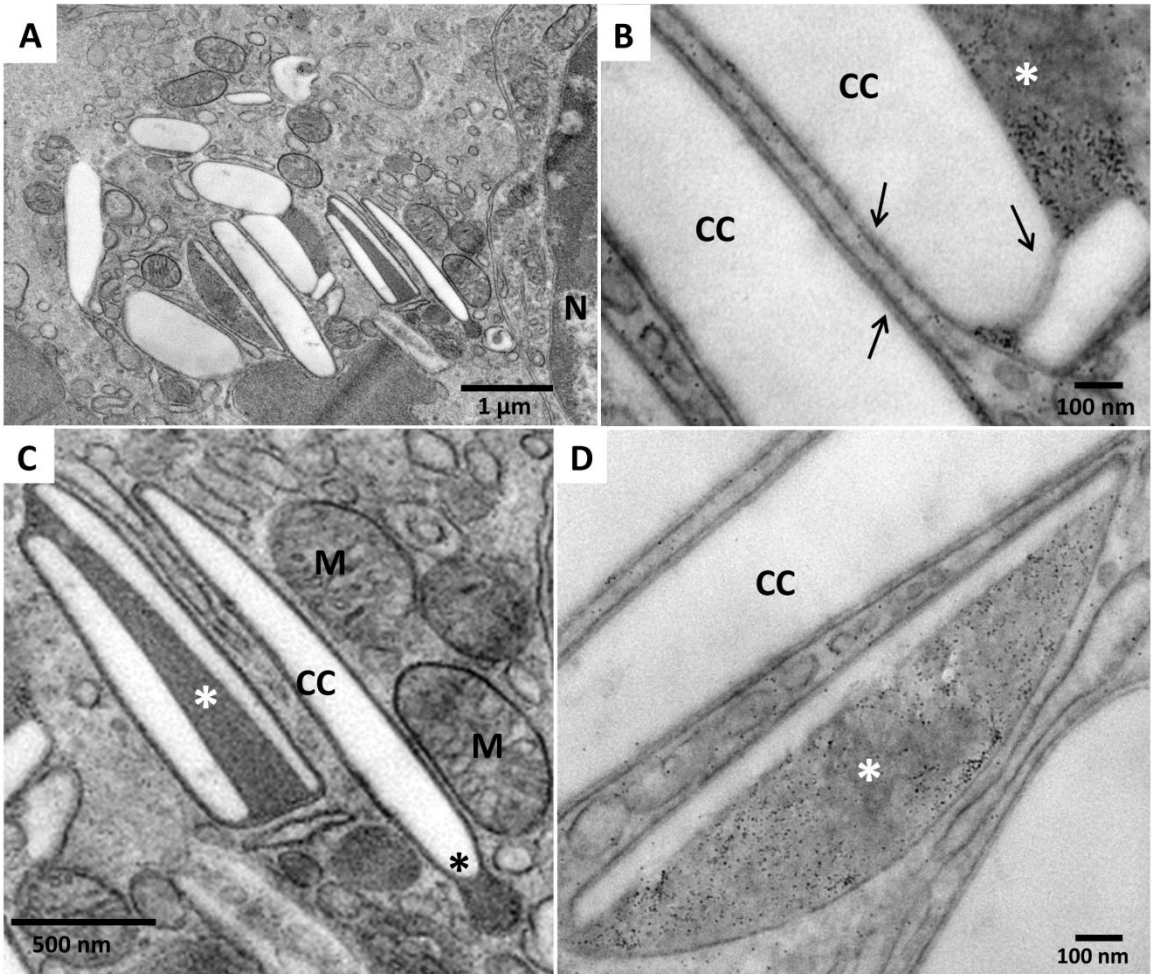

Figure 5-1 cTEM, 6 wk treated mouse liver macrophage

(**A**), Cytoplasm of liver macrophage contained CLDI cavities (CC), which appeared as polyhedral spaces of several micrometers. (**B**), CCs are double membrane bound structure (arrow), and the thicknesses of the double membranes were approximately 20 nm. (**C**), higher magnification of CC along with mitochondria (M) is shown. CLDI has multiple domains: osmiophilic materials (*) were connected to empty spaces where contents were washed out during the sample preparation. (**D**), osmiophilic body (*) was confined within the same delimiting membrane with the empty spaces.

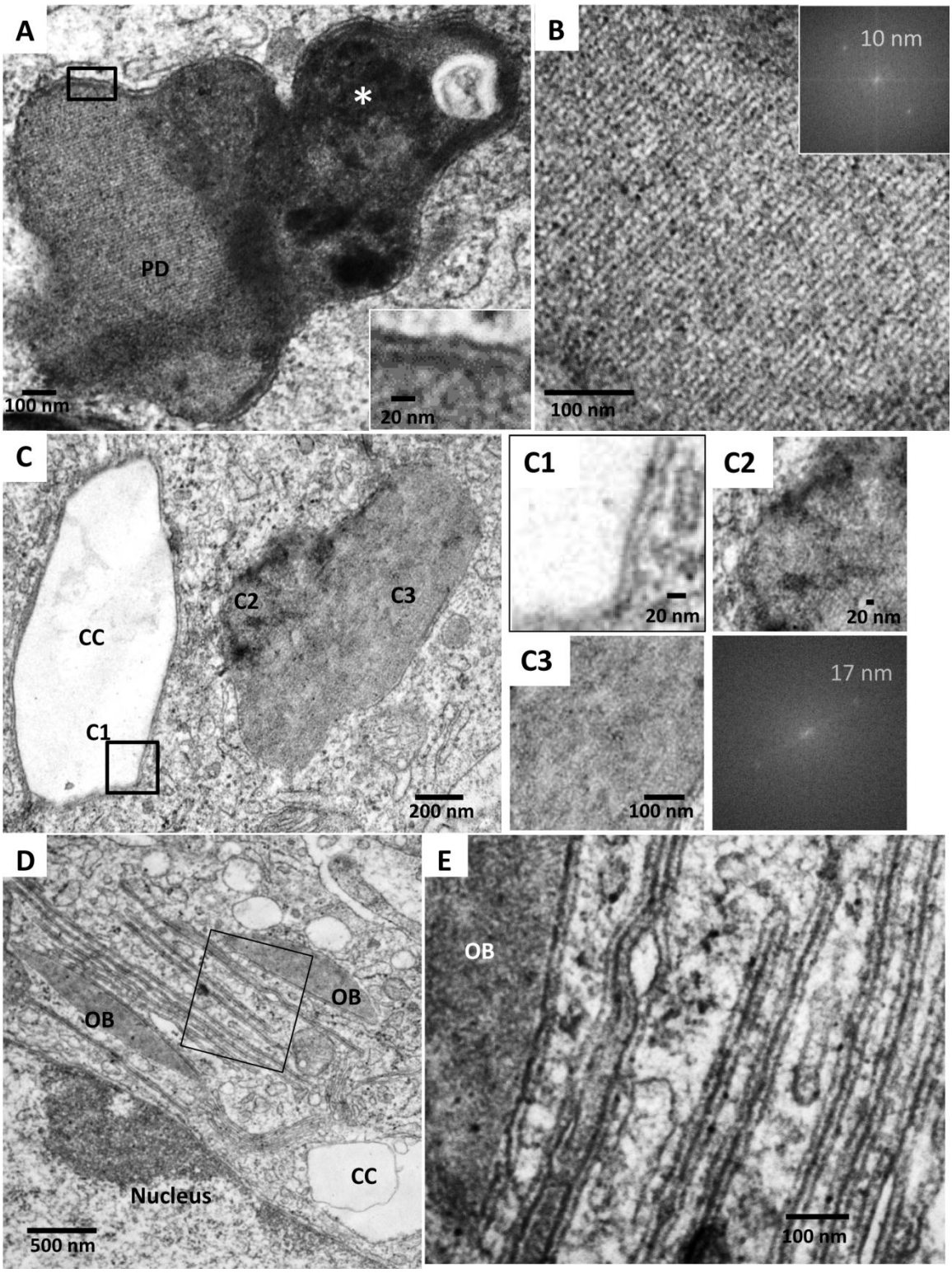

Figure 5-2 TEM, polyhedrosomes found in 8.5 wk treated mice jejunum

(**A**), Inside a macrophage found in a villus, a 20 nm membrane-bound (inset) cytoplasmic structure revealed two distinguished regions: polyhedrosome (PD) and more osmiophilic,

amorphous region (*). (**B**), PD from panel A was magnified, and Fast Fourier Transform (inset) indicated 10 nm of regular spacing. (**C**), CC and a neighboring polyhedrosome were found in a cytoplasm. Boxed region shows double membrane with 20 nm thicknesses (**C1**), while polyhedrosome also revealed two distinguishable regions: amorphous (**C2**) and crystalline region (**C3**) only which shows 17 nm spots in the FFT. (**D**), in some macrophages, there were rigid lining of tubes next to the CC. Inner portion of these tube-like structures had much darker osmiophilic stain flanked by 10 nm layers on each side (**E**).

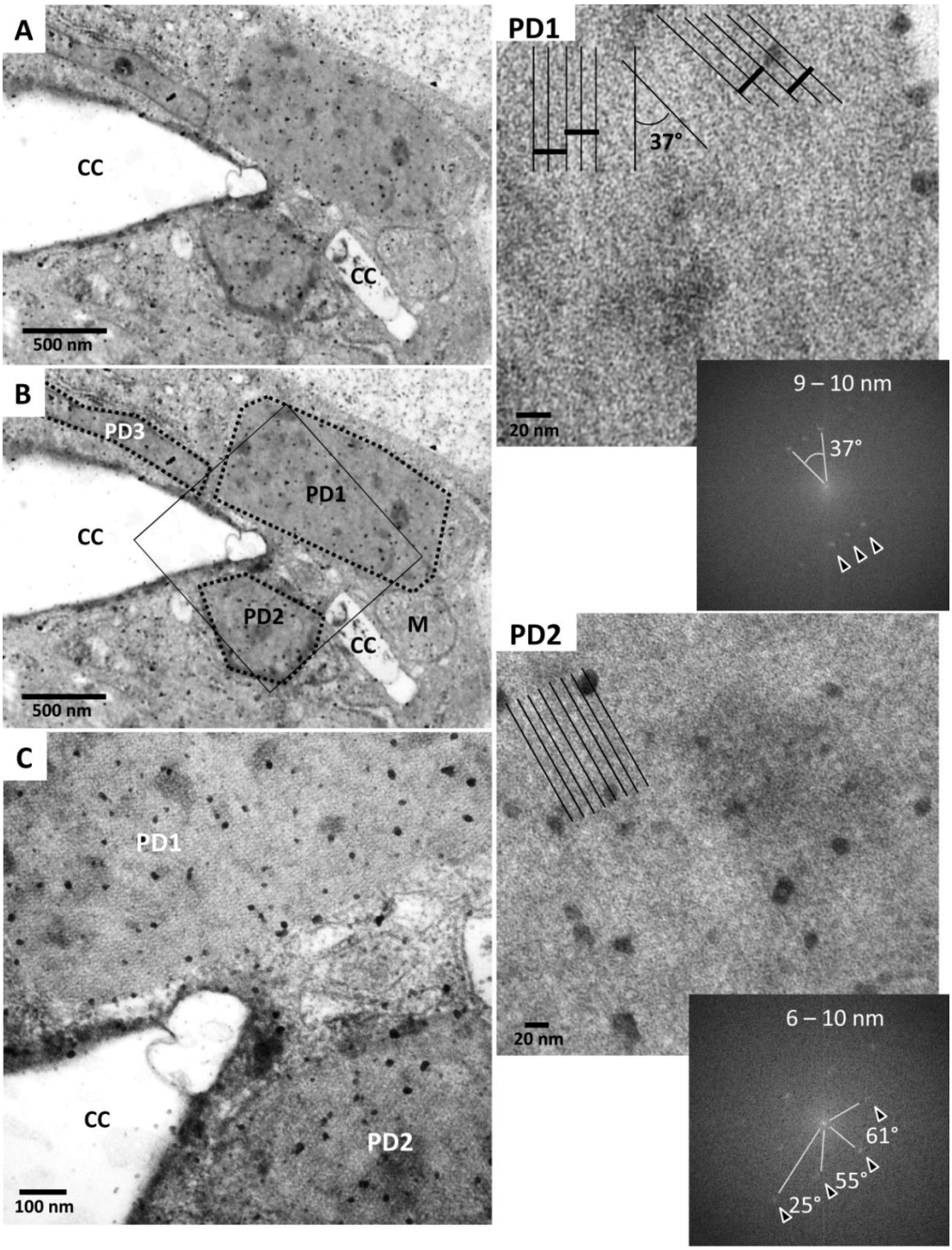

Figure 5-3 TEM, polyhedrosomes found in jejunum villus from washout

(**A**, **B**), CLDI cavities (CC) and three polyhedrosomes (PD) within a cytoplasm of a macrophage. M: mitochondrion. (**C**), Magnified region of the box from panel B shows lattice organization in two different polyhedrosomes, each of which are further magnified (**PD1** and **PD2**) with FFT analysis to show the regular, yet diverse spacing. Internal lamellae were intersecting at varying angles.

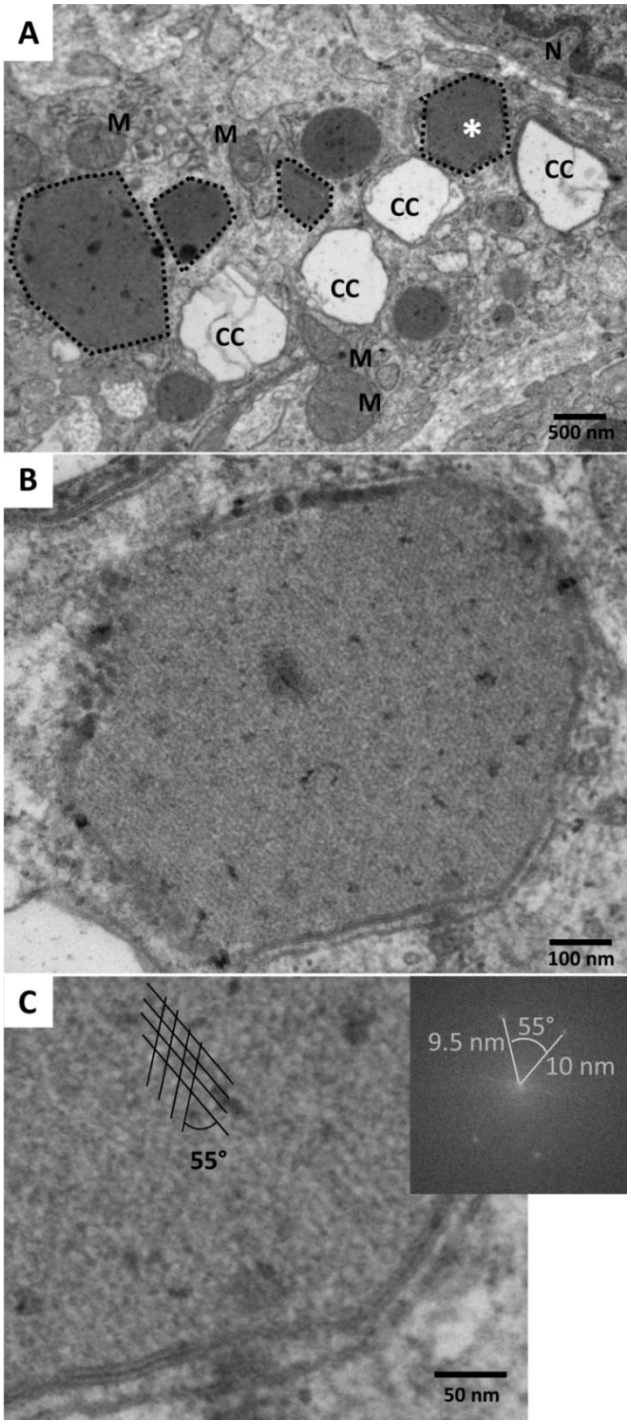

Figure 5-4 TEM, cross section of polyhedrosomes in a macrophage

(**A**), In a section from a washout mouse jejunum, polyhedrosomes were delimited by dashed lines. M: mitochondria, N: nucleus. (**B**), one of the PDs (*) from panel A was magnified. (**C**), internal lamellae revealed a meshwork organization with about 10 nm thickness intersecting at 55° angle in FFT.

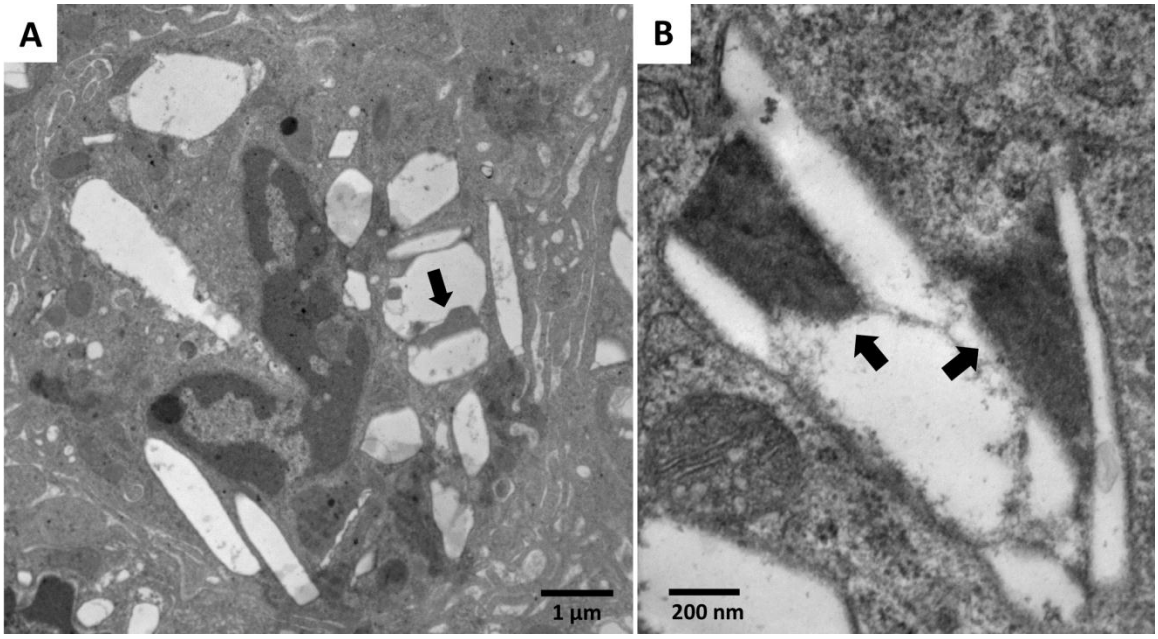

Figure 5-5 TEM, macrophage from liver microgranulomas

Samples from a washout mouse (**A**) and 8.5 wk treated mouse (**B**). Among CLDI cavities, polyhedrosome formed in between (A, arrow). Equivalent region in a higher magnification of another cell shows similar osmiophilic components between the CCs (B, arrows).

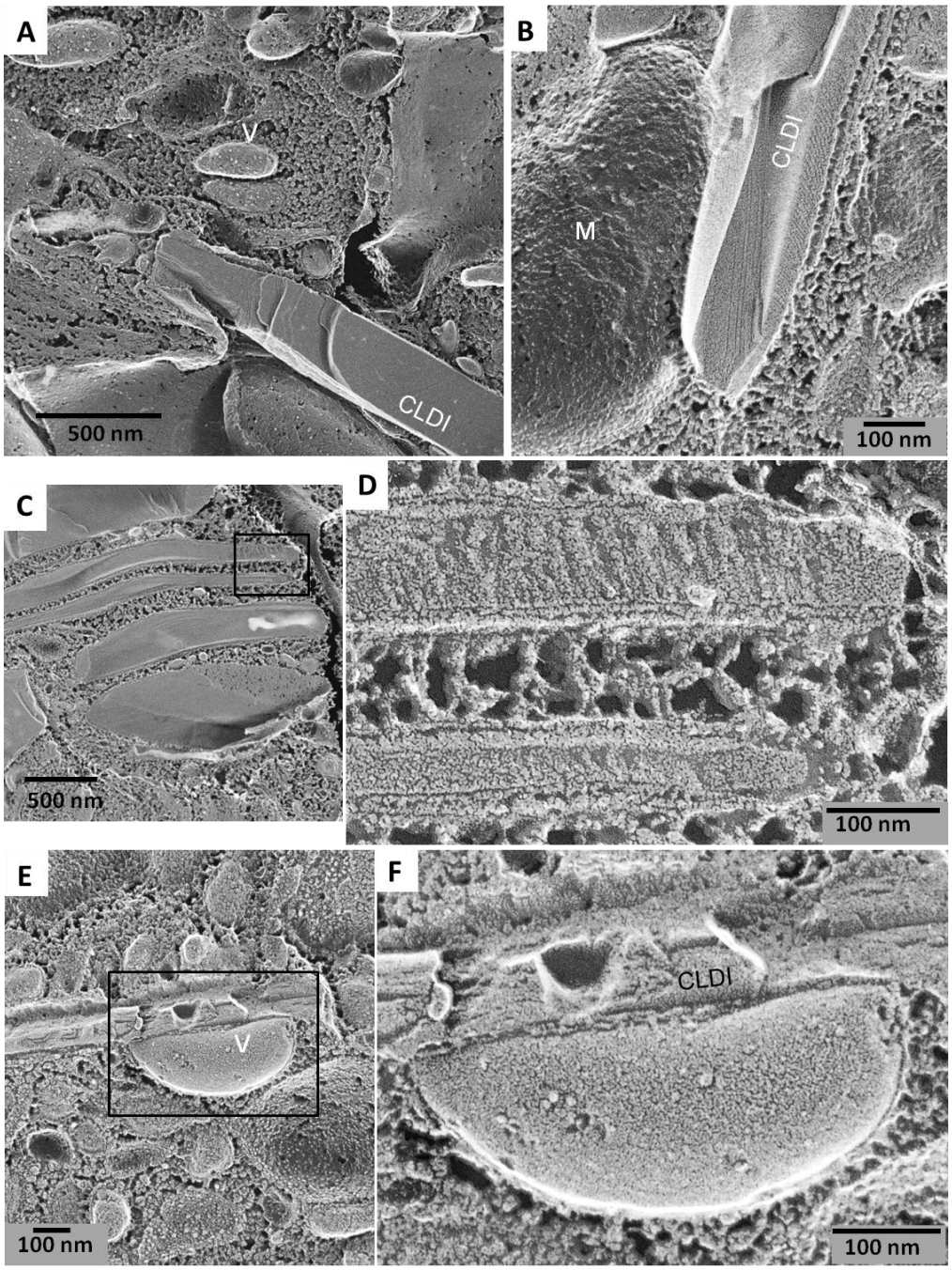

Figure 5-6 FEEM, 6 wk treated mouse liver showing CLDIs

(**A** and **B**), Needle shaped CLDIs found in liver macrophages had distinctive features compared to other cytoplasmic organelles, such as vesicles (V) or mitochondria (M). (**C**), elongated, rigid bodies appeared in close proximity to the CLDIs. (**D**), higher magnification of inner structure for the rigid bodies are shown. (**E**), CLDIs were observed with a structural addition from nearby vesicle, which were possibly fusing onto existing CLDI (**F**).

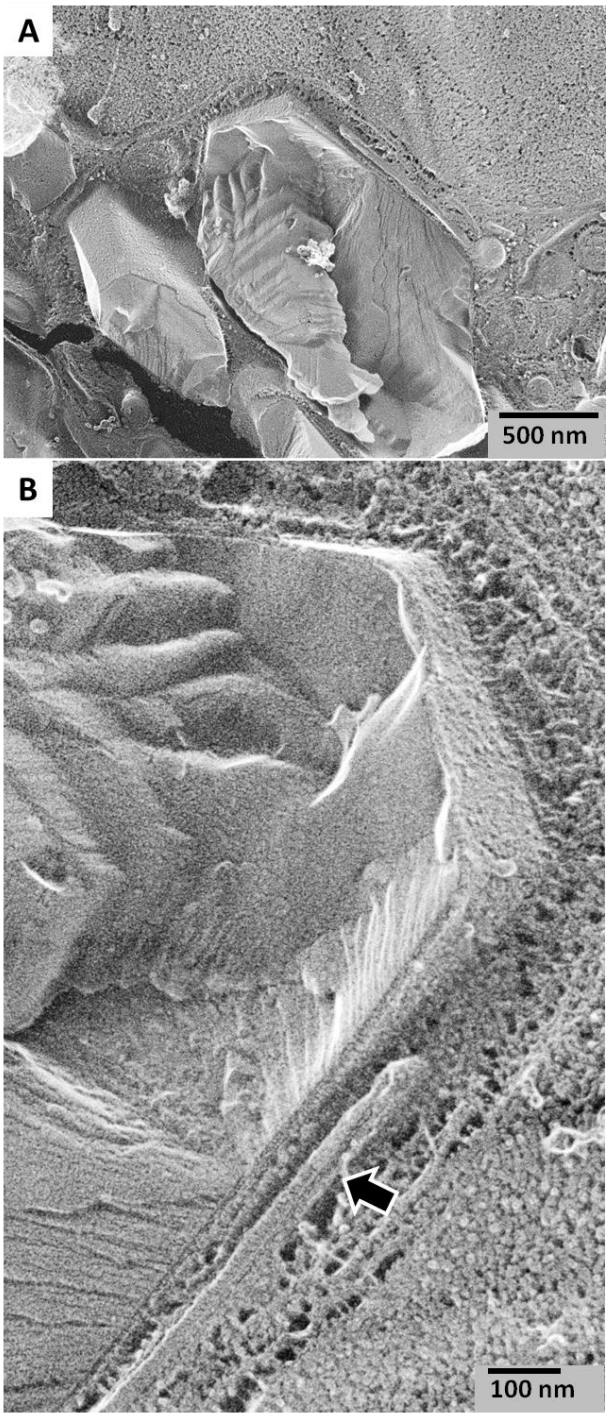

Figure 5-7 FEEM, polyhedrosome, CLDI with internal organization

(**A**), A CLDI emerging from cytoplasm of a liver macrophage showed hexagonal outlining and inner layers. (**B**), magnified view of the structure in panel A. The arrow indicates juxtaposing rigid body, partly merging onto the pre-existing polyhedrosome.

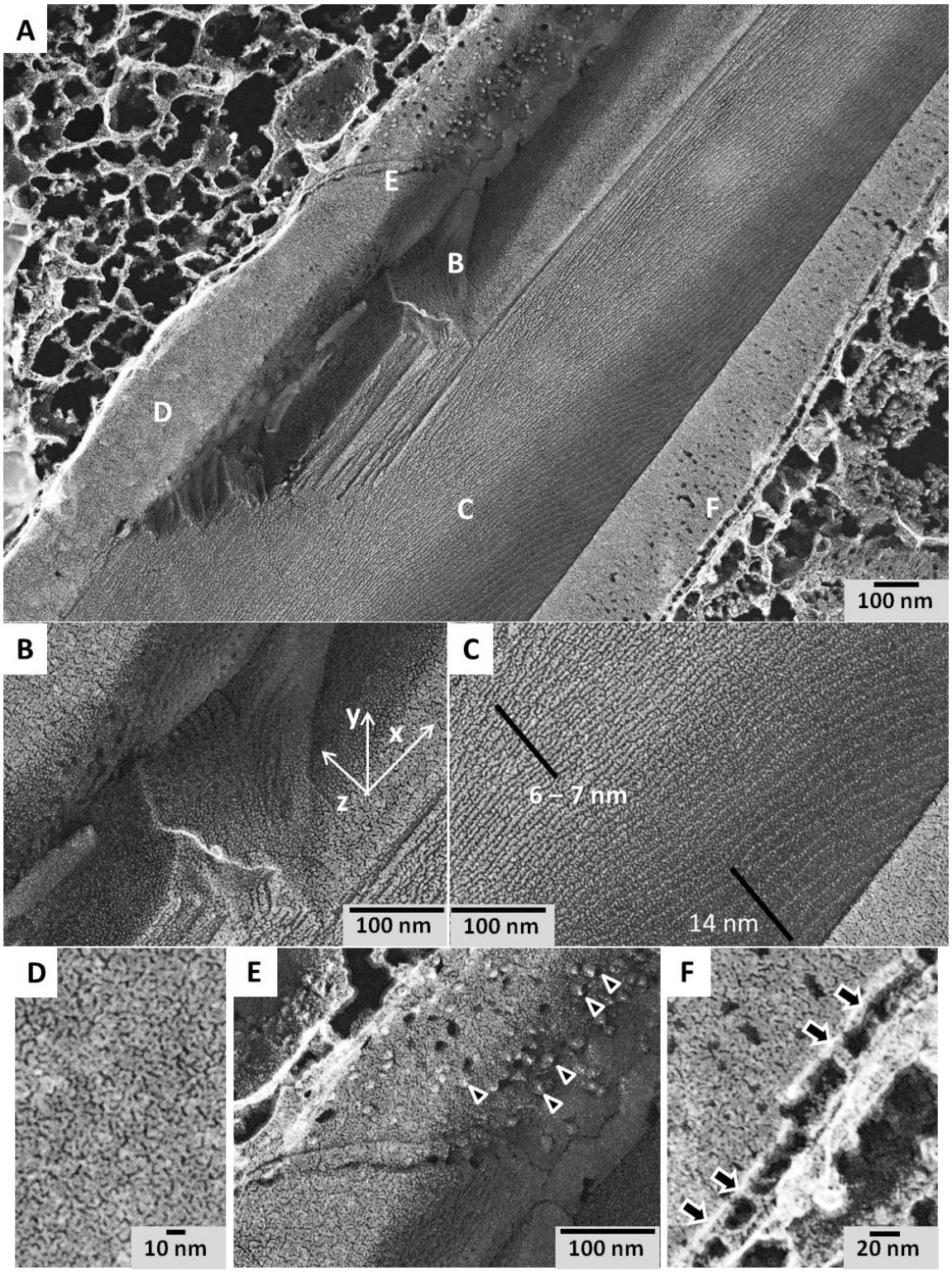

Figure 5-8 FEEM, a polyhedrosome has multiple structural domains.

(**A**) A polyhedrosome presented diagonally with outer membrane peeled open. (**B**), thin layers were stacked in z-direction parallel to x-y plane. (**C**), due to uneven fracture plane,

layers were spaced in gradient from 6 to 14 nm. (**D**), the inner texture of the delimiting double membrane shows distinct patterning. (**E**), the internal space of the separated double layer, which contained inter-membrane globules ranging 12 – 13 nm in size (triangles). (**F**), cross section of the delimiting double membrane is greater than 30 nm in thickness. Between the inner and outer layer, the connecting pillars (arrow) appeared to be approximately 20 nm in height and 12 – 13 nm in width.

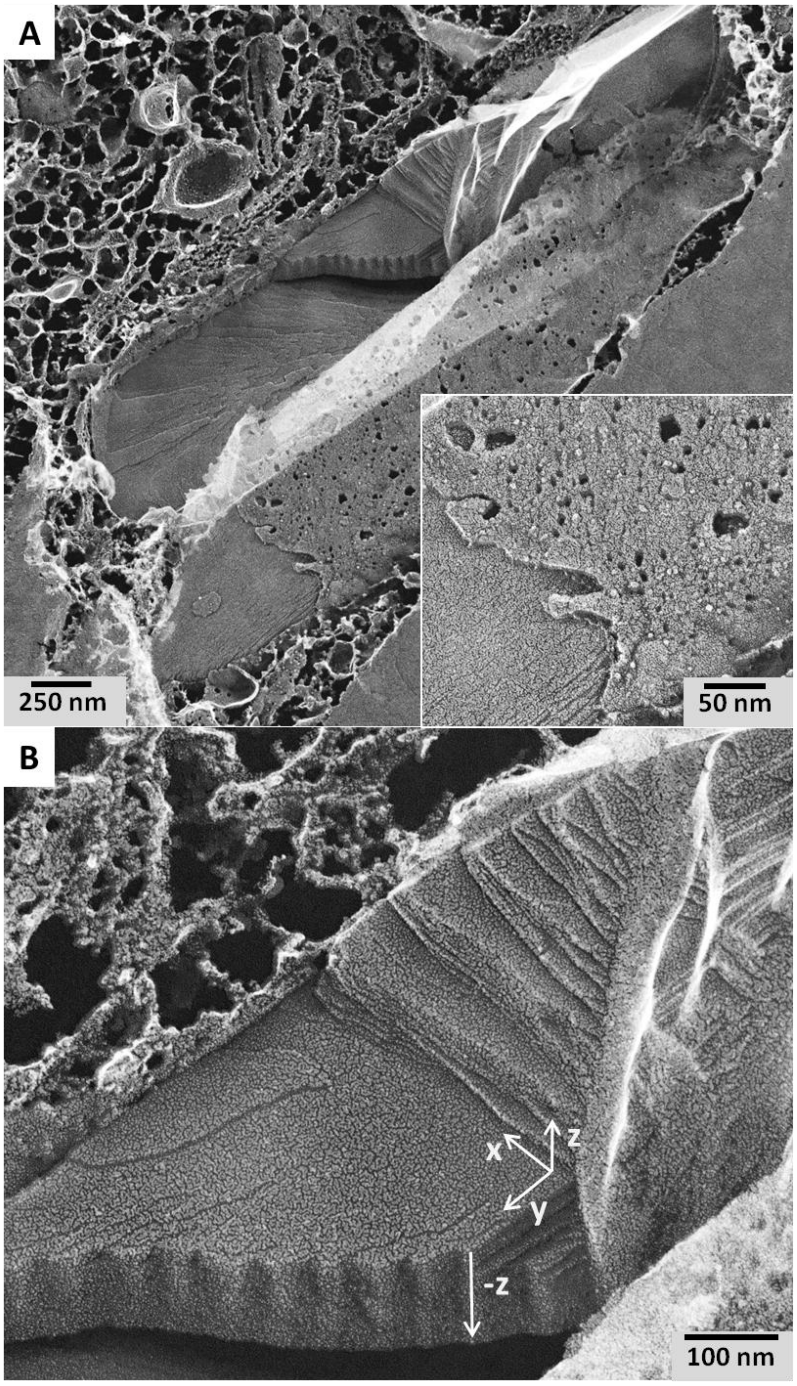

Figure 5-9 FEEM, polyhedrosome with rotational stacking

(**A**), a couple of polyhedrosomes were juxtaposed, and they showed the inner stacks and the delimiting membrane (inset). (**B**), the architecture of the stack was not normal to z-axis. Separated by the x-y plane, layers in the upper region rotated around the y-axis (from +x to +z), resulting a slanting view. In contrast, below the x-y plane, – z-axis, has an organized stack, normal to z-axis.

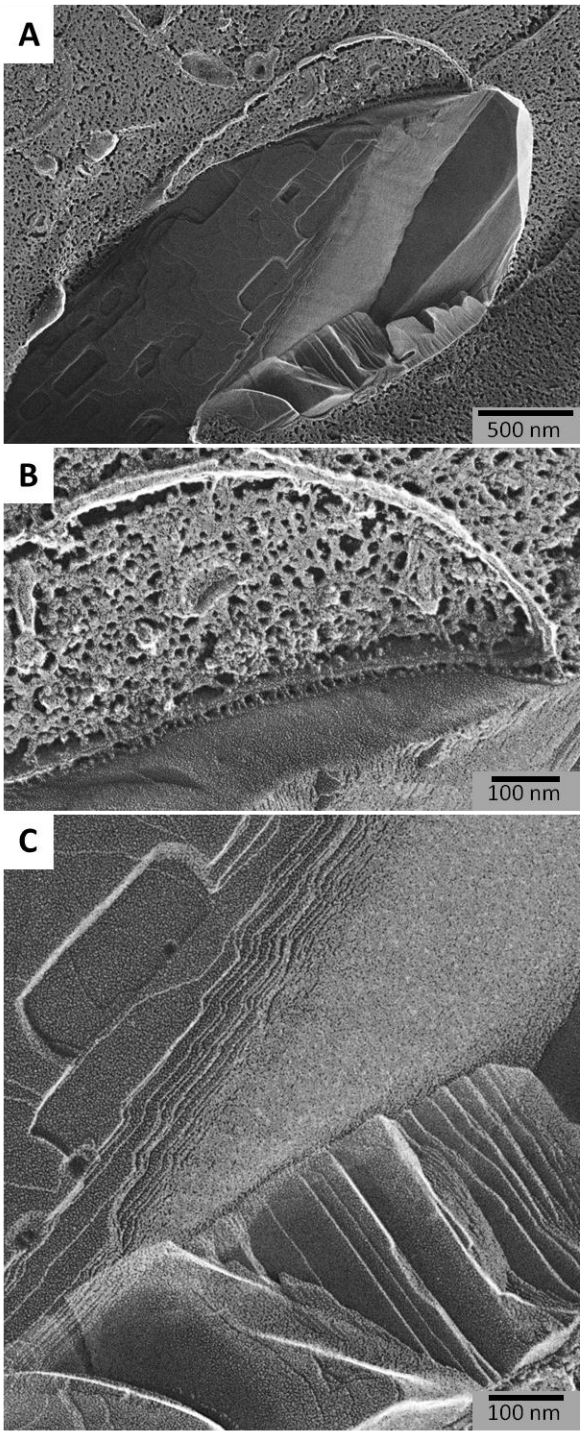

Figure 5-10 FEEM, isolated CLDIs

(**A**), structural organization was similar to what was found in liver tissues, but the size of isolated polyhedrosomes were much larger in general. (**B**), the addition of a vesicle containing cellular component onto a polyhedrosome. (**C**), inner stacks have layers, seen from the top view.

5.8 References

1. Baik, J.; Rosania, G. R. Cytoplasmic Construction of Supramolecular Structures with Organelle- and Crystal-like Features. *submitted to Pharm Res* **2011**.

2. McDougall, A. C. Electron microscope studies of the antileprosy drug B663 (clofazimine; Lamprene). *Int J Lepr Other Mycobact Dis* **1974,** *42*, (1), 1-12.

3. Heuser, J. Quick-freeze, deep-etch preparation of samples for 3-D electron microscopy. *Trends in Biochemical Sciences* **1981,** *6*, (0), 64-68.

4. Conalty, M. L.; Barry, V. C.; Jina, A. The antileprosy agent B.663 (Clofazimine) and the reticuloendothelial system. *Int J Lepr Other Mycobact Dis* **1971,** *39*, (2), 479-92.

5. Heuser, J. Protocol for 3-D visualization of molecules on mica via the quick-freeze, deep-etch technique. *J Electron Microsc Tech* **1989,** *13*, (3), 244-63.

6. Cullis, P. R.; de Kruijff, B. Lipid polymorphism and the functional roles of lipids in biological membranes. *Biochim Biophys Acta* **1979,** *559*, (4), 399-420.

7. Hope, M. J.; Wong, K. F.; Cullis, P. R. Freeze-fracture of lipids and model membrane systems. *J Electron Microsc Tech* **1989,** *13*, (4), 277-87.

8. Tarahovsky, Y. S.; Arsenault, A. L.; MacDonald, R. C.; McIntosh, T. J.; Epand, R. M. Electrostatic control of phospholipid polymorphism. *Biophys J* **2000,** *79*, (6), 3193-200.

9. Verkleij, A. J. Lipidic intramembranous particles. *Biochim Biophys Acta* **1984,** *779*, (1), 43-63.

Chapter 6

Conclusion

6.1 Multiscale biodistribution analysis

A series of biodistribution analyses was carried out at various levels for a lipophilic, poorly soluble antibacterial, clofazimine. Such a multi-scaled approach to the subject matter revealed the clofazimine's intracellular sequestration phenomena and subcellular aggregation formation at the microscopic level. Furthermore, the subcellular level accumulation was shown to impact the clofazimine's organ/tissue drug distribution and its atypical pharmacokinetic behavior at the systemic, macroscopic level.

Based on these results, we find it important to study more detailed relationships between the low solubility compounds with their pharmacokinetic and pharmacologic responses, especially owing to the significant efforts and investments of the current pharmaceutical industry focusing on poorly soluble compounds.[1] However, one of the most common descriptors used in pharmacokinetic studies, volume of distribution (Vd), does not work as informative for clofazimine as it does with other drugs. The volume of distribution is an equation-derived, calculated parameter from total clearance (CL) and plasma half-life ($t_{1/2}$), $Vd = t_{1/2} \times CL/0.693$. Therefore, the estimated values can hardly be useful for the cases like clofazimine whose mechanism of clearance is unclear or inconsistent while its half-life is extremely long. Instead of such a hypothetical, possibly-

misleading volume of solution with drug plasma concentration conjectured to account for the total drug presented in the body, we have demonstrated a new cellular and biological basis that is responsible for the drug's significant retention and long pharmacokinetic half-life. In addition, we reported the drug-induced changes of tissue structure as well as subcellular compartments, requiring modification in pharmacokinetic models.

MDCK cells treated with supersaturated clofazimine-containing medium resulted in autophagosome-like drug inclusions, the lipophilic drug forming complexes with biological membranes, and a measurable amount of drug sequestered in amorphous form. More importantly, the drug did not crystallize in cells as we originally hypothesized, whereas an apparent drug precipitation in extracellular media was observed after 5 days of incubation. Therefore, in search of the biological determinant that could induce crystal precipitation, solid aggregation, or their inhibitory mechanism, we fed Balb/c mice with drug mixed diet. As a result, unchanged clofazimine was selectively accumulating in lymphatic tissues, leaving some other tissues unaffected. At the cellular level, the drug molecules were exclusively sequestered in macrophage-like cells and also led the macrophage population to increase, which in return drastically changed the pharmacokinetic and distribution pattern after 2 months of prolonged dosage. To our surprise, we discovered that the crystal-like drug inclusions were in fact not pure drug crystals as had been commonly perceived for over 50 years. Therefore, we conclude that the subcellular level accumulation of clofazimine was biologically controlled, rather than thermodynamically crystallizing at random places in the body.

Upon further analysis using electron microscopy, we found that there was unreported and unique, ultrastructural organizations within crystal-like drug inclusions,

and therefore we dubbed the inclusions as polyhedrosomes. Their highly organized, supramolecular structure with organelle-like features suggested an efficient packing and storage of the lipophilic compound, which in return would possibly make the packed molecules not only biologically inactive but also inaccessible to plasma, conceivably leading to an elongated plasma half-life. Since the polyhedrosomes were responsive to various stimuli and extracellular environment, they possess a series of potential applications for both science and engineering.

6.2 Future investigation of polyhedrosomes and similar structures

As investigated in a previous chapter, the involvement of an immunological reaction must be further elucidated. Cytokine profiling and oxidative stress level could be tested to find whether unforeseen irritation is present, causing proliferation of the immune cells, and therefore further inducing a positive feedback to sequester more clofazimine within an expanded macrophage population. The inflammatory response could also be tested by measuring protein expression levels, such as nitric oxide[2] or manganese superoxide dismutase,[3] which are known to play significant roles in inflammatory response.

In order to further investigate the components and structural organization of the polyhedrosomes, we need to develop the physical and biochemical techniques that can resolve the subcellular structure at the molecular level. To identify molecular entities and their stoichiometry within the supramolecular organization, technical challenges related to isolation and purification of the intact polyhedrosomes must be overcome so that the lipids, proteins, or ionic species associated with clofazimine can be unveiled. Following

the purification, chromatographic approach[4] followed by mass spectrometry[5] would be suitable to measure any enrichment of protein or lipidic components that could suggest the biogenesis pathway of the atypical structure; for example, cardiolipin enrichment would suggest that the membrane has originated from mitochondria.

In addition, applying different sorts of *in situ* analytical techniques would be worthwhile; for example: X-ray diffraction for component periodicity measurement[6], small angle X-ray scattering (SAXS) for supramolecular structure periodicity[7], laser microprobe mass analysis (LAMMA) for component analysis[5], low-energy-loss electron microscopy for molecule-specific optical signal detection[8] or ^{31}P-nuclear magnetic resonance on freeze-fractured sample for phospholipid content analysis.[9-11] For example, SAXS and ^{31}P-NMR were previously implemented to characterize supramolecular organization called cubic phases,[12, 13] which are known to be three dimensional, highly organized membranous structures that can be generated both artificially[6] and naturally.[14,15]

In relationship towards earlier studies on cubic lipidic phases,[6] also known as lipidic mesophases,[7] liquid crystalline,[6] or membrane polymorphisms,[12, 13] identifying the actual supramolecular organization would require comparative studies with model systems, such as *in vitro* lipid mixtures.[6, 12, 13, 16, 17] In addition to the artificial mixtures in the test tubes, a group of researchers have found cases of highly organized lattice-like lamellae present in human and mice. Pasyk et al. reported cytoplasmic crystalloid inclusions in patients with hemangiomas (a form of benign tumor associated with the blood vessels of newborns), revealing distinctive 5 – 7 nm of triple membrane structures with alternating, dark dense layers.[18-20] In addition, splenic lipofuscinosis in mice,[21]

multilamellar bodies in the macrophages of amiodarone-treated patients,[22] and myelin fibers of Schwann cells in the nerve system from clofazimine treated patients[23] revealed whirls of concentric multilamellar structure, spaced 6 – 28 nm apart. Also, there are naturally occurring multilamellar bodies in the lungs of humans and mice that are associated with lung surfactants to share some of the morphological features with subcellular drug inclusions.[24, 25] Investigating these structurally similar macromolecular assemblies by image analysis could unravel whether polyhedrosome-like machinery in cells is related to other diseases or whether lipidic systems naturally exist.

Furthermore, there are several case reports on supramolecular structure that show needle-like structures, as investigators often referred them as crystals, crystalloid cavities, or osmiophilic rods. In mice spleen that developed lipofuscinosis, several micrometers long crystalloid bodies were observed in association with rough endoplasmic reticulum,[21] which appeared morphologically similar to the osmiophilic rods described in the previous chapter. In another study with mice, macrophages from the bone marrow and red pulp of spleen spontaneously developed needle-like crystalloids over 5 months, transforming from spherical inclusions into bundles of needles that are 10 μm in average length.[26] The authors of this study speculated that the crystalloids were related to erythropoietic activity, where certain types of macrophages may be breaking down the phagocytized blood cells and building crystalloid structure within the phagolysosomes. Similarly, rod-like crystalline structures were recorded under pulmonary infection of *Cryptococcus neoformans*, and presumably the multinucleated cells in the lungs were polymerizing an eosinophilic protein into needle-like constructions.[27] These reports suggest that there are

certain types of cells in the body which can build subcellular materials into rod-shaped, crystal-like structures ranging several micrometers long.

Since formation of these inclusions in macrophages seems to be a natural, defensive reaction of the body, we perceived formation of clofazimine crystal-like drug inclusions as a result of active sequestration of poorly soluble xenobiotics. To show that this is not a clofazimine-specific case, we found a comparable case study of the poorly soluble fluoroquinolone antibiotic, tosufloxacin (CAS 100490-36-6, clogP = 0.81 (TerraQSAR-LOGP^{TM} by TerraBase Inc), Mw: 404.3). A biopsy from a patient treated with tosufloxacin tosilate for 4 years showed intracellular drug inclusions that were birefringent. Transmitted light microscopy also revealed a significant number of crystalloid cavities and granulomatous interstitial nephritis.[28] The authors also remarked that due to such crystalloid accumulation, the drug exerts renal and hepatic toxicity leading to its limited approval and use in Japan.[29]

In extension to the bioaccumulation phenomena as to sequester the surplus of molecules in the body, cholesterol is also one of the model systems that must be closely looked into in terms of crystal formation. The cholesterol deposition is reported to cause crystal embolism and form plaque as well as crystalloid cavities in human patients.[30] Moreover, cholesterol[31] and cholesterol monohydrate[32] crystal formation in different types of macrophages were investigated, and the researchers have reported the formation of multilamellar bodies, crystalloid cavities, and the effect of composition on the phase transition within the macrophage intracellular compartments.[33, 34]

6.3 Candidates for drug-membrane complex/aggregation formation

Two issues related to pharmaceutical research must be emphasized. One is the recognition that a poorly soluble drug delivered into the body can be sequestered in a way that can change drug performance, and this may lead to unpredictability and possible failure at a later point of drug development, which would be costly. The second notion is that the anti-inflammatory response of the body related to the role of macrophages on drug sequestration, which could make pathophysiological changes on the volume or structural component of the liver or spleen. As a result of fibrosis or microgranulomas development, pharmacokinetic models assuming consistency in body state would be inapplicable and require modifications to account for the poorly soluble drugs that already have long plasma half-lives. Therefore, researchers in the field of pharmaceutical sciences are advised to pay attention to *in vivo* drug-membrane complex formation when investigating poorly soluble compounds.

There are several factors that could serve as indicators of the *in vivo* drug-membrane complex/aggregation formation that could be applied to identify the potential candidates causing unwanted bioaccumulation in the body. For example, currently known parameters can be used for draft selection, such as long half-life, large volumes of distribution and poor solubility. Also, high permeability with poor metabolism and/or slow clearance could be indicative of drug accumulation. These criteria could be considered to be a quick screen for potential *in vivo* aggregation and precipitation at an early stage of drug discovery.

As an example, selected from the literature were nine drugs that have been reported to accumulate in humans and cause temporary hyperpigmentation (Table 1).[35] Under the electron microscope, they revealed ultrastructures resembling autophagosome-like drug inclusions,[36-39] and in some cases were associated with mononuclear cells or macrophage population expansion associated with subcellular sequestration. Even though some of these drugs were reported to be cleared out through either renal excretion or extensive metabolism, others did show significantly long plasma half-lives (underlined in Table 1). Both biopharmaceutical classification systems BCS[40] (Biopharmaceutics Classification System that divides drugs with solubility and permeability) and BDDCS[41] (Biopharmaceutics Drug Disposition Classification System that divides drugs with solubility and metabolism) suggested that the drugs with long half-lives could be poorly soluble drugs based on the equation, $t_{1/2} = 0.693 \times Vd/CL$. In fact, the listed drugs were highly hydrophobic and they were subjected to hepatic metabolism; however, chloroquine did not show as much extensive biotransformation, presumably leading to a significant length of circulation despite the favorable water solubility. On the other hand, amiodarone could be imagined to be first partitioning into fatty tissue owing to its extreme lipophilicity, but at the same time, they could be extensively metabolized in the liver, making the plasma half-life highly variable. Presumably, such variability is due to the plasma's extraction efficiency against fatty tissue, which has a limited perfusion rate. In any case, these subcellular structure forming molecules need to be studied further and administered with care to prevent unwanted drug side effects.

In conclusion, multiscale biodistribution analysis on clofazimine revealed a striking biological response that the field of pharmaceutics has never seen. Understanding the

subcellular polyhedrosomes as well as the bioaccumulation and sequestration phenomena could change the concept on how a body responds to a drug.

Table 1. Drug candidates with reported hyperpigmentation and deposition in the body.[42] Long half-life and poor solubility with less extensive metabolism of a drug may suggest that it may form membrane complex and become sequestered via polyhedrosome formation. Data collected from various sources.[1, 41, 42]

Drug	Use	BCS / BDDCS	$t_{1/2}$	Vd (L/kg)	CL (ml/min/kg)	logP	Solubility (mg/mL)	Metabolism
Amiodarone	Anti-arrhythmic	2/2	15-142 d	66±44	1.9±0.4	7.8	0.7	Extens. hepatic
Busulfan	immunosuppressive	?/1	2.5 hr	0.99±0.03	4.5±0.9	-0.52	0.1	Hepatic
Bleomycin	Antibiotic	?/3	2 hr	-	-	-7.5 xLogP	20	Unchanged renal
Chloroquine	Antibiotic	2/3	30-60 d	132-261	3.7-13	4.63	100	Hepatic
Chlorpromazine	Antipsychotic	2/?	30 hr	21±9	8.6±2.9	5.41	400	Extens. Hepatic Renal
Clofazimine	Antibiotic	2/2	70 d	-	-	7.4	0.001	-
Imipramine	Antidepressant	1/1	8-20 hr	18±2	13±1.7	3.9	0.02	Extens. Hepatic
Methacycline	Antibiotic	?/?	14 hr	-	-	-0.3	7.55	?
Minocycline	Antibiotic	1/1	11-22 hr	-	-	0.05	50	Hepatic

6.4 Reference

1. Benet, L. Z.; Broccatelli, F.; Oprea, T. I. BDDCS Applied to Over 900 Drugs. *AAPS J* **2011**, DOI:10.1208/s12248-011-9290-9.

2. Nussler, A. K.; Billiar, T. R. Inflammation, immunoregulation, and inducible nitric oxide synthase. *J Leukoc Biol* **1993,** *54*, (2), 171-8.

3. Li, C.; Zhou, H. M. The role of manganese superoxide dismutase in inflammation defense. *Enzyme Res* **2011**, 387176.

4. Aplin, R. T.; McDougall, A. C. Identification of crystals of the rimino-phenazine compound B663 (Lamprene: clofazimine) in mouse spleen macrophages by thin layer chromatography and mass spectrum analysis. *Experientia* **1975,** *31*, (4), 468-9.

5. Vandeputte, D.; Jacob, W.; Van Grieken, R.; Boddingius, J. Study of intracellular deposition of the anti-leprosy drug clofazimine in mouse spleen using laser microprobe mass analysis. *Biol Mass Spectrom* **1993,** *22*, (4), 221-5.

6. Johnsson, M.; Barauskas, J.; Tiberg, F. Cubic phases and cubic phase dispersions in a phospholipid-based system. *J Am Chem Soc* **2005,** *127*, (4), 1076-7.

7. Caffrey, M.; Cherezov, V. Crystallizing membrane proteins using lipidic mesophases. *Nat Protoc* **2009,** *4*, (5), 706-31.

8. Mhawi, A. A.; Fernandes, A. B.; Ottensmeyer, F. P. Low-energy-loss electron microscopy of doxorubicin in human breast cancer MCF-7 cells: localization by color. *J Struct Biol* **2007,** *158*, (1), 80-92.

9. Burnell, E.; van Alphen, L.; Verkleij, A.; de Kruijff, B. 31P nuclear magnetic resonance and freeze-fracture electron microscopy studies on Escherichia coli. I. Cytoplasmic membrane and total phospholipids. *Biochim Biophys Acta* **1980,** *597*, (3), 492-501.

10. Burnell, E.; van Alphen, L.; Verkleij, A.; de Kruijff, B.; Lugtenberg, B. 31P nuclear magnetic resonance and freeze-fracture electron microscopy studies on Escherichia coli. III. The outer membrane. *Biochim Biophys Acta* **1980,** *597*, (3), 518-32.

11. van Alphen, L.; Verkleij, A.; Burnell, E.; Lugtenberg, B. 31P nuclear magnetic resonance and freeze-fracture electron microscopy studies on Escherichia coli. II. Lipopolysaccharide and lipopolysaccharide-phospholipid complexes. *Biochim Biophys Acta* **1980,** *597*, (3), 502-17.

12. Tarahovsky, Y. S.; Arsenault, A. L.; MacDonald, R. C.; McIntosh, T. J.; Epand, R. M. Electrostatic control of phospholipid polymorphism. *Biophys J* **2000,** *79*, (6), 3193-200.

13. Verkleij, A. J. Lipidic intramembranous particles. *Biochim Biophys Acta* **1984,** *779*, (1), 43-63.

14. Almsherqi, Z. A.; Kohlwein, S. D.; Deng, Y. Cubic membranes: a legend beyond the Flatland* of cell membrane organization. *J Cell Biol* **2006,** *173*, (6), 839-44.

15. Almsherqi, Z. A.; Landh, T.; Kohlwein, S. D.; Deng, Y. Chapter 6: cubic membranes the missing dimension of cell membrane organization. *Int Rev Cell Mol Biol* **2009,** *274*, 275-342.

16. Cullis, P. R.; de Kruijff, B. Lipid polymorphism and the functional roles of lipids in biological membranes. *Biochim Biophys Acta* **1979,** *559*, (4), 399-420.

17. Meyer, H. W.; Richter, W. Freeze-fracture studies on lipids and membranes. *Micron* **2001,** *32*, (6), 615-44.

18. Pasyk, K. A.; Grabb, W. C.; Cherry, G. W. Cellular haemangioma. Light and electron microscopic studies of two cases. *Virchows Arch A Pathol Anat Histol* **1982,** *396*, (1), 103-26.

19. Pasyk, K. A.; Grabb, W. C.; Cherry, G. W. Crystalloid inclusions in endothelial cells of cellular and capillary hemangiomas. A possible sign of cellular immaturity. *Arch Dermatol* **1983,** *119*, (2), 134-7.

20. Pasyk, K. A.; Hassett, C. A.; Cherry, G. W.; Argenta, L. C. Endothelial cell crystalloids in newborn human foreskin. *J Cutan Pathol* **1988,** *15*, (2), 84-91.

21. Crichton, D. N.; Busuttil, A.; Ross, A. An ultrastructural study of murine splenic lipofuscinosis. *J Ultrastruct Res* **1980,** *72*, (2), 130-40.

22. Dake, M. D.; Madison, J. M.; Montgomery, C. K.; Shellito, J. E.; Hinchcliffe, W. A.; Winkler, M. L.; Bainton, D. F. Electron microscopic demonstration of lysosomal inclusion bodies in lung, liver, lymph nodes, and blood leukocytes of patients with amiodarone pulmonary toxicity. *Am J Med* **1985,** *78*, (3), 506-12.

23. Kumar, V. Does clofazimine (B663) reach Mycobacterium leprae persisting in Schwann cells and endothelial cells of endoneurial blood vessels in peripheral nerves? *Microsc Res Tech* **2008,** *71*, (8), 614-8.

24. Stratton, C. J. The ultrastructure of multilamellar bodies and surfactant in the human lung. *Cell Tissue Res* **1978,** *193*, (2), 219-29.

25. Williams, M. C. Conversion of lamellar body membranes into tubular myelin in alveoli of fetal rat lungs. *J Cell Biol* **1977,** *72*, (2), 260-77.

26. Sasaki, K.; Matsumura, G.; Ito, T. Crystalloid inclusion-containing macrophages in the bone marrow and red pulp of the mouse, with particular relation to age, sex and hydrocortisone administration: qualitative and quantitative electron microscopy. *Arch Histol Jpn* **1983,** *46*, (3), 381-91.

27. Feldmesser, M.; Kress, Y.; Casadevall, A. Intracellular crystal formation as a mechanism of cytotoxicity in murine pulmonary Cryptococcus neoformans infection. *Infect Immun* **2001,** *69*, (4), 2723-7.

28. Okada, H.; Watanabe, Y.; Kotaki, S.; Ikeda, N.; Takane, H.; Kanno, Y.; Sugahara, S.; Ban, S.; Nagata, M.; Suzuki, H. An unusual form of crystal-forming chronic interstitial nephritis following long-term exposure to tosufloxacin tosilate. *Am J Kidney Dis* **2004,** *44*, (5), 902-7.

29. Rubinstein, E. History of quinolones and their side effects. *Chemotherapy* **2001,** *47 Suppl 3*, 3-8; discussion 44-8.

30. Meyrier, A. Cholesterol crystal embolism: diagnosis and treatment. *Kidney Int* **2006,** *69*, (8), 1308-12.

31. Klinkner, A. M.; Waites, C. R.; Kerns, W. D.; Bugelski, P. J. Evidence of foam cell and cholesterol crystal formation in macrophages incubated with oxidized LDL by fluorescence and electron microscopy. *J Histochem Cytochem* **1995,** *43*, (10), 1071-8.

32. Tangirala, R. K.; Jerome, W. G.; Jones, N. L.; Small, D. M.; Johnson, W. J.; Glick, J. M.; Mahlberg, F. H.; Rothblat, G. H. Formation of cholesterol monohydrate crystals in macrophage-derived foam cells. *J Lipid Res* **1994,** *35*, (1), 93-104.

33. Snow, J. W.; Glick, J. M.; Phillips, M. C. The phase behavior of cholesteryl esters in intracellular inclusions. *J Biol Chem* **1992,** *267*, (26), 18564-72.

34. Veloski, C. A.; McCann, R. A.; Snow, J. W. An analytical model for the phase behavior of cholesteryl esters in intracellular inclusions. *Biochim Biophys Acta* **1994,** *1213*, (2), 183-92.

35. Granstein, R. D.; Sober, A. J. Drug- and heavy metal-induced hyperpigmentation. *J Am Acad Dermatol* **1981,** *5*, (1), 1-18.

36. Hashimoto, K.; Joselow, S. A.; Tye, M. J. Imipramine hyperpigmentation: a slate-gray discoloration caused by long-term imipramine administration. *J Am Acad Dermatol* **1991,** *25*, (2 Pt 2), 357-61.

37. Hashimoto, K.; Wiener, W.; Albert, J.; Nelson, R. G. An electron microscopic study of chlorpromazine pigmentation. *J Invest Dermatol* **1966,** *47*, (4), 296-306.

38. Ming, M. E.; Bhawan, J.; Stefanato, C. M.; McCalmont, T. H.; Cohen, L. M. Imipramine-induced hyperpigmentation: four cases and a review of the literature. *J Am Acad Dermatol* **1999,** *40*, (2 Pt 1), 159-66.

39. Treister, N. S.; Magalnick, D.; Woo, S. B. Oral mucosal pigmentation secondary to minocycline therapy: report of two cases and a review of the literature. *Oral Surg Oral Med Oral Pathol Oral Radiol Endod* **2004,** *97*, (6), 718-25.

40. Amidon, G. L.; Lennernas, H.; Shah, V. P.; Crison, J. R. A theoretical basis for a biopharmaceutic drug classification: the correlation of in vitro drug product dissolution and in vivo bioavailability. *Pharm Res* **1995,** *12*, (3), 413-20.

41. Wu, C. Y.; Benet, L. Z. Predicting drug disposition via application of BCS: transport/absorption/ elimination interplay and development of a biopharmaceutics drug disposition classification system. *Pharm Res* **2005,** *22*, (1), 11-23.

42. Wishart, D. S.; Knox, C.; Guo, A. C.; Cheng, D.; Shrivastava, S.; Tzur, D.; Gautam, B.; Hassanali, M. DrugBank: a knowledgebase for drugs, drug actions and drug targets. *Nucleic Acids Research* **2008,** *36*, (suppl 1), D901-D906.

Appendices

Appendix A

Clofazimine logD

Clofazimine lipid/water distribution coefficient was simulated using logD function in program MarvinSketch 5.3.8, developed by ChemAxon Ltd. Optional electrolyte concentration was set to 0.1M Cl^- and 0.1M Na^+K^+. Weighted method was set to VG=1, KLOP=1, PHYS=1.

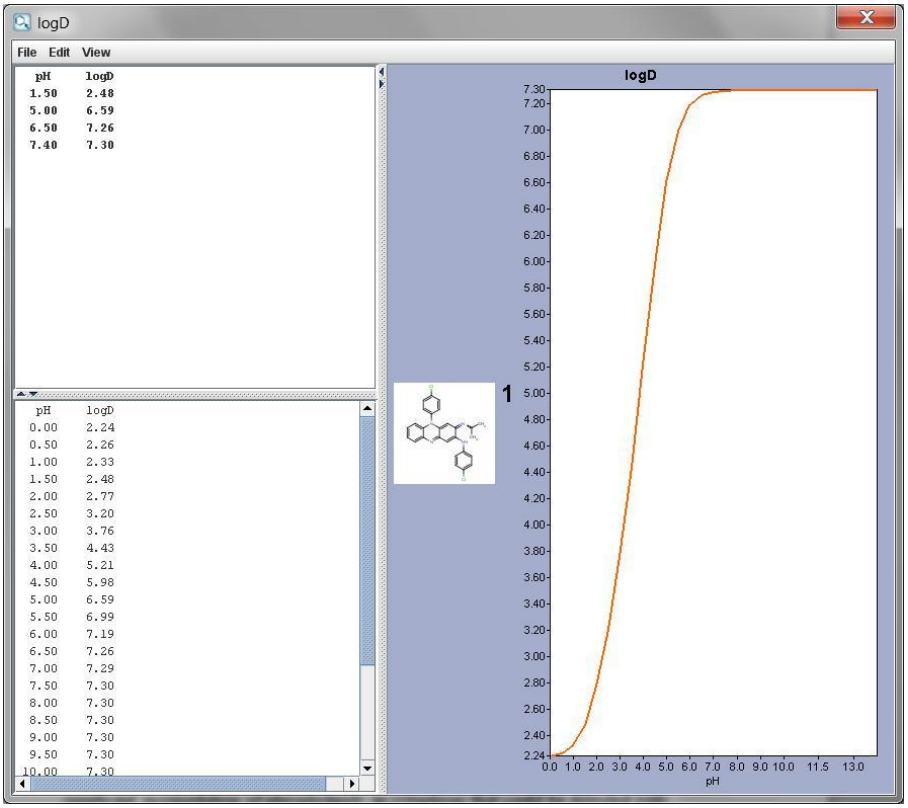

Appendix B

Supporting Information in Chapter 2

SI 1. (A) CFZ is present in solution as protein-bound form as 10 mg/ml BSA in DPBS prevented CFZ to precipitate out from the solution. (B) In the supernatant, significant amount is present in protein bound form and only a small fraction is observed to be protein-unbound, freely dissolved in the solution containing 90% of $(NH_4)_2SO_4$ in DPBS. About 22% of the amount was unrecoverable owing to non-specific adsorption of the tips, eppendorf tubes, conical tubes as well as the loss from calculation error etc. (C) As the control, without BSA, DPBS containing over 90% saturation of the ammonium sulfate was shown for retaining CFZ in solution, where significant amount was adsorbed onto the walls of the glass vials at 2, 5, and 10 µM of CFZ final concentration. Precipitation was negative and adsorption to the wall was visible at certain portion in the vial, top of the liquid phase.

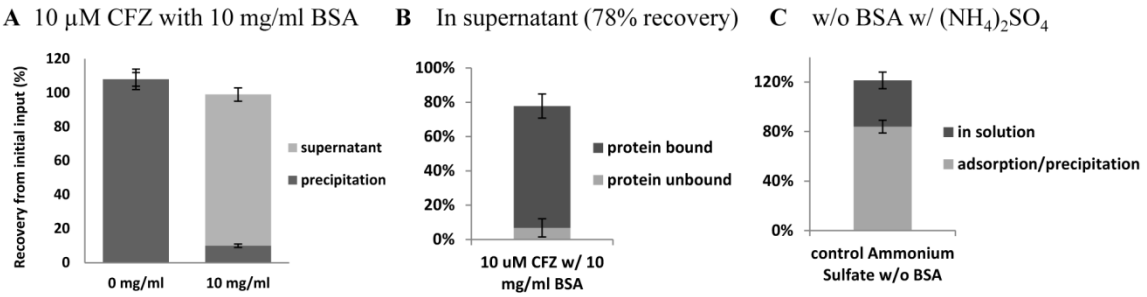

SI. 2 LC-MS metabolism study result indicates there are no major drug metabolism. Detailed method was described in main section. Briefly, pure drug was dissolved in MeOH (1 µg/ml) for standard, whereas the pure drug was mixed with cell lysate for positive control. For metabolism analysis, two experiments were separately carried out for cells treated with 10 µM CFZ for 90 or 96 hours, which virtually showed the same result. Two major peaks were analyzed under multiple reaction monitoring (MRM) mode observing possible biotransformation. Among 44 listed biotrransformations and pairs of 178 fragments in combination, the peaks indicated 473 or 431 m/z which is the parent compound rather than any of its metabolites.

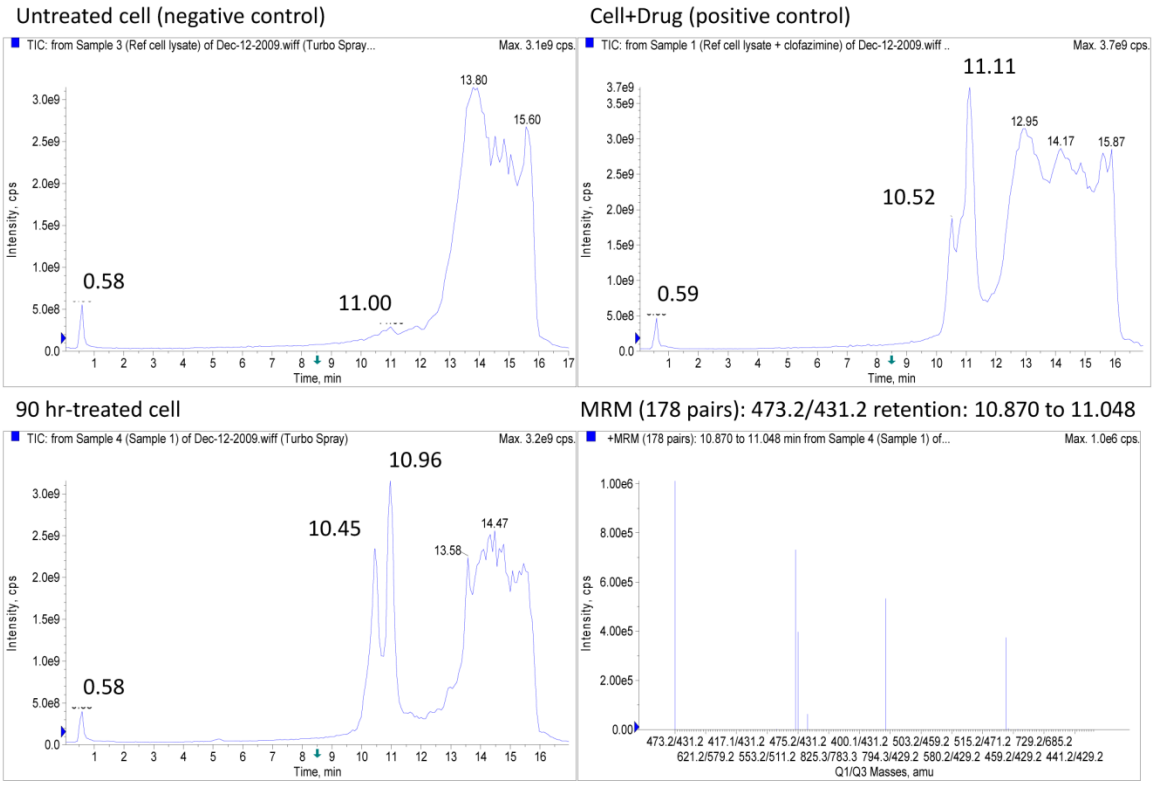

SI. 3 Proliferation rate measured over 24 – 48 hours of exposure under various FBS contents. Within same serum concentration, fitted cell proliferation factor k is inversely proportional to the extracellular drug concentration in the cell culture medium. Fitted curve was $y = y_0e^{kt}$ assuming exponential increase in cell number without reaching confluency.

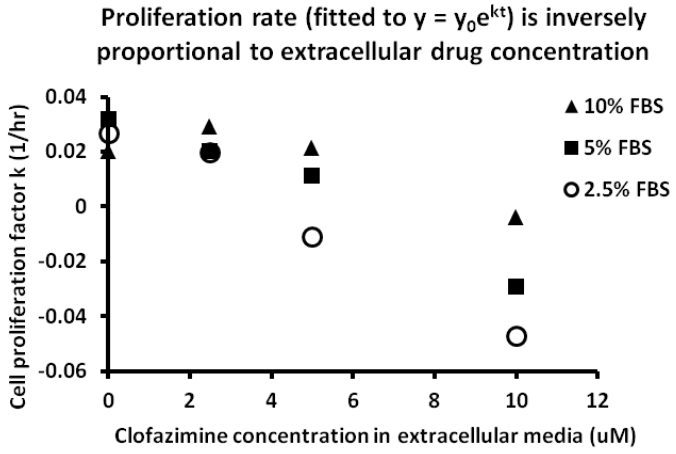

SI. 4 Intrinsic fluorescence of CFZ is quenched for aggregation at higher concentration in 0.2 M phosphate buffer: pH at 5.58, 6.89, and 8.09, with varying CFZ content. Fluorescence excitation at 450 nm and emission 528 nm, dichroic mirror 510 nm was used. After linear increase, signal in more basic solution showed greater extent of quenching owing to CFZ being monobasic compound that decreases solubility with increasing pH.

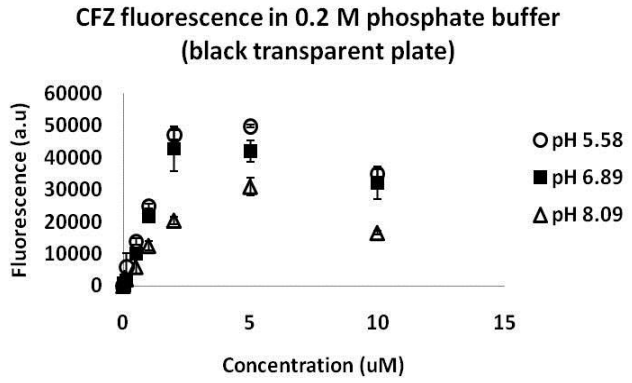

SI. 5 Polarization microscopy (L) and dark field image (R) of CFZ treated MDCK cells with extracellular drug crystal (positive control). The MDCK cells show significant amount of drug inclusions yet alive, but no polarization or birefringence in the dark field is observed in contrast to extracellular crystal shows significant birefringence. 500x magnification (no scale bar is available, but cell dimension is approximately 20 µm x 30 µm)

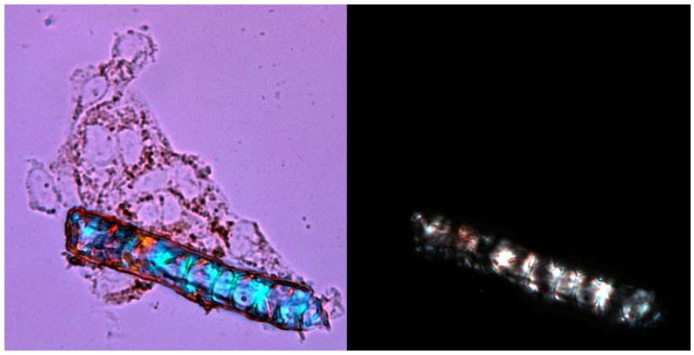

SI. 6 Focus on amorphous vs. crystal sample suspended in different buffer system for confocal Raman microscopy. Corresponding spectra were shown in main figure.

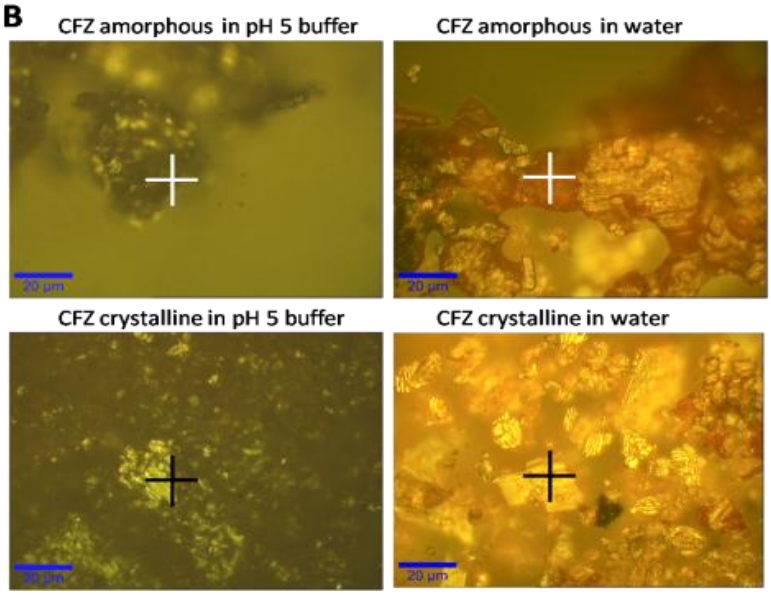

SI. 7 Organelle morphology category used to count the objects observed in particular TEM section. In general one section cannot be representative of the entire object, however, it is assumed that larger organelle comes from small one(s), and complex internal structure should originate from less complicated structures. Postulated sequence develops from top to bottom of the figure. Each row represents one category: Normal (a – c) -> Degenerating/Abnormal (d – f) -> MVB/MLB (g – i) -> early ALDI (j – l) -> late ALDI (m – p). Although we cannot confirm early ALDIs are actually small objects rather than a particular section from larger, it represents less complicated internal structures. Images were not drawn to same scale.

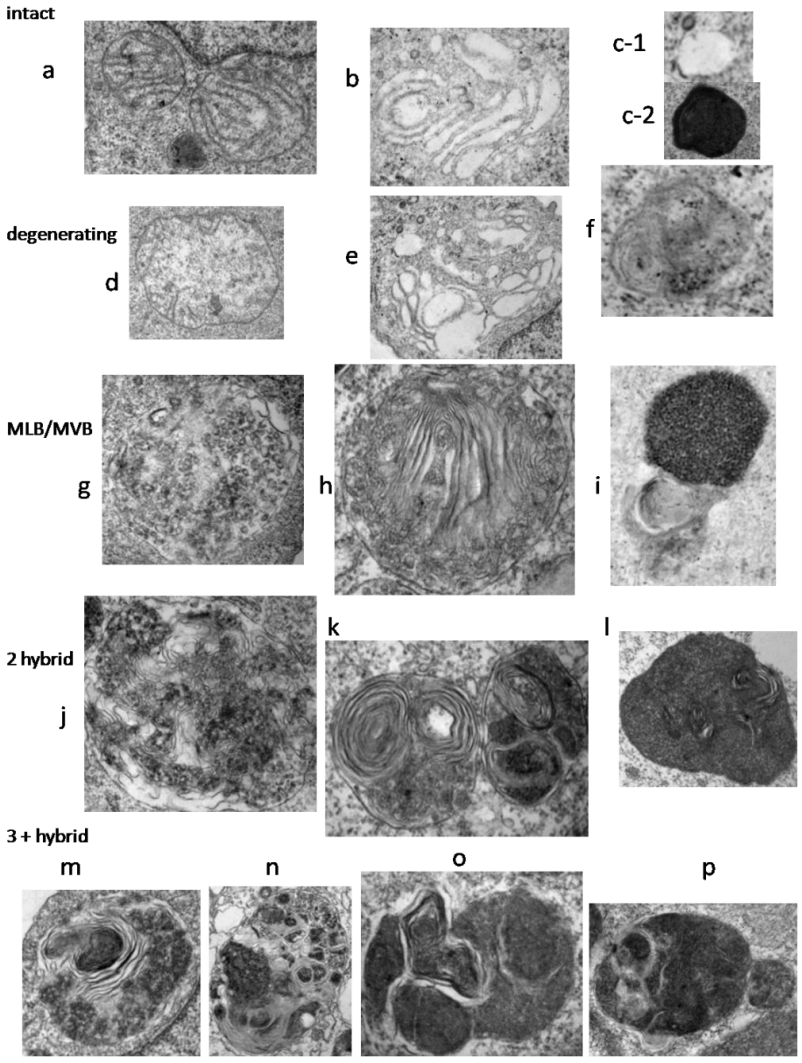

Appendix C

In Vitro Phenotypic Characteristics of Peritoneal Macrophages Forming Crystal-like Drug Inclusions

C.1 Abstract

Mice fed with clofazimine (CFZ) developed crystal-like drug inclusions (CLDIs) in various organs in association with resident tissue macrophages. In order to further study the characteristics and composition of the CLDIs, mass production of this subcellular structure is needed. Here, we tested the possibility of producing CLDIs *in vitro* to evaluate the factors of their formation in a simpler and controlled manner. We isolated peritoneal macrophages from CD-1 mice (PMC) and cultured them on tissue culture plates with different concentrations of CFZ to investigate the relationship between the formation of different types of inclusions/crystals and cell viability. Epifluorescence microscopic imaging revealed that the drug accumulated inside the macrophages, which was similar to the previous study using MDCK cells.[1] PMC treated with 1 μM of CFZ for 48 – 96 hours produced intracellular CLDIs similar to those observed *in vivo* as well as producing autophagosome-like drug inclusions (ALDIs) and extracellular CFZ crystals.[1, 2] Cells associated with crystals remained attached, well spread, and produced formazan from MTT assay used to test the cell viability. ALDI, CLDI, and CFZ crystals did not

show any sign of cytoprotective function upon doxorubicin treatment. In conclusion, we successfully demonstrated the bioaccumulation of CLDIs in peritoneal macrophages.

C.2 Introduction

Immunohistochemical analysis and ultrastructural image analysis revealed that tissue macrophages play crucial roles in pharmacokinetic distribution of the poorly soluble drug clofazimine (CFZ).[2] This in fact is related to the anti-inflammatory response phenomenon observed in cases such as paraffin or parasitic infection as elaborated in previous chapters.[3, 4] One of the most significant pathological responses related to these foreign body reactions is the formation of microgranulomas which is the colonizing macrophages accumulating in the liver to counteract the inflammation.[5]

In previous work, intracellular drug inclusions were categorized into two: autophagosome-like drug inclusions (ALDI) and crystal-like drug inclusions (CLDI), both prevalent in cytoplasm of affected cells. In order to study this unique bioaccumulation phenomenon, we aimed to create an *in vitro* environment that could reproduce what was shown in mice and humans. Previous work done on Madin-Darby Canine Kidney (MDCK) cells *in vitro* only produced ALDIs and failed to form CLDIs. Here, we hypothesized that cell specificity and functionality is key to CLDI formation, and therefore we tested various macrophage cell lines to demonstrate formation of CLDIs *in vitro.*[1]

Usually the isolation of CLDI is followed by labor intensive work involving animal sacrifice with series of homogenization and density gradient centrifugation which takes time and energy only to gain a small amount of intact material that we cannot be sure that

has not been disrupted by these processes.[2] Hence, the establishment of an *in vitro* set up would promote the study of bioaccumulation of xenobiotics in a more effective way.

CLDIs are membrane bound polyhedral inclusions that display distinct optical and physicochemical properties from CFZ crystals, which are extracellular, orange-red, and have needle-like morphology.[2] Utilizing these characteristics, and under different concentrations and treatment durations, we implemented epifluorescence and polarization microscopy to successfully demonstrate phenotypical changes of inclusions or crystals in macrophages. In addition, since several investigators suggested that autophagosomes have cytoprotective function, we tested whether ALDI or CLDIs might alleviate the toxicity of the anti-cancer reagent Doxorubicin (DOX) by combining with CFZ treatment.

C.3 Materials and Methods

Chemicals. Reagents were purchased from Sigma-Aldrich (St. Louis, MO), unless otherwise indicated. Doxorubicin was obtained from (BEDFORD Laboratories).

Peritoneal macrophage isolation and in vitro culture. Peritoneal macrophages (PMC) were obtained from the peritoneal cavity of 8 – 12 wk old female CD-1 mice (Harlan laboratory). 1.5 – 2 ml of 4% thioglycollate solution was injected into both sides of the abdomen as previously described.[2] After 4 days of peritoneal macrophage recruitment into peritoneum, mice were euthanized under sterile environment and wash collected with cold DPBS (Gibco® 14190). Cells were cultured on T-75 flasks at 37^{o} C, 5% CO_2 supplied sterile incubator treated with DMEM plus 10% FBS (Gibco® 10082), 10% non-essential amino acids (Gibco® 11140), and 10% penicillin/streptomycin (Gibco® 15140). Culture media was changed every 1 – 2 days and cells were sub-cultured at 90%

confluency with 0.25% Trypsin-EDTA (Gibco® 15050). They were plated to 96 well or 6 well with carbonated cover glass for biochemical experiment or microscopic imaging as previously described.[1]

Cell viability assay upon treatment. PMC cells in different conditions were tested with standard MTT assay (American Type Culture Collection 30-1010K) following manufaturer's manual. Absorbance between 550 nm and 600 nm (Synergy-2, Biotech instruments, Winooski, VT) were measured, background subtraction and cell number was estimated with standard curve generated separately.

Formation of ALDI/CLDI/CFZ crystals in PMC. Seeded in different densities in 96 well plates for 24 – 96 hours, doubling time was estimated using 1st order exponential increase with $y = y_o e^{kt}$. Positive control of intracellular CLDI in PMC were experimented for feasibility of microscopic analysis, and cells were treated with isolated CLDI previously collected from the liver of CFZ-chow fed mice.[2]

CFZ of 0, 0.1, 1, 5 and 10 µM in DMEM were diluted from a 5 mM in DMSO stock and the PMC were treated for 48 and 96 hours. Doxorubicin solution of 0, 3, 9, 18, 25, 36, 50 µM were treated for 48 hours. After generating the Hill curve for toxicity, PMCs were treated with 5 µM CFZ for 48 hours and then co-treated with 18 µM DOX for additional 48 hours to observe if CFZ crystal inclusions had any cytoprotective function towards DOX treatment. Student's T-test was performed for statistical significance using Microsoft Excel.

Light and fluorescence microscopy. Olympus 51X upright epifluorescence/polarization microscope equipped 100× objective (1.40 NA, PlanApo oil emersion), cross polarizers, U-MWIBA3 (eGFP) for green, U-MWG2 (rhodamine) filter cube for red channel, and an

Olympus DP-70 color camera. Images were acquired using DP controller 3.1.1.267 under same exposure settings. Nikon Eclipse TE2000-S microscopy and MetaMorph^{TM} imaging software were used for image analysis. Different optical properties allowed us to distinguish PMC alone, ALDIs, CLDIs, extracellular CFZ crystals and isolated CLDIs.

C.4 Results

Isolation of peritoneal macrophages and their phagocytic activity on CLDI isolated from CFZ treated mouse liver

After 4% thioglycollate injection into the peritoneum, the anaerobic environment helped recruitment of unactivated macrophages which were isolated by repeated washing with cold DPBS.[6] They were collected in DMEM supplemented with 10% of FBS, penicillin/streptomycin, and non-essential amino acids, and plated on tissue culture flasks kept in a sterile incubator to remain viable (Fig 1A). After a couple of days, macrophages were tested for phagocytic activity by treatment of the crystal-like drug inclusions that were isolated previously from CFZ-chow fed mice (Fig 1B). Macrophages readily phagocytosed the particle, however they could not metabolize or degrade the material. The CLDI structure inside the macrophages was used as the positive control to test optical microscopy properties in order to distinguish CLDI from autophagosome-like drug inclusions (ALDIs) which appeared as birefringent and non-fluorescent in the green channel (FITC), but brightly fluorescent in the red channel (RHOD) (Fig 1B). In the previous study, autophagosome-like drug inclusions were non-birefringent, but at the same time, appeared brightly fluorescent in the green channel, suggesting that ALDIs and

CLDIs are different types of cytoplasmic structures. These characteristics were used as distinguishing criteria for extracellular clofazimine crystals as well which were visibly different in terms of larger crystal size bright yellow in color, but most importantly brightly fluorescent in the green channel.

PMC proliferation

MTT assay was carried out to measure cell viability relying on enzymatic reactions to convert tetrazolium salt into formazan crystals. Mitochondrial dehydrogenases for this reaction are known to be active only in live cells, and therefore, by measuring production of the formazan after complete lysis and dissolution we could extrapolate the number of the cells under different conditions.[7-9] An equal number of PMCs were seeded and grew for 72 hours and they were compared to the standard curve generated separately on formazan produced from a known number of cells (Figure 2A). Cells within the first 24 hours decreased in number due to the subculture, by which activated and adherent macrophages would undergo apoptotic death upon forced detachment from flasks. However, after 24 hours, PMC proliferated slowly but steadily, resulting in approximately 145 ± 42 hours of doubling time depending on the seeding density (Figure 2B). Therefore, we used controlled seeding density and incubation time to carry out further analyses for consistency (Figure 2C).

PMC viability after treatment with CFZ and DOX

10 μM CFZ revealed toxicity and decreased cell viability significantly (Fig 3A). Lower concentrations at 1 μM CFZ with longer incubation times only slightly decreased cell numbers and PMC with formazan crystals were verified under microscopy at 24, 48 and 72 hours (Fig 3B). The LC50, the concentration of CFZ required to decrease the cell

viability to under 50%, was significantly lowered during this prolonged treatment, from greater than 10 μM at 24 hours to 7 and less than 4 μM for 48 and 72 hours, respectively. Notably, 10 μM in DMEM showed formation of extracellular CFZ crystals associated with MTT positive cells (Fig 3B, indicated by arrows) which presumably precipitated from an initially supersaturated drug solution that is known to stay protein bound as previously reported.[1] They grew about 50 μm per day *in vitro* and were also found in 5 μM solution, although to a significantly lesser extent during 72 hours of CFZ treatment. Therefore, we applied 1 μM CFZ for 48 hours to see the CFZ effect on PMCs without toxicity or extracellular crystal precipitation.

In order to show a positive toxic effect, we treated PMC with the anti-mitotic reagent doxorubicin (DOX). LC50 was approximately 18 μM during 48 hours of treatment (Fig 4A) and at 50 μM, cells were completely dead and did not produce formazan (Fig 4B). Meanwhile, 24 hours of DOX treatment was insufficient to show cytotoxicity.

CLDI forms at 1 μM CFZ treatment for 96 hours

Relying on optical characteristics of CFZ crystals, CLDI, and ALDI, formations of different drug inclusions inside the cytoplasm of PMC were assessed after 1 μM CFZ treatment for 96 hours (Fig 5). The CLDI and ALDI formed and revealed their characteristic optical features as tested in the positive control above (Fig 1B). The CLDIs were 10 – 20 μm in length, 1 – 2 μm in width needle-like cytoplasmic structures, and dark red in color. They were birefringent under polarized light (PL) while selectively fluorescent in the red channel but not in the green channel. ALDIs were not birefringent but brightly fluorescent in the green channel as scattered, cytoplasmic punctate.

Depending on the orientation of the needle shaped CLDI on the stage, fixed polarized light shined as different colors, and sometimes birefringence was completely off-set by a post-polarization filter, and as a result, CLDI appeared as black (Fig 6A). The same exposure time and background correction settings were applied throughout the experiment and contrast-enhanced in pairs with the negative control, unexposed to CFZ containing media.

Different CFZ inclusions formed after 48 hours

We also found that 48 hours of 1 μM CFZ treatment was sufficient to induce the formations of CLDIs (Fig 6A) and ALDIs (Fig 6B) similar to what was previously found *in vitro* and *in vivo.* 5 μM treatments exhibited a mixed population of CLDIs and ALDIs (Fig 6C and D, indicated as arrows). The ALDIs appeared fluorescent in the green channel but did not polarize light. Under the same condition, CFZ crystals were observed and categorized as such, depending on their optical property shining as orange-red with positive fluorescence in the green channel (Fig 6C). 5 and 10 μM treatments demonstrated a significant increase in ALDI formations confirmed by a brighter fluorescence signal under the same exposure setting (Fig 6D and E). At this concentration extracellular CFZ crystals were much elongated, shining in orange-red, and associated with PMC. Most interestingly, no intracellular CLDI was observed (Fig 6E) indicating the supersaturated concentration drives crystallization of the CFZ too fast to allow the cells to take in a sufficient amount of molecules. It also suggests that there is no simple relationship between ALDI formation and CLDI formation in terms of one preceding the other. At this condition ALDIs were darker and heterogeneous in size and density, but retained their morphology rather than developing into CLDI.

CFZ inclusions do not have cytoprotective function towards doxorubicin

Since autophagosomes were reported to have cytoprotective function,[10, 11] we hypothesized CFZ induced ALDI could function to rescue or alleviate the cells from DOX toxicity. We treated PMCs for 48 hours with CFZ containing media to induce a sufficient number of ALDIs, but toxicity appeared to be additive when they were pre-treated for 48 hours with 1 or 5 μM CFZ solutions and then exposed to a CFZ+DOX solution for an additional 48 hours (Fig 7A and B). Cytotoxicity of the CFZ and DOX showed that 50% of the cells survived after 48 hours, further decreasing to less than 10% at even longer period, after an 18 μM DOX treatment. Therefore, we conclude that doxorubicin was toxic to cells regardless of any inclusions formed, which were not cytoprotective in the given condition (Fig 7C).

C.5 Discussion

PMCs were successfully isolated and subcultured *in vitro.* Their phagocytosis on isolated CLDIs showed similar characteristics to CLDIs under polarization and fluorescence microscopy from the *in vivo* study,[2] in which we distinguished the different types of inclusions through experimental processes. Based on CFZ crystal formations at 1 μM concentration, we can infer that PMC can develop CLDIs as well as ALDIs, which is a significant finding compared to the previous study on MDCK cells resulting in ALDIs exclusively, despite the longer treatment of over 5 days. The longer period of treatment exhibited more CLDI formation, as similar to what was seen *in vivo*.[2] Also this prolonged treatment accompanied significant cell death, producing a large margin of error in quantitative study on CFZ accumulation and cell proliferation. In relation to the

microgranulomas *in vivo*,[2, 5] the cells in the center of the tissue macrophage colonies were found necrotic. Nevertheless, we have demonstrated that weeks of treatment in mice is unnecessary to create CLDIs as the 48 hour treatment at 1 μM concentration could successfully produce them in PMCs. To further investigate the formation of CLDIs in future, we could simplify the supply chain of these biosynthetic drug inclusions.

Although CFZ crystals were differentiated from CLDIs, they cannot be confirmed to be polyhedrosomes as well until EM analysis was made to reveal the ultrastructure with highly organized membrane lamellae in cytoplasm as previous chapters has described. Therefore, EM study with a significant number of cells *in vitro* is strongly recommended.

ALDI formations occurred in all conditions tested, and suggested that PMC phagocytosis can be a way of intake and accumulation at the site of exposure. However, cells that had CLDI were not the PMC containing the more of ALDIs, indicating that ALDI does not necessarily coalesce to form crystal-like features. Despite the higher concentrations of CFZ in the medium led to the aggregation of ALDIs into much larger and more pronounced number of inclusions, the populations between CLDI positive vs ALDI positive cells were distinct. On the other hand, extracellular CFZ crystals, either attached or unattached to PMCs, have displayed the pure CFZ crystal morphology without forming CLDIs in PMCs. It is possible that the extracellular CFZ crystal formation could induce the CFZ to crystallize out from culture medium, limiting the amount of the drug that could be delivered into cytoplasm restraining the formation of intracellular ALDIs or CLDIs.

In order to establish a condition for mass production of CLDI-storing macrophages, we have tested various cell lines in DMEM culture media, including HepG2 (human hepatocarcinoma), NR8383 (rat lung macrophage), bone marrow-derived macrophages (isolated from mouse femur), Raw 264.7 (mouse monocyte/macrophage), P388D1 (lymphoblasts). HepG2 developed ALDIs only, while other macrophages appeared to be too sensitive to subculture which made it hard to reproduce experimental outcomes. If we could identify the stable cell lines and conditions suitable for inclusion formations, it would be interesting to run a comparative study on similarities and differences among cell lines that form varying types, number, and morphology of inclusions.

C.6 Acknowledgements

The author thanks Esteban Montemayor (West Texas A&M University) for his contribution during June – August 2011, supported by Interdisciplinary Research Experiences for Undergraduates Program 2011 funded by National Science Foundation.

C.7 Figures

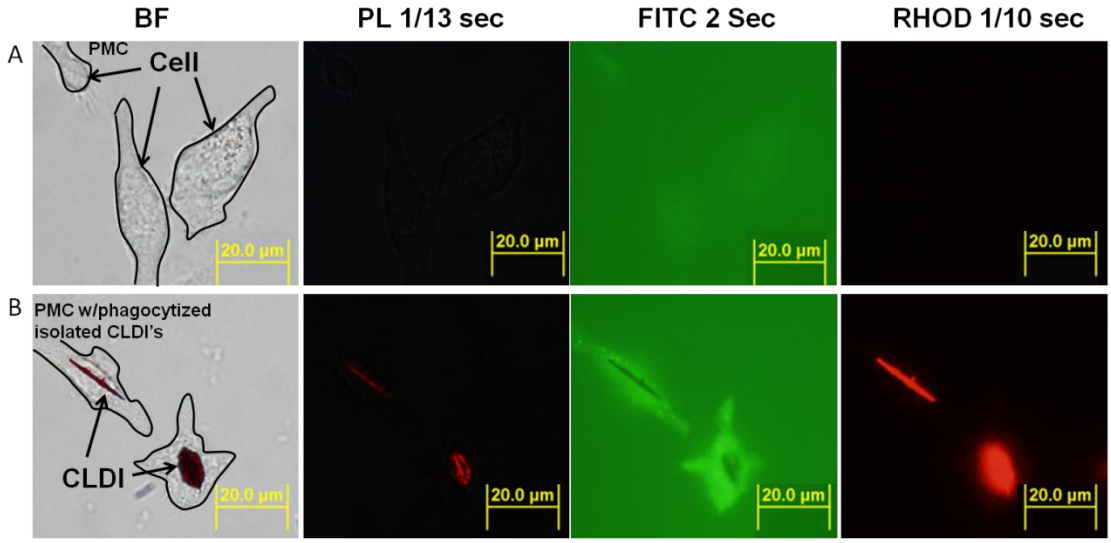

Figure 1. Optical property of PMC with phagocytosed CLDIs.

(A) Isolated PMC cells seeded on cover slip showed negative optical properties for polarized light (PL), green (FITC) and red (RHOD) fluorescence channel for indicated exposure. **(B)** PMC phagocytosed isolated CLDIs as positive control. They showed birefringence (PL +) and red fluorescence (RHOD +), while appeared negative in the FITC channel. Under the green fluorescence, cytoplasmic area appears brighter due to small endo/lysosomal accumulation of the CFZ as reported in the previous study.

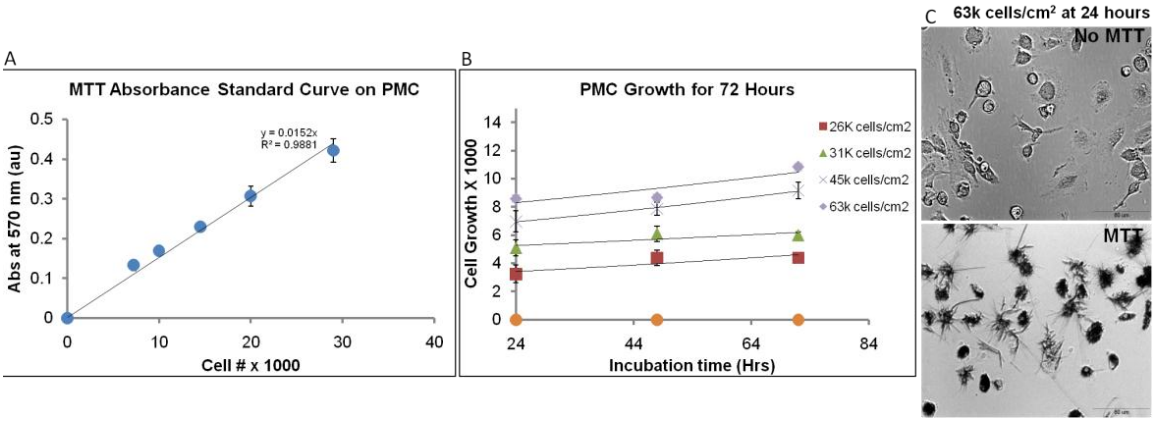

Figure 2. MTT assay on PMC proliferation.

(A) Standard curve for formazan production showing linear relationship between PMC cell numbers vs. absorbance at 570 nm. **(B)** Growth curve of PMC for 72 hours at different seeding. N=3, average doubling time was 145 hours. **(C)** Transmitted light microscopy image of PMC before and after MTT treatment. 30 minute incubation was sufficient to produce purple crystalline formazan.

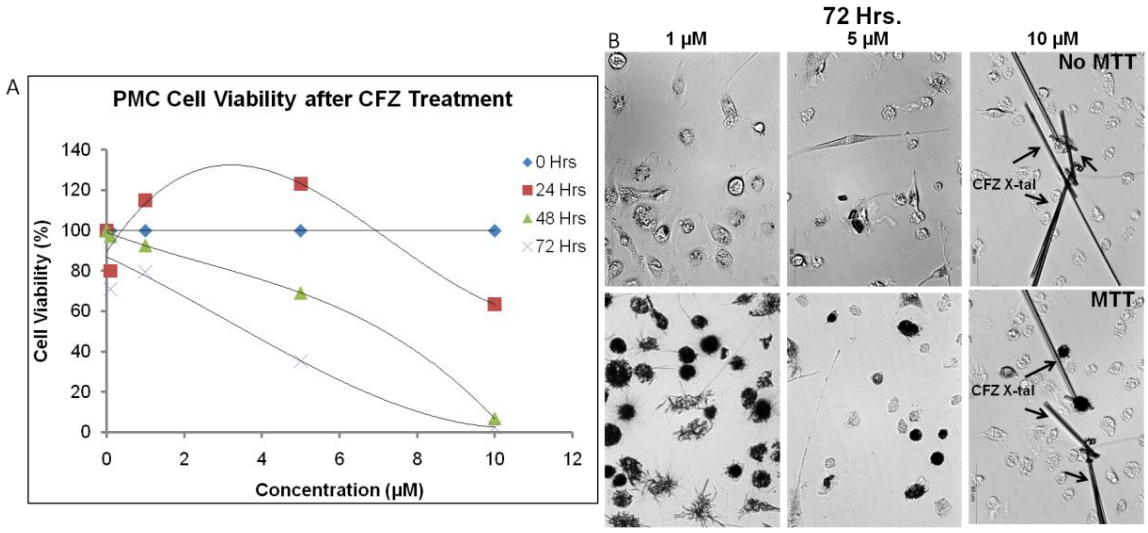

Figure 3. MTT assay on PMC with CFZ treatment.

(A) Cell viability calculated from MTT assay after 0.1 – 10 µM CFZ treatment for 24 – 72 hours. Approximated LC50 decreased for prolonged treatment. **(B)** PMC treated with CFZ at different concentrations with and without MTT reagent. Notably 10 µM CFZ treatment showed significant elongation of extracellular crystals while PMC did not show formazan production. Experiments were duplicated.

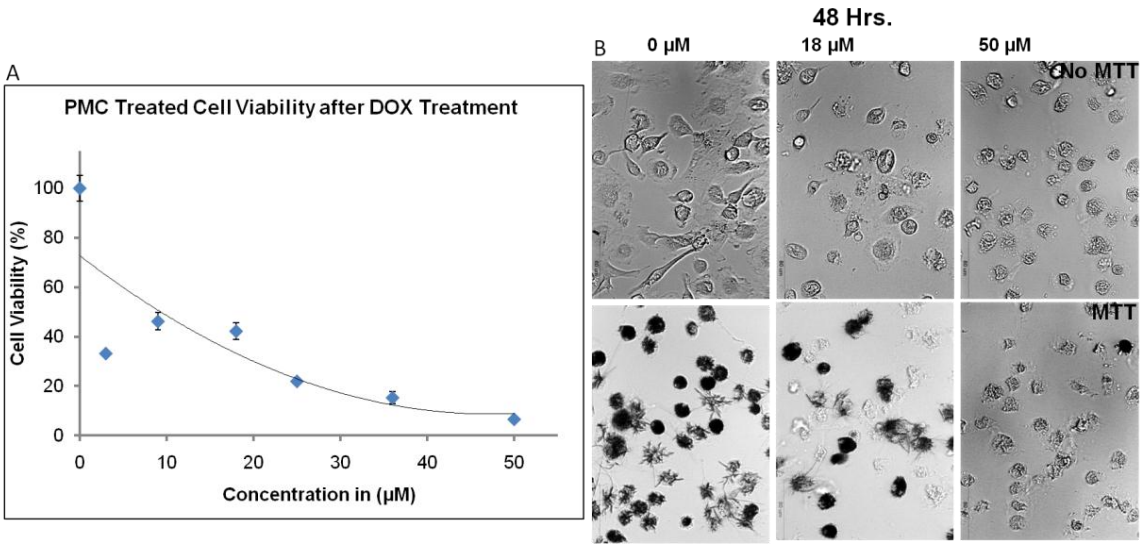

Figure 4. Doxorubicin toxicity analysis on PMC.

(A) Cell viability of PMC from MTT assay after 48 hours of DOX treatment showed LC 50 around 18 µM. **(B)** Brightfield image of PMC cells after DOX treatment with and without MTT. Negative control at 0 µM, LC 50 at 18 µM and positive control at 50 µM was shown with corresponding MTT treatment.

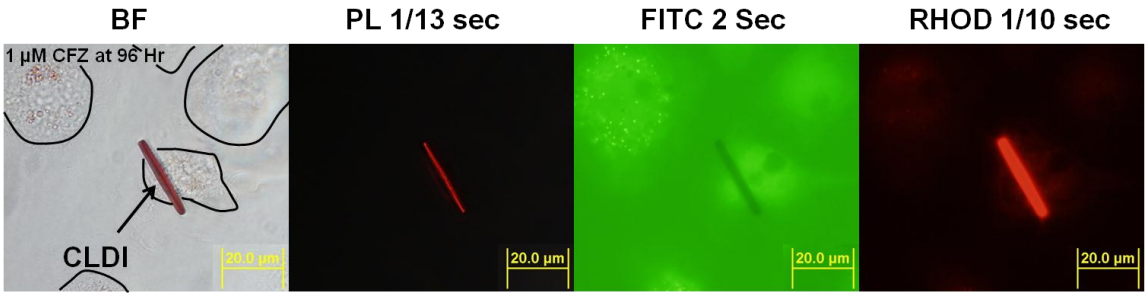

Figure 5. A CLDI formed in PMC cells after treatment of 1 µM CFZ for 96 hours.

CLDIs appeared as bright red needles about 20 µm in length, 1 – 2 µm in width with birefringent (PL positive), negative green fluorescence (FITC), and positive red fluorescence (RHOD). ALDIs (autophagosome-like drug inclusions) were also positive in other PMCs which did not polarize light but fluorescent in the green channel.

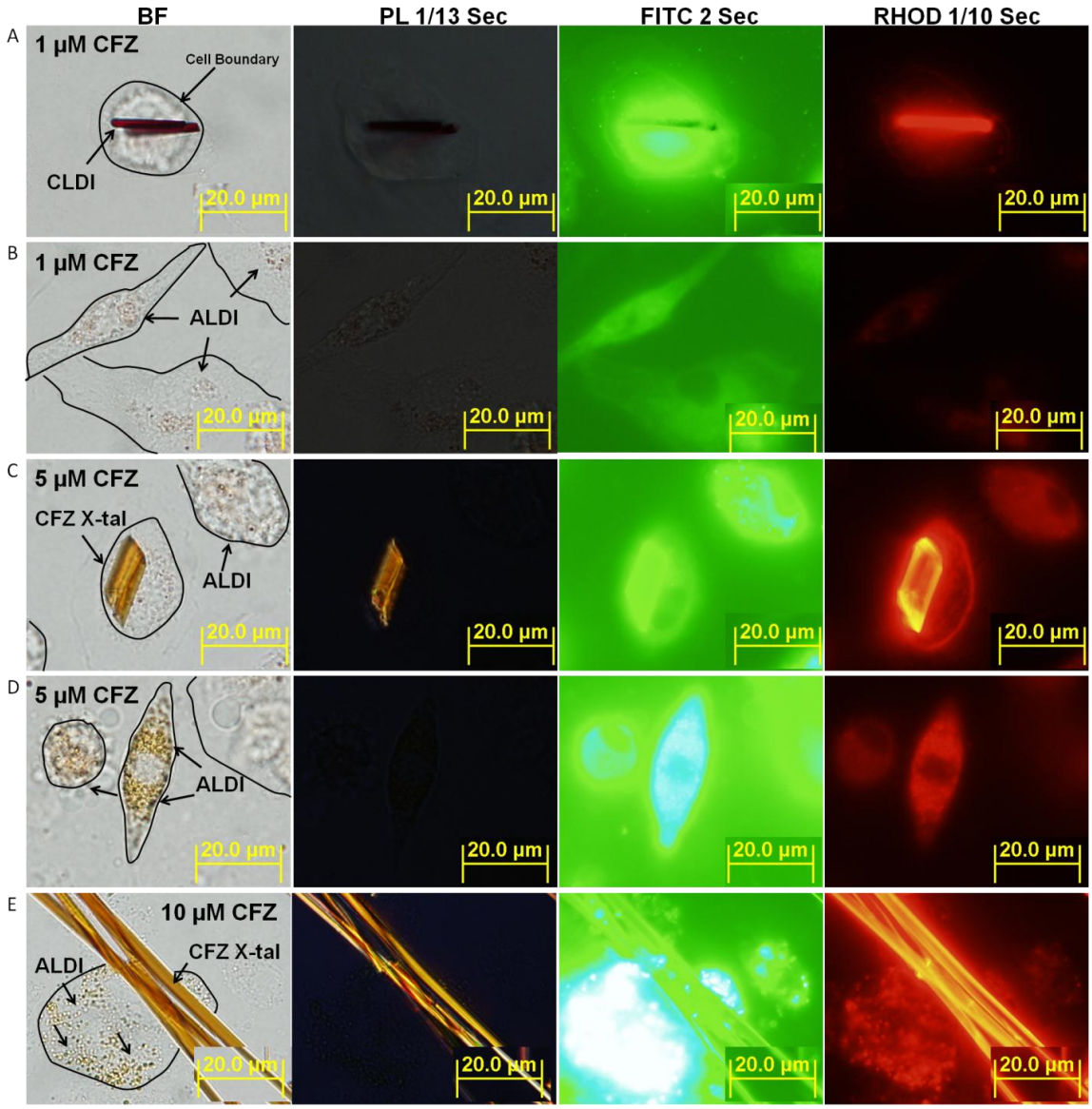

Figure 6. PMC with CLDI, ALDI, and CFZ crystals (X-tal)

(A) CLDI formed in PMC after 1 µM CFZ treatment for 48 hours. **(B)** ALDI formed in PMC as well in same treatment. **(C)** Although it appears intracellular, orange-red colored, thick object is CFZ crystal. They appear birefringent but green fluorescent as well. **(D)** Darker and larger number ALDI formed in PMC after 5 µM CFZ treatment which revealed stronger green fluorescence. **(E)** Elongated, orange-red, extracellular CFZ crystals with ALDI formed at 10 µM CFZ treatment for 48 hours.

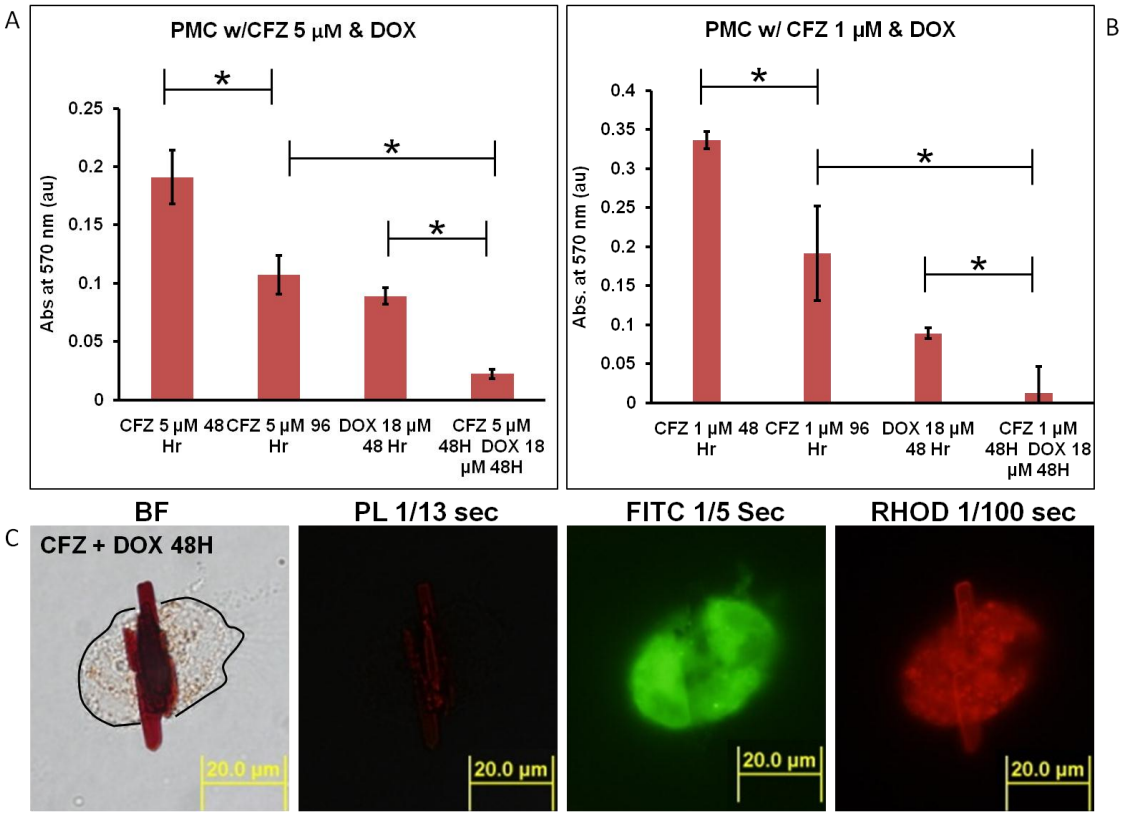

Figure 7. Co-treatment of CFZ with DOX

(A) MTT assay on PMC treated with 5 µM CFZ with 18 µM DOX. N=3 ***:** P<0.05 using student's T-test. **(B)** PMC w/ CFZ 1 µM demonstrated similar pattern with 5 µM which showed CFZ and DOX has additive toxicity. **(C)** CLDI formations at CFZ + DOX treatment for 48 hours under different optical properties.

C.7 References

1. Baik, J.; Rosania, G. R. Molecular Imaging of Intracellular Drug-Membrane Aggregate Formation. *Molecular Pharmaceutics* **2011**, DOI:10.1021/mp200101b.

2. Baik, J.; Rosania, G. R. Cytoplasmic Construction of Supramolecular Structures with Organelle- and Crystal-like Features. *submitted to Pharm Res* **2011**.

3. Griffis, L. C.; Twerdok, L. E.; Francke-Carroll, S.; Biles, R. W.; Schroeder, R. E.; Bolte, H.; Faust, H.; Hall, W. C.; Rojko, J. Comparative 90-day dietary study of paraffin wax in Fischer-344 and Sprague-Dawley rats. *Food Chem Toxicol* **2010,** *48*, (1), 363-72.

4. Jenkins, S. J.; Ruckerl, D.; Cook, P. C.; Jones, L. H.; Finkelman, F. D.; van Rooijen, N.; MacDonald, A. S.; Allen, J. E. Local macrophage proliferation, rather than recruitment from the blood, is a signature of TH2 inflammation. *Science* **2011,** *332*, (6035), 1284-8.

5. Williams, G. T.; Williams, W. J. Granulomatous inflammation--a review. *Journal of Clinical Pathology* **1983,** *36*, (7), 723-733.

6. Leijh, P. C.; van Zwet, T. L.; ter Kuile, M. N.; van Furth, R. Effect of thioglycolate on phagocytic and microbicidal activities of peritoneal macrophages. *Infect Immun* **1984,** *46*, (2), 448-52.

7. Berridge, M. V.; Tan, A. S. Characterization of the cellular reduction of 3-(4,5-dimethylthiazol-2-yl)-2,5-diphenyltetrazolium bromide (MTT): subcellular localization, substrate dependence, and involvement of mitochondrial electron transport in MTT reduction. *Arch Biochem Biophys* **1993,** *303*, (2), 474-82.

8. Liu, Y.; Peterson, D. A.; Kimura, H.; Schubert, D. Mechanism of cellular 3-(4,5-dimethylthiazol-2-yl)-2,5-diphenyltetrazolium bromide (MTT) reduction. *J Neurochem* **1997,** *69*, (2), 581-93.

9. Vellonen, K. S.; Honkakoski, P.; Urtti, A. Substrates and inhibitors of efflux proteins interfere with the MTT assay in cells and may lead to underestimation of drug toxicity. *Eur J Pharm Sci* **2004,** *23*, (2), 181-8.

10. Pallet, N.; Bouvier, N.; Legendre, C.; Gilleron, J.; Codogno, P.; Beaune, P.; Thervet, E.; Anglicheau, D. Autophagy protects renal tubular cells against cyclosporine toxicity. *Autophagy* **2008,** *4*, (6), 783-91.

11. Sarkar, S.; Perlstein, E. O.; Imarisio, S.; Pineau, S.; Cordenier, A.; Maglathlin, R. L.; Webster, J. A.; Lewis, T. A.; O'Kane, C. J.; Schreiber, S. L.; Rubinsztein, D. C. Small molecules enhance autophagy and reduce toxicity in Huntington's disease models. *Nat Chem Biol* **2007,** *3*, (6), 331-8.